Journal of Materials Chemistry A

ROYAL SOCIETY OF CHEMISTRY

REVIEW

View Article Online
View Journal | View Issue

Cite this: J. Mater. Chem. A, 2021, 9, 4379

Oxygen-induced defect-healing and photo-brightening of halide perovskite semiconductors: science and application†

Like Huang, *[ab] Ziyi Ge, *[ac] Xiaoli Zhang[d] and Yuejin Zhu[b]

Solution-processed metal halide perovskite (MHP) semiconductors have shown remarkable success in diverse optoelectronic device applications, especially in solar cells, despite having a non-negligible density of defect states. The photoluminescence quantum yield (PLQY) is usually taken as a proxy to evaluate the optoelectronic quality of MHPs. Higher PLQYs imply a reduction of nonradiative deactivation pathways, which can contribute to a lower nonradiative voltage loss and higher open circuit voltage of the final device. Many studies have reported various methods to passivate the defect states in MHPs and to enhance their PLQYs. An interesting observation that has been repeatedly reported recently is a drastic PLQY enhancement upon exposure of MHPs to dry air or oxygen under illumination, which is the so-called photo-brightening phenomenon associated with oxygen-induced defect-healing (OIDH) of MHPs. This phenomenon involves the interaction between oxygen and defects in MHPs, as the adsorption and diffusion of oxygen can mediate the perovskite lattice and passivate the defects (such as halogen vacancies and interstitials, halogen migration and aggregation) on the surface or in the bulk of MHPs. In this review, we mainly focus on the recent advances and the related sciences in enhancing the optoelectronic quality of emerging MHP semiconductors by effective defect passivation though a facile oxygen post-treatment, which is the so called OIDH effect and the associated photo-brightening effect, as well as their wide applications in solar cells, LEDs, oxygen/ozone sensors, X-ray detectors, *etc.* Our work highlights the great potential of the efficient and convenient *in situ* defect passivation of emerging MHP semiconductors by oxygen (abundant in an ambient atmosphere) towards various perovskite based optoelectronic applications.

Received 10th November 2020
Accepted 21st December 2020

DOI: 10.1039/d0ta10946k

rsc.li/materials-a

1 Introduction

With excellent optoelectronic properties and simple solution processing, metal halide perovskites (MHPs), as excellent emerging semiconductors, have shown great potential in various optoelectronic applications in the last decade, especially in the photovoltaic field. The power conversion efficiency (PCE) of single-junction perovskite solar cells (PSCs) has rapidly increased from initial 3.8% (ref. 1) to a certified value of 25.2% (ref. 2) presently. However, whilst great strides have been made

[a]Ningbo Institute of Materials Technology and Engineering (NIMTE), Chinese Academy of Sciences (CAS), Ningbo 315201, China. E-mail: huanglike@nbu.edu.cn
[b]Department of Microelectronic Science and Engineering, School of Physical Science and Technology, Ningbo University, Zhejiang 315211, China
[c]Center of Materials Science and Optoelectronics Engineering, University of Chinese Academy of Sciences, Beijing 100049, China
[d]School of Materials Science and Engineering, Zhengzhou University, Zhengzhou 450001, China. E-mail: geziyi@nimte.ac.cn

† Electronic supplementary information (ESI) available. See DOI: 10.1039/d0ta10946k

Like Huang received his M.S. degree in solid state electronic physics from Ningbo University and PhD degree in electronic science and technology from Nankai University. He conducted his postdoctoral research on perovskite solar cells at the Ningbo Institute of Materials Technology and Engineering, Chinese Academy of Science. Then he moved to Ningbo University as an associate professor. His research interests focus on photovoltaic materials and solar cell device physics.

Ziyi Ge got a PhD from the Institute of Chemistry, Chinese Academy of Sciences. He conducted his postdoctoral research on organic electronics at the Tokyo Institute of Technology, Kanagawa University, Japan and the University of New South Wales, Australia. Currently, he is the leader of the Organic Electronic Material and Device Group at the Ningbo Institute of Material Technology and Engineering, Chinese Academy of Sciences. His research interests focus on OLEDs, organic solar cells, and the related materials.

in photovoltaic performance, our understanding of the fundamental properties of these materials is still incomplete.[3] Especially, this achievement is fulfilled mainly based on solution processed polycrystalline perovskite films with inevitable defects, which is usually adopted as the absorption layer.[4]

To further increase the PCE of PSCs, it is important to further reduce the unavoidable defects in polycrystalline perovskite films, including surface, grain boundary and bulk defects, which are very sensitive to the film fabrication process.[5,6] To date, many passivation strategies have been reported to reduce the charge trap density present in perovskite films, such as the introduction of functional molecules (such as PbI_2, MACl, FACl, and PEAI), metal ions (such as Li^+, K^+, Rb^+, and Cs^+), and halogen ions into the bulk or onto the surface of perovskite films.[6] For example, an organic halide salt, PEAI, was recently introduced as an effective additive layer for surface defect passivation of perovskites, and a certified efficiency of 23.32% was once obtained.[7] Fig. 1A presents the common imperfections in perovskite films and their passivation by ionic bonding, coordinate bonding, and conversion to wide band gap materials, and suppression of ion migration at extended defects.[8] Fig. 1B shows the experimentally determined energy levels associated with defects in $MAPbI_3$ and determined by different techniques.[9] These structural defects can introduce different trap levels in the band gap of MHPs, which may have a varying degree of influence on the final device performance. Therefore, effective passivation measures are urgently needed to remove these defects and to further improve the device performance.

In addition to the above-mentioned defect passivators, Lewis acids and bases are a class of substances that have a particular effect on the specific defects of perovskites.[10] Generally, a Lewis acid refers to a molecule or ion that accepts a foreign electron pair, while a Lewis base represents a molecule or ion that gives an electron pair. Such molecules could combine with perovskites *via* covalent bonds to form acid–base complexes without electron transfer. Consequently, Lewis acids have unique passivation capabilities for defects with lone pairs of electrons like free iodide ions and lead iodine antiside defects; electron-deficient defects such as Pb^{2+} interstitials can be strongly bonded by Lewis bases. Deep-level trap recombination centers induced by anion and cation defects can be well eliminated, and the overall device performance can be significantly improved. For example, Snaith *et al.* have increased the efficiency of solution-processed planar heterojunction perovskite solar cells from 13% to 15.3% and 16.5% using Lewis bases thiophene and pyridine treatments, respectively (Fig. 1C(a)).[10] The increase in the PL lifetime close to an order of magnitude demonstrated that thiophene and pyridine have good passivation effects on defects, which stems from the fact that these Lewis base molecules can bind to the under-coordinated Pb ions in the perovskite crystal. Ginger *et al.* observed photoluminescence lifetimes exceeding 8 μs and a photoluminescence quantum yield (PLQY) exceeding 30% in polycrystalline films by a variety of Lewis base treatments on $MAPbI_3$ films (Fig. 1C(b)).[11] Yang *et al.* synthesized a new molecule D-4-*tert*-butylphenylalanine (D4TBP) with 4-*tert*-butylphenyl, amine, and carboxyl, which has a very significant passivation effect on Lewis acid defects (Fig. 1C(c)).[12] The passivation ensures an extremely small open-circuit voltage (V_{oc}) loss of only 0.34 V in PSCs, which is the lowest value reported in the literature.

Apart from these organic molecule-based Lewis acids/bases that can function as defect passivators, other simple small molecules or ions, such as O_2, O_3, H_2O, H_2O_2, O, O^{2-} and Cl^-, may also serve as efficient defect passivators to enhance the optoelectronic quality of perovskite films and crystals towards various applications. Especially, oxygen, abundant in the ambient atmosphere, has been reported to serve as an efficient and convenient *in situ* defect passivator during the deposition of inorganic MHP semiconductor films.[13] Fig. 1D provides a comprehensive list of the types of defects that are important to be considered and eliminated for solar cell applications, wherein the halogen vacancy defect gets the most attention.[7] Below we will see the interplay between oxygen and the halogen vacancy that has a significant influence on the optoelectronic properties and thus the device performance.

For actual optoelectronic application of perovskites, the effect of ambient O_2 is an important issue that should be addressed. In classical inorganic semiconductor materials, the effect of oxygen on the material properties and thus device performance has been widely reported. For instance, Ding *et al.* revealed the influences of oxygen passivation of silicon nanocrystals on their trap states, electron mobility, and hybrid solar cell performance.[13] It is found that controlled particle oxidization can efficiently reduce carrier traps and improve electron mobility, while excessive oxidation can introduce an oxygen rich layer on the particle surface blocking carrier transport and deteriorating electrical properties inversely (Fig. S1A†). Zhang *et al.* found that in-gap states (IGSs) near the

Xiaoli Zhang obtained her PhD in materials chemistry from Pukyong National University. Then, she worked as a research fellow at Monash University and the University of Melbourne. She commenced her vice-chancellor's research fellowship at the University of New South Wales (2012–2015) and then worked at the University College London (2014–2015), before taking a full faculty position at Zhengzhou University in 2016. She won the Marie Sklodowska-Curie Actions Seal of Excellence Award from the European Commission Horizon 2020 research and innovation funding programme.

Yuejin Zhu is a professor in the Department of Microelectronic Science and Engineering, School of Physical Science and Technology, Ningbo University. He got his PhD from the Department of Physics, Nanjing University. He is now a member of the steering committee of physics major in Zhejiang province and a doctoral supervisor. He is mainly engaged in the research of semiconductor materials and devices. He has published more than 150 papers in Adv. Energy Mater., ACS Nano, Phys. Rev. B and other famous international academic journals, and has obtained 16 invention patents.

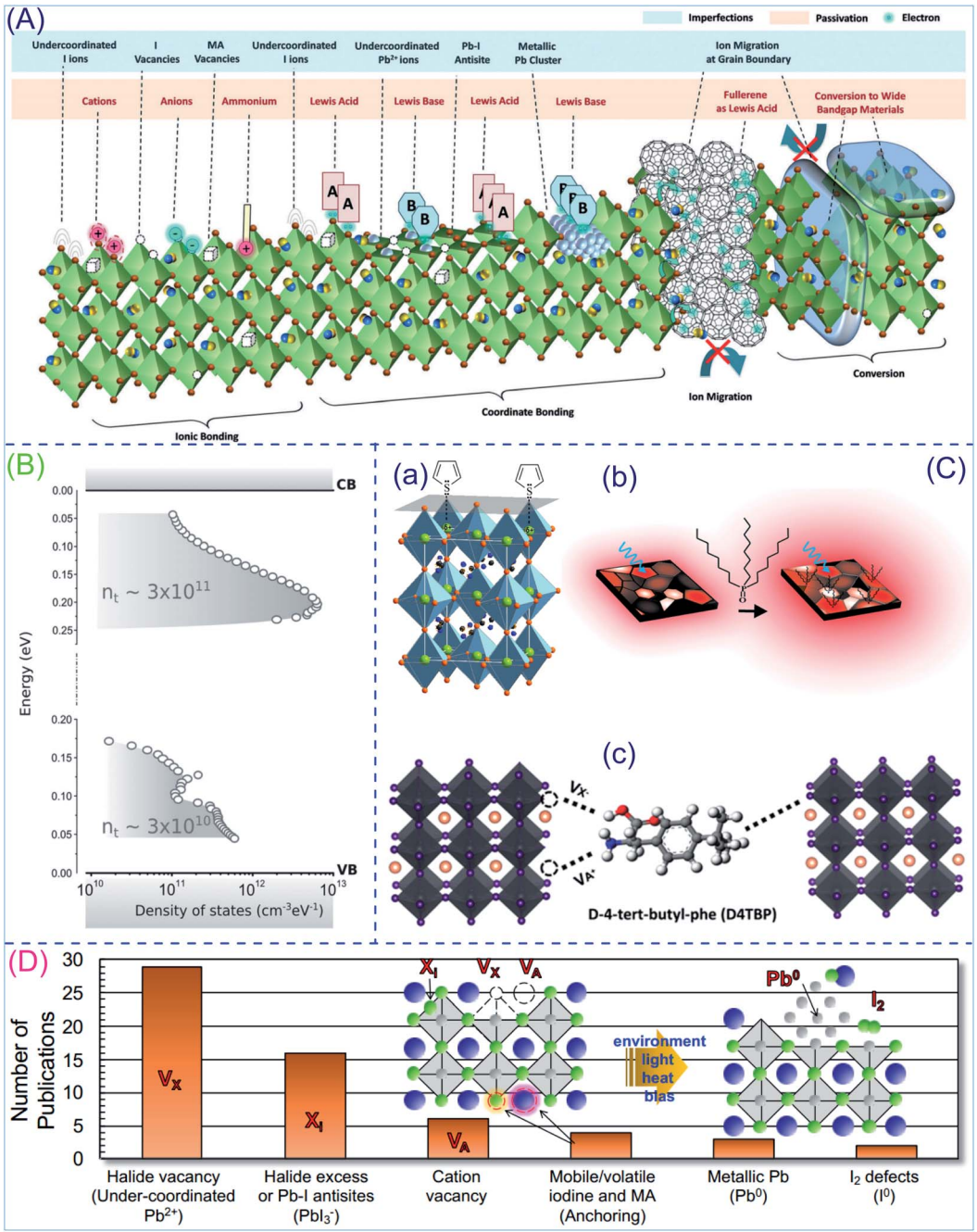

Fig. 1 (A) Imperfections in a perovskite film and their passivation by ionic bonding, coordinate bonding, and conversion to wide band gap materials, and suppression of ion migration at extended defects. Reprinted with permission from ref. 8. Copyright 2019 Royal Society of Chemistry. (B) Experimentally determined defect levels in $MAPbI_3$ (by different techniques). Reprinted with permission from ref. 9. Copyright 2018 Nature Publishing Group. (C) Passivation by a Lewis base. Proposed passivation mechanism of thiophene or pyridine (a). Reprinted with permission from ref. 10. Copyright 2014 American Chemical Society. Schematic diagram of PLQY enhancement (b). Reprinted with permission from ref. 11. Copyright 2016 American Chemical Society. Schematic illustration of the D4TBP passivation effect on defect sites (c). Reprinted with permission from ref. 12. Copyright 2019 American Chemical Society. (D) Histogram of published studies on the experimentally assigned types of defects in perovskites employing passivation strategies. Reprinted with permission from ref. 7. Copyright 2019 Wiley-VCH.

valence band occur frequently in artificial semiconductor quantum dots (QDs) except when treated with reducing agents (such as hydrazine).[14] By virtue of experimental and theoretical study, they revealed that the oxygen molecule is most likely the origin of these IGSs. They further expect these impurity-induced deep in-gap states to be a common occurrence in ionic semiconductors, where the intrinsic vacancy defects either do not produce IGSs or produce shallow states near band edges. Tang *et al.* reported that oxygen addition during Sb_2Se_3 film evaporation significantly improves the CdS/Sb_2Se_3 heterojunction quality through effective passivation of interfacial defect states, which results in a substantial enhancement in

device performance (Fig. S1B†).[15] Schwermann *et al.* proposed the incorporation of oxygen atoms as a mechanism for photoluminescence enhancement of chemically treated MoS_2 (Fig. S1C†).[16] Nan *et al.* also reported strong photoluminescence enhancement of MoS_2 through defect engineering and oxygen bonding (Fig. S1D†).[17] These studies confirm the vital role of oxygen as an efficient and universal defect passivator of various classical semiconductors, which implies the great potential of oxygen induced defect passivation in halide perovskites as emerging new semiconductors.

Recently, experimental and theoretical research about the contradictory and controversial effect of O_2 on hybrid perovskites has attracted increasing attention with several research groups noting that O_2 can also affect the performance of PSCs.[18–20] In fact, theoretical calculations have demonstrated that oxygen atoms can effectively passivate traps in MHPs and occupy halogen vacancies, thus suppressing halogen redistribution and phase separation. Within this review, we take a bird's-eye view of the recent advance in the understanding of the effect of oxygen on hybrid perovskite properties and perovskite-based device performance, with applications in PSCs, PLEDs, *etc.* as typical examples.

2 Oxygen annealing process in PSCs: phenomenon and experience in early research

Perovskites have shown great success in various optoelectronic applications, especially in the photovoltaic field, though with various defects that cannot be ignored. There have been many review articles published on defects and their passivation in the past decade as mentioned, and here we will mainly focus on the oxygen-induced defect-healing effect of perovskites.

In early studies, the "missing" Cl and its role in improving the optoelectronic properties of Cl-included perovskites has once been the focus of intensive study. Delugas and coworkers revealed the defect role of Cl in $MAPbI_3$ perovskites with Cl inclusion.[21] In their work, methyl-ammonium fragmentation in amines is confirmed as a source of localized trap levels in the band gap, while an amount of 2% additional interstitial Cl is capable of removing these localized defect states. Polycrystalline $MAPbI_3$ perovskite shows complex optoelectronic behavior, largely because its 3D semiconducting inorganic framework is strongly perturbed by the organic cations and ubiquitous structural or chemical inhomogeneity. Based on a newly developed time-dependent DFT formalism, Beljonne *et al.* found that lead and iodine vacancies can yield deep trap states that can be healed by dynamic effects (rotation of the methyl-ammonium cations in response to point charges), or through slight changes in chemical composition, for example, by introducing a tiny amount of Cl dopant into the defective $MAPbI_3$ (Fig. S2†).[22] This is supported by the enhanced PL intensity and lifetime of $MAPbI_{3-x}Cl_x$ with increasing Cl content (x). By DFT calculations, Yin *et al.* suggested that Cl and O can spontaneously segregate into grain boundaries (GBs) and passivate those defect levels and deactivate the trap state, implying a similar role of electronegative Cl and O as electron acceptors in passivating the defects in MHPs.[27] This work laid the theoretical foundation for oxygen as an effective passivator for MHPs.

The photoluminescence quantum yield (PLQY) is usually taken as a proxy to evaluate the optoelectronic quality of lead halide perovskites. Higher PLQYs imply a reduction of non-radiative deactivation pathways, which can contribute to a lower non-radiative voltage loss and higher V_{oc}. Apart from the above-mentioned thermodynamics or chloride dominant self-induced defect-healing,[23–26] published studies have reported many other methods to passivate the defect states in perovskites and to enhance their PLQYs. An interesting observation that has been repeatedly reported is a drastic PLQY enhancement upon exposure of prototypical lead halide perovskites to dry air or oxygen under illumination, which is the so-called photo-brightening phenomenon associated with oxygen-induced defect-healing of perovskites. This confirms the correct foresight of the theoretical work of Yin *et al.* as mentioned above.

In fact, in early research, there have been reports about oxygen annealing perovskites to improve the device performance, while the mechanism behind is not clear. Ren *et al.* revealed the effect of post-atmosphere treatment on the performance of $MAPbI_3$-based n–i–p planar PSCs.[28] It is found that annealing $MAPbI_3$ in O_2 (placing the films in dry O_2 at 65 °C prior to electrode deposition) can lead to a substantial increase in the PCEs of the devices. Also, strong dependence on the annealing temperature for the PCEs of the devices suggests that a thermally activated process may underlie the observed phenomenon (Fig. 2A(a)). It is believed that the annealing process may facilitate the diffusion of O_2 into spiro-MeOTAD for inducing p-type doping of the hole transport material, which enhances its conductivity (Fig. 2A(b)). Furthermore, the process can decrease the localized state density at the GBs as well as the bulk of perovskite. Utilizing thermal assisted O_2 annealing, highly efficient devices with good reproducibility can be achieved. Their results suggest that the improvement in device performance by the O_2 annealing process is due to the reduction in the defect density of the perovskite film as well as the enhancement in the conductivity of spiro-MeOTAD. This work highlights the critical role of post-O_2 annealing treatments in enhancing the device performance and reproducibility.

Snaith *et al.* investigated the atmospheric influence upon crystallization and electronic disorder and its impact on the photophysical properties of $MAPbI_{3-x}Cl_x$ films as well as the final device performance (Fig. 2B).[29] It was found that the crystal formation and photophysical properties of $MAPbI_{3-x}Cl_x$ films are kinetically driven by the annealing atmosphere, time and temperature. Generally, annealing in air produces an improved crystallinity and large grain domains as compared to nitrogen. Lower photoluminescence quantum efficiency (PLQE) and shorter photoluminescence (PL) lifetimes are observed for nitrogen annealed perovskite films as compared to their air-annealed counterparts (Fig. 2B(a and b)). The air annealed perovskite films show higher absorption in the visible region than the nitrogen-annealed one, a trend that is surprisingly reversed in the near-IR region (Fig. 2B(c and d)). This indicates that a change in crystal symmetry is partially responsible for the

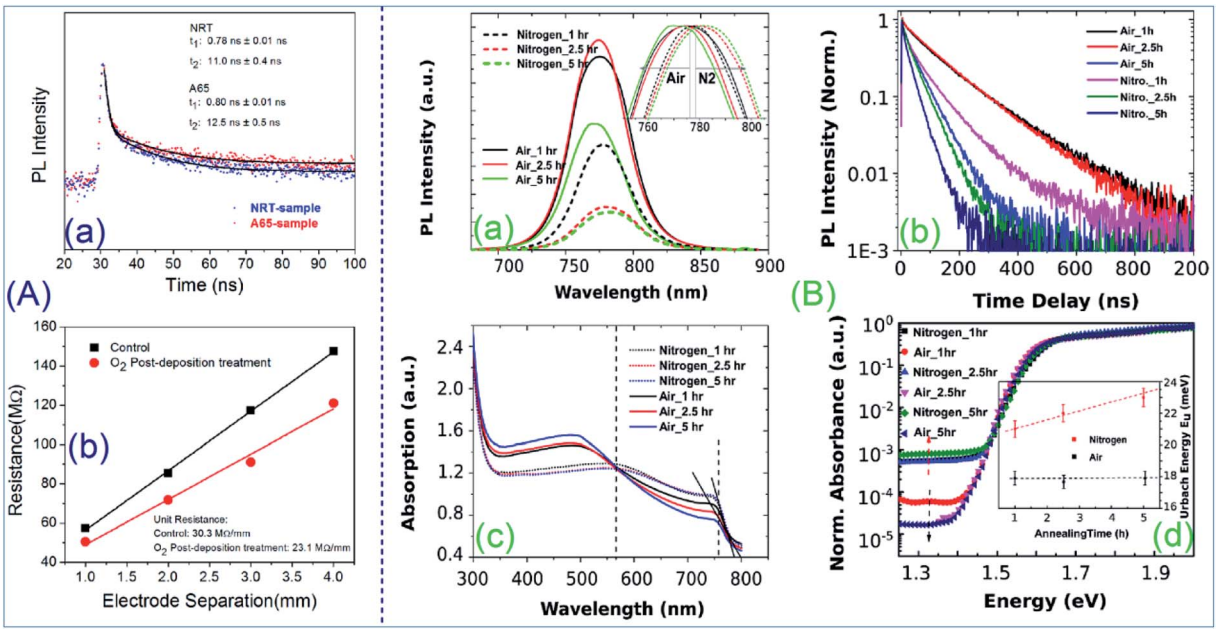

Fig. 2 (A) Effect of thermal-oxygen annealing: transient PL spectrum of the perovskite film with or without O_2 post-annealing treatment (a). The resistance of the spiro-MeOTAD film with and without O_2 post-annealing (b). Reprinted with permission from ref. 28. Copyright 2014 Nature Publishing Group. (B) Atmospheric influence upon the crystallization, electronic and photophysical properties of the perovskite: steady-state (a) and time-resolved (b) PL spectra, absorption spectra (c) and PDS spectra (d) of $MAPbI_{3-x}Cl_x$ films prepared under nitrogen and ambient conditions for different annealing times and temperatures. Reprinted with permission from ref. 29. Copyright 2015 American Chemical Society.

observed red shift in PL emission and is not exclusively due to the energy relaxation. A higher degree of crystal disorder could lead to lower PLQEs, PL lifetimes and higher recombination in nitrogen-annealed samples. Photothermal deflection spectroscopy (PDS) suggests that air annealed films exhibit a remarkably lower level of disorder than the nitrogen annealed one. Janssen *et al.* reported the complex effect of oxygen on the efficiency of planar p–i–n metal PSCs with a PEDOT:PSS hole transport layer.[30] It is shown that processing of a perovskite layer on top of PEDOT:PSS *via* spin coating of a precursor solution chemically reduces the oxidation state of PEDOT:PSS. This reduction leads to a lowering of the work function of PEDOT:PSS and the perovskite layer on top of it. As a consequence, the solar cells display inferior performance. The reduced PEDOT:PSS can be re-oxidized by thermal annealing of the PEDOT:PSS/perovskite layer stack in the presence of oxygen. As a consequence, thermal annealing of the perovskite layer in air provides PSCs with increased performance.

These early results suggest that oxygen has a significant effect on the properties of perovskite materials and device performance thereof, but the underlying mechanism is not clear.

3 Oxygen–perovskite interaction and its effects

3.1 Oxygen–perovskite interaction: adsorption, diffusion, binding and reaction

Since the above-mentioned reports on oxygen annealing to improve the device performance, the mechanism behind such a phenomenon has attracted researchers' attention. The effect of oxygen adsorption and diffusion on the structure, stability, electronic structure and properties of perovskites has been comprehensively studied by combined experiments and theoretical calculations.

As for the effect of oxygen adsorption and diffusion, Grancini *et al.* revealed the surface photo-physics of $MAPbI_3$ single crystals (SCs) and their interaction with the environment.[31] They found that water molecules can permeate across the perovskite structure to form a partly hydrated phase, occurring spontaneously due to hydrogen bonding interactions with the perovskite lattice, as the formation energy of $4MAPbI_3 \cdot H_2O$ is negative (−0.45 eV) indicating spontaneous water incorporation into the perovskite lattice, while the incorporation of oxygen molecules is unfavorable, with a positive formation energy of 0.17 eV. This implies that the oxygen diffusion in the perfect single crystal is not fast.

As for the effect of oxygen binding and reaction, Hao *et al.* revealed the synergistic effects of water and oxygen molecule co-adsorption on the (001) surfaces of tetragonal $MAPbI_3$ using DFT calculations to uncover the possible effect of oxygen on the degradation process of $MAPbI_3$.[32] Fig. 3A shows the possible adsorption sites for water molecule or oxygen molecule co-adsorption. They found that oxygen molecules have strong interactions with the (001) surfaces of tetragonal $MAPbI_3$ through the formation of a chemical Pb–O bond on the PbI_2-terminated surface and a hydrogen bond on the MAI-terminated surface. The adsorbed oxygen molecules introduce empty states near the Fermi level of the surfaces, which can facilitate charge transfer between the surface and oxygen molecules (Fig. 3B).

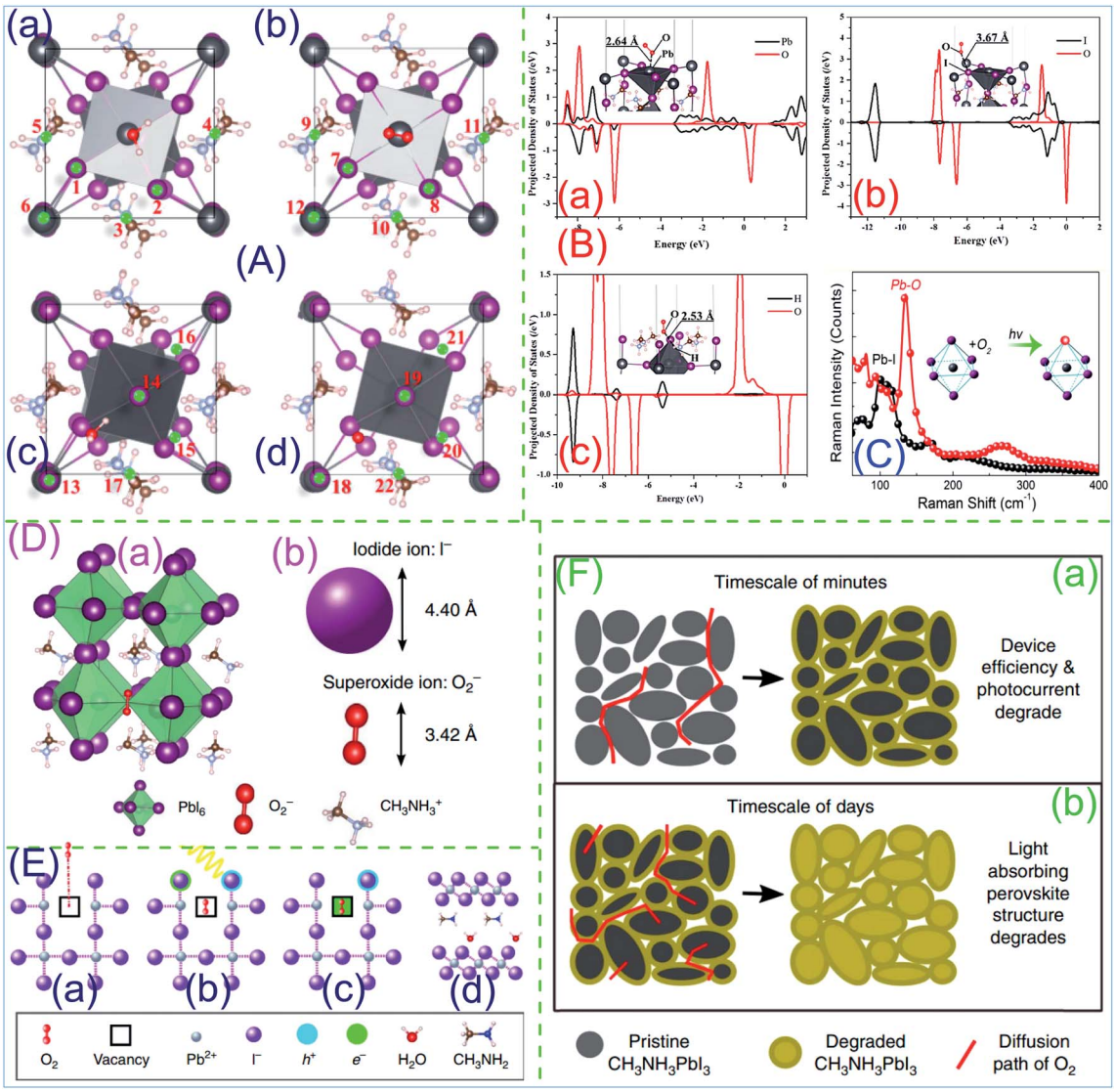

Fig. 3 (A) Possible adsorption sites for oxygen molecules. (B) Geometric structures and pDOS of an oxygen molecule at different sites on surfaces. Reprinted with permission from ref. 32. Copyright 2016 American Chemical Society. (C) Raman spectra of pristine and PbO-like $MAPbI_3$. Reprinted with permission from ref. 33. Copyright 2016 American Chemical Society. (D) Size comparison of superoxide and iodide anions. (E) Oxygen-induced photo-degradation. (F) Oxygen diffusion pathways and associated degradation regions. (a) O_2 diffusion in inter-particle regions and the initial reaction with particle surfaces on a timescale of hours leading to reduction in device efficiency, V_{oc} and photocurrent and (b) O_2 diffusion into bulk regions on a time scale of days leading to a phase change from the photo-absorbing perovskite phase into the non-absorbing lead iodide phase (yellow). Reprinted with permission from ref. 35. Copyright 2017 The Author(s).

Furthermore, when an oxygen molecule is located atop a Pb atom on the PbI_2-terminated surface, the calculated adsorption energies indicate that the surface is more attractive to water molecules, making the surface even more sensitive to humidity. These results suggest that oxygen molecules play an important role in the initial stage of the degradation of perovskite materials.

In another relevant study by Kong *et al.*, resonance Raman spectroscopy is combined with surface and bulk crystal characterization to interpret the oxygen intercalation phenomenon on the surface of $MAPbI_3$ (Fig. 3C).[33] It is found that oxygen can intercalate into the frameworks of $MAPbI_3$ with the assistance of laser excitation. By lowering down the pressure in the experimental chamber, the intercalated oxygen can be readily removed. XPS and XRD characterization results suggest that Pb–O bonds are mainly formed on the surface of $MAPbI_3$ but are constrained to avoid the formation of the PbO compound. DFT calculation supports the above conclusions. PL characterization shows that the intercalation of oxygen into $MAPbI_3$ results in evident luminescence quenching. Thus, the oxygen intercalation on the surface of $MAPbI_3$ could potentially be used as an oxygen sensor with high sensitivity and repeatability. In the work by Zhang *et al.*, the interactions between the MAI-terminated $MAPbI_3$ (110) surface and O_2 molecules in the presence of excess mobile electrons were studied by DFT calculations.[34] Their results show that molecular O_2 only weakly interacts with the perovskite surface. However, a superoxide,

which is formed from the reaction between an oxygen molecule and an excess electron, reacts readily with the perovskite surface by forming a Pb–O covalent bond with a surface Pb ion. By further introducing an excess electron, the superoxide is converted into a peroxide and the two O atoms form two covalent bonds with the surface Pb in a side-on configuration. During these processes, the local Pb–I octahedral structure disintegrates. The formation of the P–O covalent bonds can be the precursor of the PbO in the degradation products.

Although oxygen only weakly interacts with the perovskite surface and has a positive binding energy with the single crystal perovskite lattice, as mentioned above, the perovskite films in actual solar cells are mostly polycrystalline. Oxygen molecules may diffuse rapidly through the loose grain boundary zone. Haque *et al.* reported that fast oxygen diffusion and iodide defects mediate the oxygen-induced photo-degradation of PSCs (Fig. 3D–F).[35] In fact, oxygen diffusion into perovskite polycrystalline films is observed to occur remarkably fast with, for example, a typical film (500 nm thick) reaching complete saturation within 10 min (Fig. 3F). It is shown that the fast oxygen diffusion into $MAPbI_3$ films is accompanied by photo-induced formation of highly reactive superoxide species and iodide vacancies are the preferred sites in mediating the photo-induced formation of superoxide species from oxygen (Fig. 3E), as superoxide species have a smaller size than iodide ions. Also, $MAPbI_3$ polycrystalline films composed of smaller crystal grains show a higher yield of superoxide generation and a higher degradation rate than $MAPbI_3$(Cl) films with larger grains, suggesting a direct correlation between the yield of superoxide generation (and subsequently degradation rate) and perovskite crystal size and thus grain boundary density. These results suggest that oxygen diffuses rapidly in the polycrystalline perovskite with the aid of halogen vacancies and grain boundaries.

3.2 Effects of oxygen–perovskite interaction on the electronic structures and electrical properties of MHPs

Surface oxygen adsorption and bulk oxygen diffusion may lead to changes in the electronic structure and electrical properties of perovskites.[36] As for the electronic structure, Koch *et al.* addressed the effect of water, oxygen, and air exposure on $MAPbI_{3-x}Cl_x$ perovskite surface electronic properties by a comprehensive photoelectron spectroscopy (PES) study.[37] It is shown that pure oxygen exposure reduces the typically observed pronounced n-type surface character (Fig. S3A†), while pure water exposure increases it. A very low water partial pressure, *e.g.*, as encountered in inert-gas glove boxes and in a high vacuum of 10^{-6} mbar, reduces the perovskite work function due to water physisorption, which is fully reversible upon mild annealing (room temperature to 50 °C) in an ultrahigh vacuum. Upon exposure to ambient air, the effect of oxygen prevails over that of water, and the perovskite becomes less n-type as seen by a 0.6 eV Fermi level shift toward the mid-gap. The results help in understanding variations of the surface electronic properties reported for perovskites, which in turn impact the energy level alignment at heterojunctions in devices.

For electrical properties, Cahen *et al.* tracked the electronic processes in $MAPbI_3$(Cl) films *in vacuo*, and in N_2, air, and O_2, using impedance spectroscopy (IS), contact potential difference (CPD), and surface photovoltage measurements, which provides direct evidence for perovskite sensitivity to the ambient environment (Fig. S3B†).[38] A 2-orders of magnitude decrease in the film resistance upon transferring the film from an O_2-rich ambient atmosphere to vacuum was observed (Fig. S3B(b and c)†). The same change under ambient conditions also results in a 0.5 V decrease in the material work function. These results suggest that facile adsorption of oxygen onto the film dedopes it from n-type semiconductor to intrinsic semiconductor. While appearance of negative capacitance *in vacuo* or *post vacuo* N_2 exposure, indicates for the first time an electrochemical process in the perovskite (Fig. S3B(d and e)†). These effects influence any material characterization, *i.e.*, results may be ambient-dependent due to changes in the material's electrical properties and electrochemical reactivity, which can also affect material stability. These results stress the crucial importance of stringent environment control during perovskite material characterization in future studies.

The above-mentioned studies have pointed out that oxygen adsorption on the surface will lead to the change of the electronic structure and energy level of perovskites, but the theoretical blueprint of the specific mechanism behind it is still not clear.

4 Oxygen-induced defect-healing (OIDH) and photo-brightening of MHPs

The interaction between oxygen and the perovskite can not only affect the structure, stability and energy levels, but also interact with the surface and/or bulk defects of the perovskite as it adsorbs on the surface and further invades into the bulk phase of polycrystalline perovskite films, thus passivating defects on the surface, at the grain boundary and in the bulk phase and improving the PLQY. Especially, fast O_2 diffusion into $MAPbI_3$ has been proven and found to be mediated by defects as mentioned above.[35] The PLQY is usually taken as a proxy to evaluate the optoelectronic quality of halide perovskites. Higher PLQYs imply a reduction of non-radiative deactivation pathways, with long-lived and long-transported charge carriers allowing efficient charge collection at selective contacts. An interesting observation that has been repeatedly reported is a drastic PLQY enhancement upon exposure of halide perovskites to dry air or oxygen. This observation indicates that controlled exposure to oxygen or mild oxidants could lead to trap annihilation and improved solar cell performance. Interestingly, the effect can be reversible over a few cycles, which further suggests that the mechanism underlying such a behavior should be related to a fairly weak chemical interaction between O_2 and the perovskite. Impedance spectroscopy results also suggested a reversible effect of oxygen on $MAPbI_3$ electronic properties, associated with a dedoping of the material. It was also proposed that the effect of light and oxygen adsorption can significantly reduce

the density of these trap states in $MAPbI_3$. Thus, parasitic non-radiative charge carrier losses can be eliminated and the PLQY can be improved.

4.1 Oxygen-induced defect-healing effect at the grain boundaries of MHPs

The mechanism of oxygen passivation of defect states at the grain boundary was first reported compared with the surface and bulk. In 2015, inspired by an early study of the Cl-induced passivation effect of defects at CdTe grain boundaries, Yin *et al.* reported the passivation effect of Cl and O at the GBs of $MAPbI_3$ by DFT calculations (Fig. 4), considering different I positions as Cl/O substitution sites.[27] They found that the spontaneous segregation of extrinsic elements such as Cl and O can weaken the wrong bond at GBs and thus reduce the shallow trap state with a level close to the valence band maximum (VBM). As the GB state can increase the hole effective mass and act as a shallow trap state which hinders the hole diffusion, oxygen passivation of GBs may enhance the device performance of polycrystalline perovskite based solar cells. Their theoretical results provide a fundamental understanding of the oxygen passivation mechanism at perovskite GBs. However, the work does not mention any experimental observations that oxygen passivation of GB defects could improve the luminescence of the perovskite.

4.2 Oxygen-induced defect-healing effect on the surface and in the bulk phase of MHPs

4.2.1 Impact of the atmosphere on the luminescence properties of MHPs. As for the impact of the atmosphere, in 2015, Galisteo-López *et al.* reported the environmental effects on the photophysical properties of $MAPbI_3(Cl)$.[39] They demonstrated that the luminescence properties of $MAPbI_3(Cl)$ are determined by the interplay between photoinduced activation and darkening processes, which strongly depend on the atmosphere surrounding the samples. They have isolated oxygen and moisture as the key elements in each process, activation and darkening, both of which involve an interaction with photogenerated carriers. These findings show that environmental factors play a key role in the performance of lead halide perovskites as efficient luminescent materials. From the results of Fig. 5A, it is evident that the strong photo-darkening is mainly due to the presence of moisture in the atmosphere surrounding the samples when the sample is illuminated in air. Furthermore, from the results in Fig. 5B, it can be seen that the photo-darkening during illumination in air is partially reversible when the sample is placed in O_2 at a later time. They also noted that such recovery upon changing the atmosphere from air to O_2 demands illumination, that is, it is a photoactivated process.

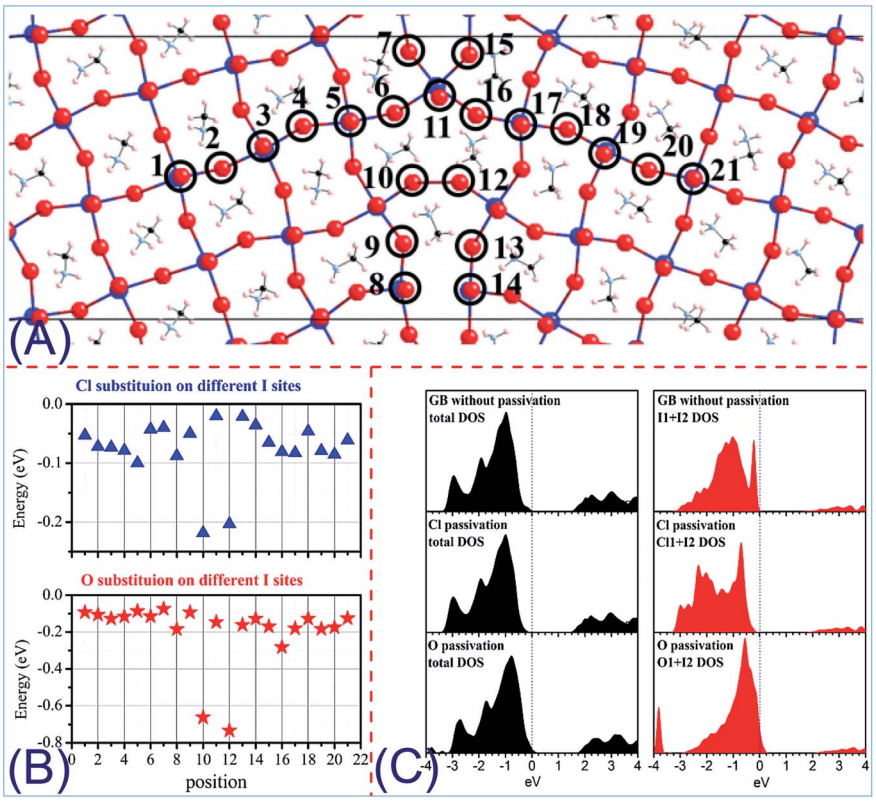

Fig. 4 (A) Different I positions considered as Cl/O substitution sites in $MAPbI_3$ Σ5(310) GBs. (B) The relative total energies when Cl/O substitutes on different I sites in (A). The unsymmetrical behavior is attributed to the random orientations of the CH_3NH_3 molecule. (C) Total DOS and partial DOS at wrong bonds of unpassivated, Cl-passivated and O-passivated $MAPbI_3$ Σ5(310) GBs. Reprinted with permission from ref. 27. Copyright 2015 Wiley-VCH.

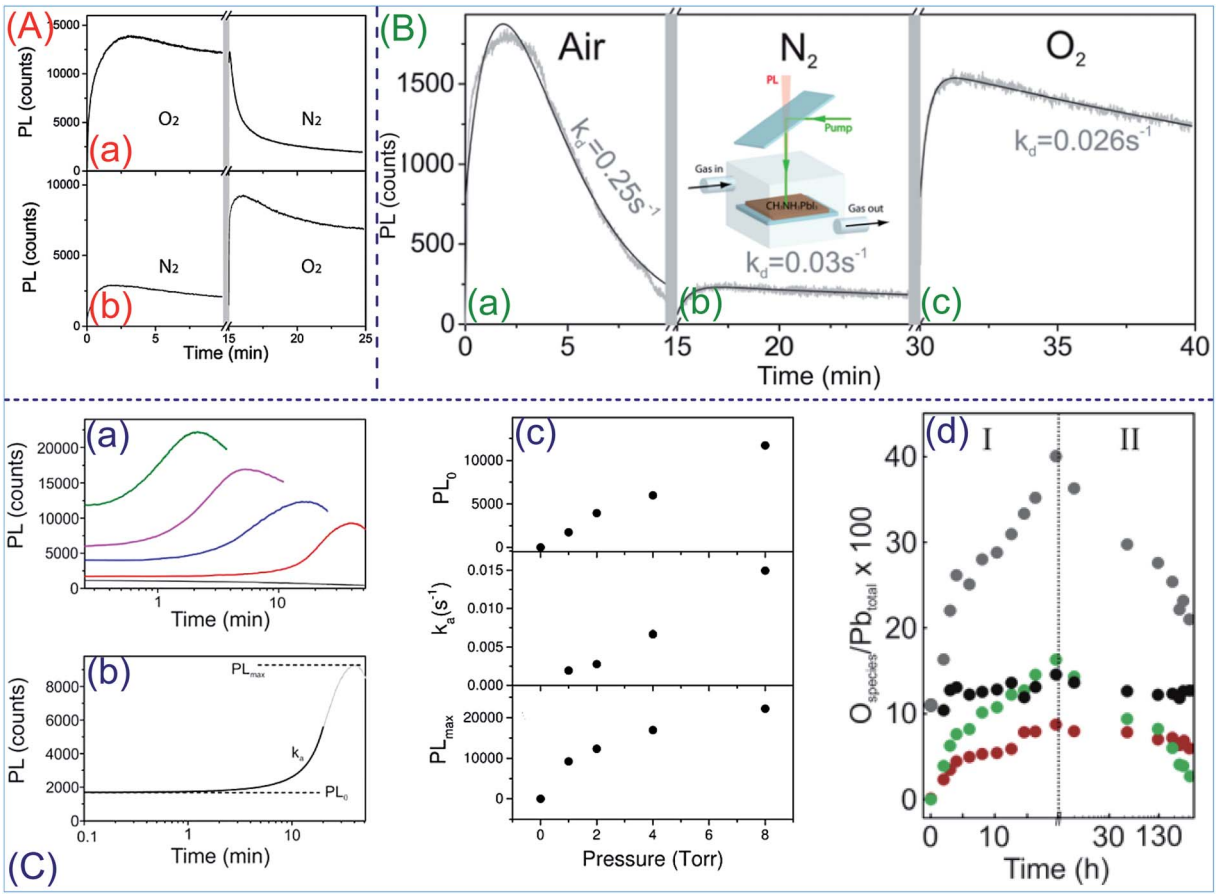

Fig. 5 Environmental effects on the photo-physics of $MAPbI_3$ perovskite: (A) dynamics of the PL maximum under constant pumping conditions for bulk $MAPbI_{3-x}Cl_x$ under different atmospheric conditions. (a) Passing an O_2 flux followed by a N_2 one. (b) Passing a N_2 flux followed by an O_2 one. (B) Evolution of the PL maximum with the sample exposed to different atmospheres. Reprinted with permission from ref. 39. Copyright 2015 American Chemical Society. (C) Origin of light-induced photophysical effects in $MAPbBr_3$ perovskites in the presence of oxygen: time evolution of the PL of a $MAPbBr_3$ film under different O_2 pressures: 0.75×10^{-8} (black), 1 (red), 2 (blue), 4 (magenta), and 8 Torr (green curve) (a). Characteristic PL activation curve (gray line) indicating the initial (PL_0) and maximum PL (PL_{max}) and the PL activation constant (k_a) (b). The black curve represents the exponential growth fit. The evolution of these parameters with O_2 pressure are shown in (c) for k_a, PL_{max}, and PL_0. Evolution of the O_{total}/Pb_{total} (gray circles), H_2O/Pb_{total} (black circles), O_2^-/Pb_{total} (red circles), and O_2^-/Pb_{total} (green circles) atomic ratios for the whole experiment (d). Reprinted with permission from ref. 40. Copyright 2018 American Chemical Society.

After that, to further reveal the origin of light-induced photophysical effects in MHPs in the presence of oxygen, they presented a combined study of the evolution of both the photoluminescence and the surface chemical structure of $MAPbBr_3$ perovskite as the environmental oxygen pressure rises from ultrahigh vacuum up to a few thousandths of an atmosphere (Fig. 5C).[40] They found direct evidence of the formation of a superficial layer of negatively charged oxygen species capable of repelling the halogen anions away from the surface and toward the bulk. The reported PL transient dynamics, the partial recovery of the initial state when photoexcitation stops, and the eventual degradation after intense exposure times can thus be rationalized. These findings can help understand better the fundamental optically induced chemical processes that occur in these semiconductors.

In addition to the study of the effect of the atmosphere on the luminescence properties of perovskite films, Scheblykin *et al.*, then, found that light curing $MAPbI_3$ perovskite crystals with oxygen can boost the PL yield by a thousandfold and mechanistic insights into such a light-induced PL enhancement effect have been put out.[41] They found the PL intensity to increase up to three orders of magnitude upon light illumination with an excitation power density of 0.01–1 W cm^{-2} (Fig. 6A). The PL enhancement is accompanied by an increase of the PL lifetime from several nanoseconds to several hundred nanoseconds and also by an increase of the initial amplitude of the PL decay. The PL enhancement can be reversed by switching on/off the excitation light or switching the atmosphere between oxygen and nitrogen (Fig. 6B), while only a small PL enhancement was observed for the sample placed in a vacuum. So, it is concluded that the major contribution for the PL enhancement comes from a photo-induced reaction in $MAPbI_3$ involving oxygen. They proposed a model where the trapping sites responsible for non-radiative charge recombination can be deactivated by a photochemical reaction involving oxygen (Fig. 6C). The reaction zone is spatially limited by the excitation

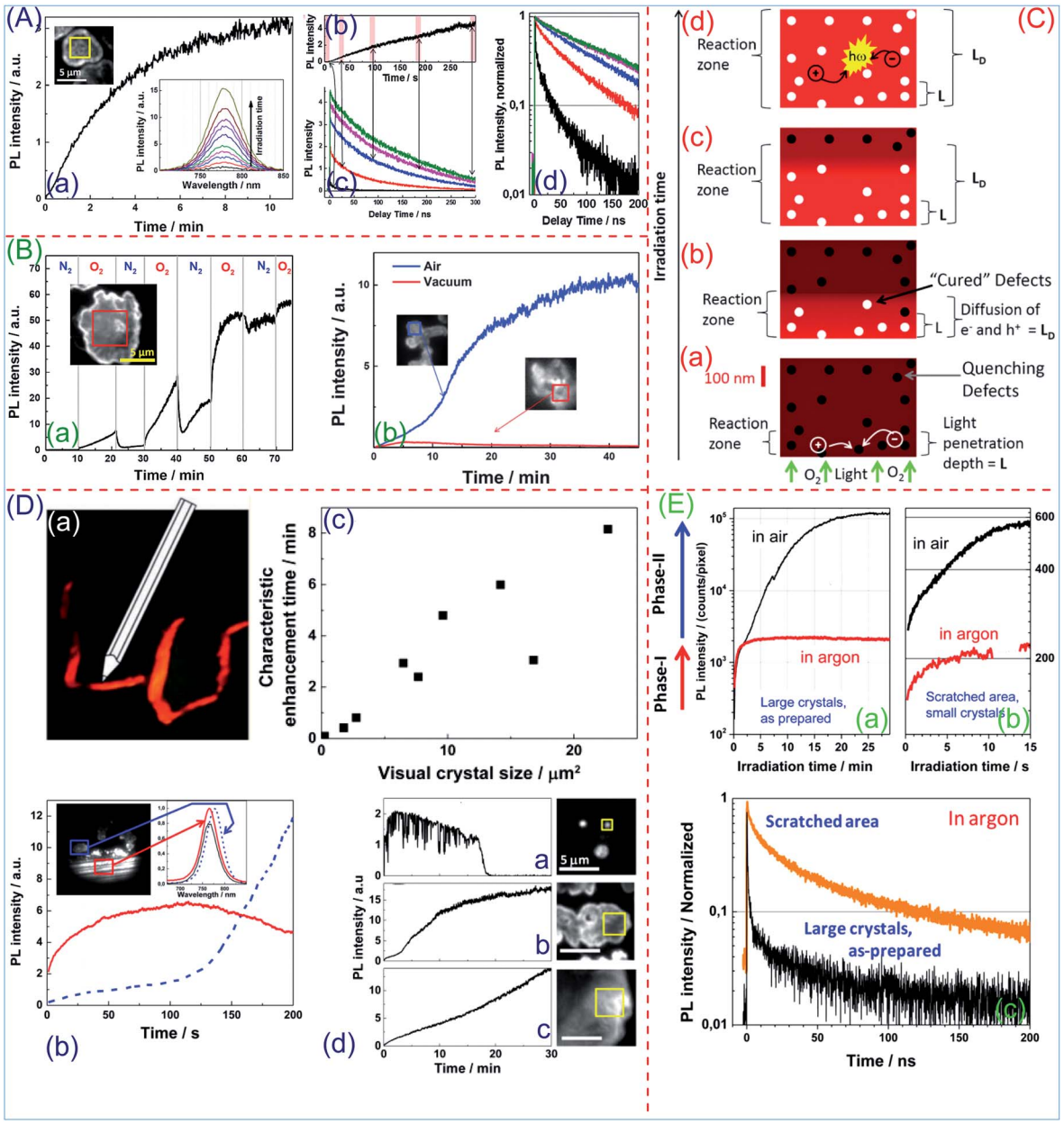

Fig. 6 Light curing with oxygen enhances the PL of $MAPbI_3$ crystals: (A) PL intensity of $MAPbI_3$ crystals upon light irradiation for 11 minutes (a). The inset shows the PL image and selected area where the PL light was collected. The PL decay and PL steady-state intensity as a function of light irradiation time: a PL enhancement trace upon light irradiation (b) and the corresponding PL dynamics (c) through the enhancement process measured at the indicated times (the data in (b) and (c) were obtained in one experiment; the intensity units are the same). The same data on a logarithmic scale (d). (B) The atmosphere effect on the PL enhancement of $MAPbI_3$ (a) and PL enhancement of $MAPbI_3$ films in air and in a vacuum (b). Propagation of the light-curing reaction to the interior of the crystal (C). Reprinted with permission from ref. 41. Copyright 2015 Royal Society of Chemistry. PL enhancement of nanosized defect-free $MAPbI_3$ crystallites: (D) enhanced PL of a mechanically scratched $MAPbI_3$ film prepared on glass (a). Light-induced PL enhancement of the scratched part (red line) and untreated part (blue dashed lines) of the same film (b). Correlation between the characteristic enhancement time (time to reach $(1 - 1/e) = 0.63$ of the saturation intensity) and the visual crystal size (c) and PL intensity traces of $MAPbI_3$ crystallites of different sizes: 1 small, 2 middle, and 3 large (d). (E) PL enhancement of large (a) and small (b) perovskite crystals in ambient air and in argon. Normalized PL kinetics of the as-prepared micrometer-sized crystals and scratched area (<100 nm grains) of the sample in argon (c). Reprinted with permission from ref. 42. Copyright 2015 American Chemical Society.

light-penetration depth and diffusion length of the charge carriers. The latter increases in the course of the light-curing process making the reaction zone spread from the surface towards the interior of the crystal. The PL enhancement can be reversed by switching on/off the excitation light or switching the atmosphere between oxygen and nitrogen. Soon after, they investigated the visible light induced PL enhancement of $MAPbI_3$ crystals with different grain sizes using PL microscopy and super-resolution optical imaging. It is found that the PL of ~100 nm crystals enhances much faster than that of larger,

micrometer-sized ones (Fig. 6D and E). This crystal-size dependence of the photochemical light passivation of charge traps responsible for PL quenching suggests that traps are present in the entire crystal volume rather than at the surface only. Because of this effect, "dark" micrometer-sized perovskite crystals can be converted into highly luminescent smaller ones just by mechanical grinding (Fig. 6D).[42]

The excitation intensity is also a variable that greatly affects the luminescence properties of perovskites. Petrozza *et al.* investigated the photoinduced emissive trap states in lead halide perovskite semiconductors by investigating the luminescence properties of polycrystalline $MAPbBr_3$ films as a function of the excitation density and the environment (Fig. 7).[43] It is found that, in an inert environment, photoinduced formation of emissive sub-band gap defect states occurs, independently of the chemical composition of the lead halide semiconductor, which quenches the band-to-band radiative emission (Fig. 7C). Carrier trapping occurs in the subnanosecond time regime, while trapped carriers recombine in a few microseconds. The relative PLQY and time trace of integrated PL (Fig. 7A(a and b)) suggest that oxygen is the main active agent in the enhancement of PL. The microscopy maps shown in Fig. 1 provide further visualization of this effect (Fig. 7C(c and d)). The changes in the PL spectrum when increasing (Fig. 7B(a)) and then decreasing (Fig. 7B(b)) the excitation density in a range between 10^{15} and 10^{17} cm^{-3} reveal the presence of a broad emission band centered at around 600 nm. This broad sub-band gap emission can be strongly quenched within a few seconds when exposed to air, while the band-to-band emission recovers its intensity (Fig. 7B(c and d)). The presence of oxygen, even in a very small amount, is able to compensate for such an effect, improving the PLQY. The relative PLQY of the low-energy band as a function of the excitation density shown in Fig. 7B(e) confirms that this new emission band originates from emissive trap states. Further study of $MAPbI_3$ and $CsPbBr_3$ polycrystalline thin films presents the same trends. This work only gives a preliminary model of oxygen defect induced passivation (Fig. 7C), while a combination of deeper theoretical and experimental investigations to rationalize such an observation is still needed.

Among these published studies, only preliminary models of oxygen passivation were proposed by discussing the

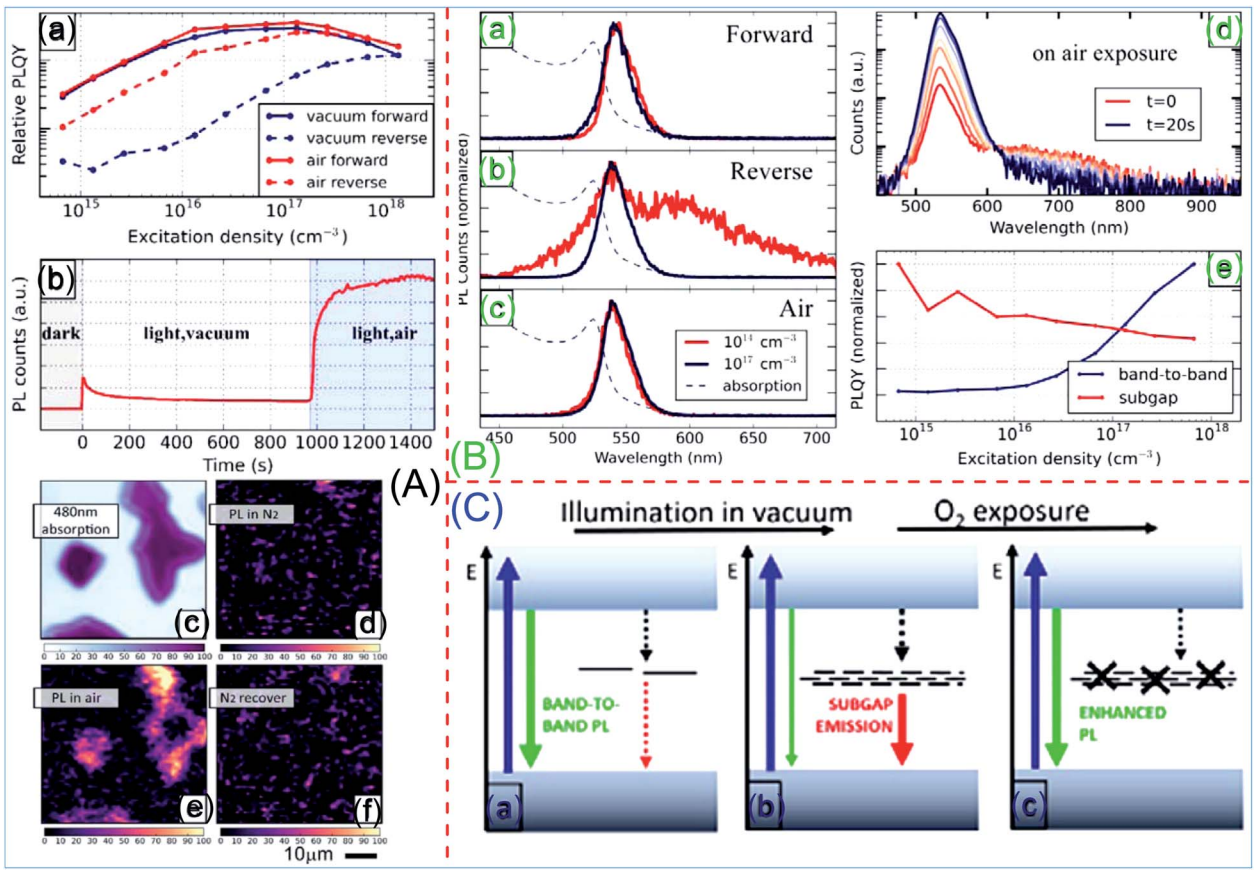

Fig. 7 (A) Relative PLQY curves of $MAPbBr_3$ polycrystalline thin films in air (red) and active vacuum (blue), recorded with increasing (solid lines) or decreasing (dashed lines) excitation densities (a). Time trace of integrated PL under illumination in a vacuum, where excitation light is unblocked at $t = 0$ and the sample is exposed to ambient air at $t = 1000$ s (b). Transmission (taken at 480 nm) (c) and (d–f) PL maps of $MAPbBr_3$ isolated crystallites on glass under a N_2 flow and air. (B) PL spectra of $MAPbBr_3$ at low (red) and high (blue) excitation densities in (a) forward and (b) reverse orders. (c) PL spectra after air exposure. (d) Evolution in time of PL spectra during air exposure. (e) Relative PLQY from 500 to 580 nm (blue) and from 630 to 850 nm (red). (C) Inert environment photoinduced formation of emissive sub-band gap defect states and their oxygen induced passivation. Reprinted with permission from ref. 43. Copyright 2016 American Chemical Society.

luminescence dynamics of perovskite and the change of its parameters with the external environment. As for the specific interaction between oxygen and defects in perovskite with respect to the underlying passivation mechanism, the current work is not involved. Especially, it has been shown that O_2 molecules may only weakly interact with non-defective $MAPbI_3$, with O_2 incorporation into the perovskite lattice being endothermic by 0.17 eV. Fast O_2 diffusion into $MAPbI_3$ was recently proven and found to be mediated by defects. However, how does O_2 boost the PLQY in lead halide perovskites is still not clear. The following studies will give the answers.

4.2.2 Oxygen passivation of halogen vacancies: effect of the oxidation state of halogen vacancies. For high-performing optoelectronic device application, polycrystalline perovskite films are still limited by nonradiative losses due to charge carrier trap states that can be affected by illumination. Li *et al.* revealed the oxidation state of halogen vacancy controlled charge recombination in $MAPbI_3$ using *ab initio* nonadiabatic molecular dynamics (Fig. 8A–C).[44] It is demonstrated that charge recombination in PSCs depends strongly on the oxidation state of the halogen vacancy, which constitutes the most common type of defect due to its low formation energy. Fig. 8A and B present the optimized structures and the projected density of states (pDOS) of the considered $MAPbI_3$ with neutral (I_V), anion (I_V^{+1}) and cation (I_V^{-1}) iodine vacancies, respectively. Specifically, a missing iodine anion (I_V^{+1}) in $MAPbI_3$ has almost no effect on charge losses as it creates no trap states. In fact, it can be beneficial to the performance because it causes minor changes to the charge carrier lifetime, while increasing the charge carrier concentration. The neutral iodine vacancy (I_V) acts as an electron donor, creates a hole trap near the conduction band (CB), increases nonadiabatic electron–phonon coupling, and accelerates charge recombination by a factor of 5. However, when the vacancy is reduced, the recombination is accelerated by up to 2 orders of magnitude. The doubly reduced vacancy accelerates the recombination by a factor of 50. Fig. 8C

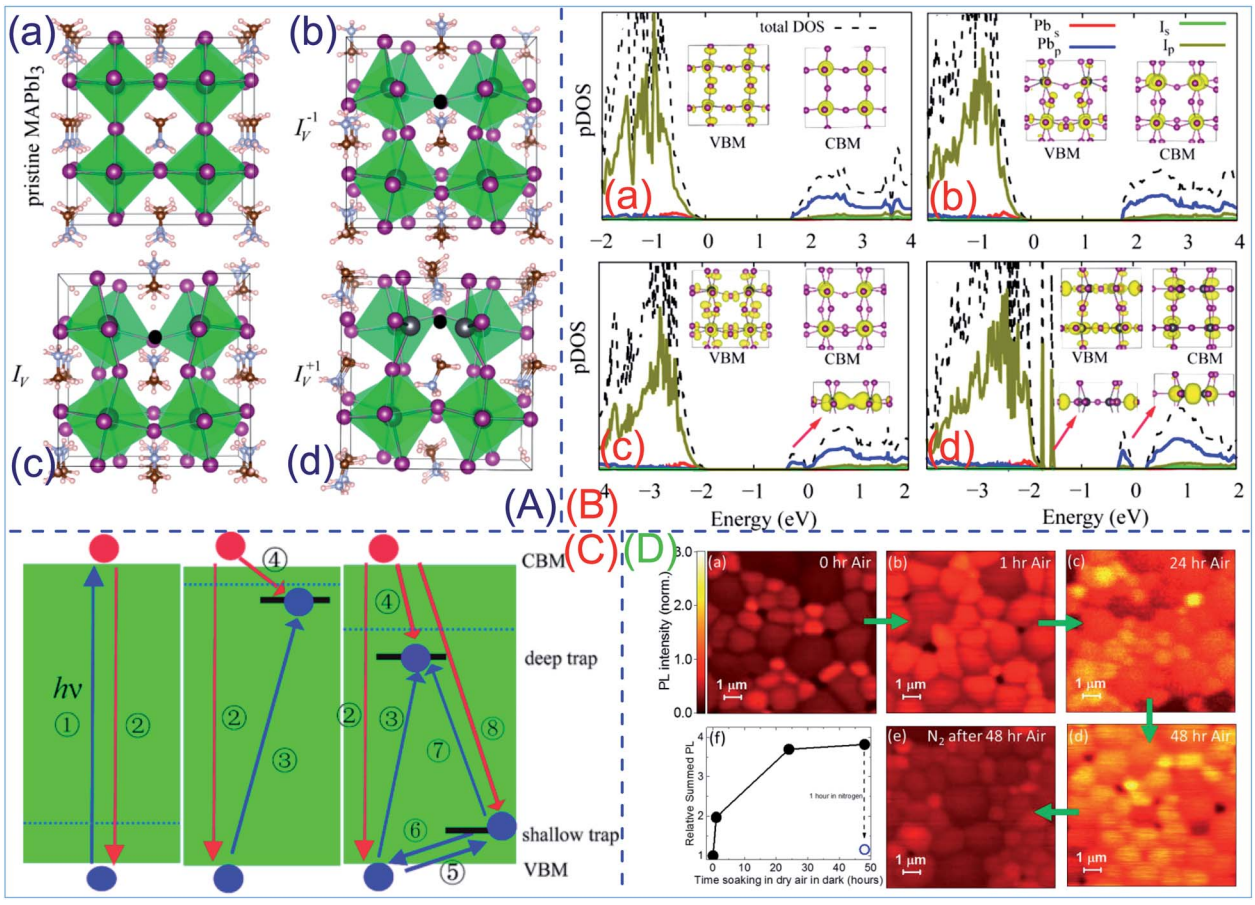

Fig. 8 (A) Optimized structures of (a) pristine $MAPbI_3$, and $MAPbI_3$ with (b) I_V^{-1}, (c) I_V and (d) I_V^{+1} defects. (B) pDOS for (a) pristine $MAPbI_3$, and $MAPbI_3$ with (b) I_V^{-1}, (c) I_V and (d) I_V^{+1} defects. Investigated charge carrier trapping, detrapping and relaxation processes in pristine and $MAPbI_3$ with (b) I_V^{-1}, (c) I_V and (d) I_V^{+1} defects. (C) Charge carrier trapping, detrapping and relaxation processes in pristine $MAPbI_3$ and $MAPbI_3$ with different iodine vacancies. Reprinted with permission from ref. 44. Copyright 2018 American Chemical Society. (D) Confocal PL map of $MAPbI_3$ films prepared in a nitrogen glove box and maps acquired (a) in dry nitrogen, and in dry air after (b) 1 hour, (c) 24 hours and (d) 48 hours in dry compressed air. (e) A film stored for 48 hours in dry air but then measured in dry nitrogen after 1 hour storage in dry nitrogen, suggesting that the oxygen pre-soaking (loading) effects can be removed. The map intensities are given relative to the maximum value in (a), which is normalized to 1. (f) Total summed intensity of each map relative to the summed intensity of (a), which is normalized to 1. The blue symbol corresponds to the map in (e). Reprinted with permission from ref. 45. Copyright 2018 Wiley-VCH.

presents the charge carrier trapping, detrapping and relaxation processes in pristine $MAPbI_3$ and $MAPbI_3$ with different iodine vacancies: ① formation of electrons and holes *via* photoexcitation across the band gap; ② nonradiative electron–hole recombination between the conduction band minimum (CMB) and valence band maximum (VBM), bypassing traps; ③ and ⑤ capture of a hole by a trap state in I_V and I_V^{+1}; ④ and ⑧ recombination of trapped holes with electrons in the CBM (trap-assisted recombination) in I_V and I_V^{+1}; ⑥ detrapping of holes by excitation from the shallow trap to the CBM in I_V^{+1}; ⑦ decay of trapped holes from the shallow trap to the deep trap. The blue (red) ball refers to a hole (electron). The dashed lines denote the Fermi level. These results indicate strongly that the conditions of synthesis and operation of perovskite materials should be carefully controlled to suppress the formation of neutral iodine and iodine cation vacancies, in order to optimize the material performance.

In the work by Stranks *et al.*, *in situ* micro-PL measurements are used to elucidate the impact of light-soaking individual $MAPbI_3$ grains in high-quality polycrystalline films while exposing them to different atmospheric environments (Fig. 8D).[45] It is shown that emission from each grain depends sensitively on both the environment and the nature of the specific grain, *i.e.*, whether it shows good (bright grain) or poor (dark grain) luminescence properties. It is found that the dark grains show substantial increases in emission, while the bright grain emission is steady when illuminated in the presence of oxygen and/or water molecules. DFT calculations reveal strong adsorption energies of the molecules to the perovskite surfaces. It is also found that oxygen molecules bind particularly strongly to surface iodide vacancies which, in the presence of photoexcited electrons, lead to efficient passivation of the carrier trap states that arise from these vacancies (Fig. S4†). This work reveals a unique insight into the nature of nonradiative decay and the impact of atmospheric passivation on the microscale properties of perovskite films.

Mixed-halide perovskites (M-MHPs), such as $MAPb(Br_xI_{1-x})_3$, are very promising candidates for tandem solar cells and wavelength-tunable light-emitting diodes (LEDs) with their tunable band gaps. However, uniform M-MHPs undergo

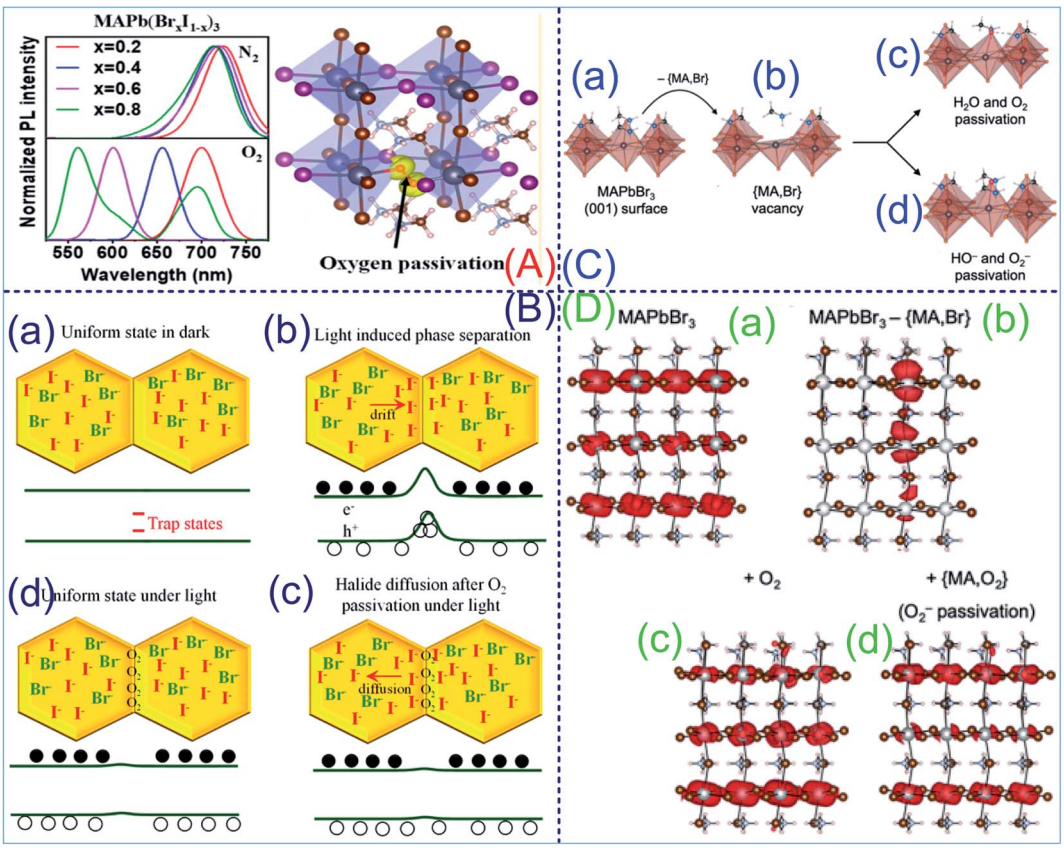

Fig. 9 (A) Oxygen passivation suppressed light-induced phase separation of $MAPb(Br_xI_{1-x})_3$. (B) Schematics of the reversion of phase separation in $MAPb(Br_xI_{1-x})_3$ due to O_2 passivation. (a) Uniform state in the dark, (b) light-induced phase separation caused by the trapped charges at the surface, (c) iodide diffusion back to the bulk due to the concentration gradient, and (d) uniform state under light. Reprinted with permission from ref. 46. Copyright 2019 American Chemical Society. Oxygen passivation of $MAPbBr_3$: (C) top layer of the pristine $MAPbBr_3$ (001) surface (a). The same as a missing (MA, Br) pair (b). Passivation of the defect by a neutral molecule (H_2O or O_2) (c). Passivation by an anionic molecule (HO^- or O^{2-}) (d). Pb, Br, O, N, C, and H atoms are depicted in gray, orange, red, blue, black, and pale pink, respectively. (D) The partial charge density computed at the CBM of the (001) surface of pristine $MAPbBr_3$ (a) and with (MA and Br) vacancies (b), and passivated by O_2 (c) or O^{2-} (d). Reprinted with permission from ref. 47. Copyright 2019 American Chemical Society.

phase separation under visible light irradiation or an electric field, and the reason is still under debate. Xiao *et al.* found that the phase separation can be dramatically suppressed by oxygen passivation under light illumination (Fig. 9A).[46] Also, phase-separated M-MHPs can be recovered to their original uniform state in an oxygen environment. Theoretical calculations demonstrate that oxygen atoms can effectively passivate traps in M-MHPs and occupy halogen vacancies, thus suppressing halogen redistribution and phase separation. A model was proposed to explain the suppression and recovery of phase separation of M-MHP films in O_2 under light illumination as shown in Fig. 9B: under light illumination, the trapped charges cause band bending and the generated electric field causes halogens, most likely iodide ions, drift to the crystal surface (Fig. 9B(b)). Oxygen can passivate the surface traps, so that the band bending near the surface can be reduced (Fig. 9B(c)). Therefore, the accumulated iodide ions are expected to diffuse back to the bulk due to the concentration gradient (Fig. 9B(d)), resulting in uniform M-MHP films under light illumination.

As a simplified case of M-MHP, Che *et al.* reported charge trap formation and passivation in $MAPbBr_3$.[47] It is proposed that the quenching and revival of surface photoluminescence properties are due to the formation and passivation of surface charge traps (Fig. 9C and D). Moreover, they established that bulk properties are preserved either because molecules are unlikely to penetrate the bulk or because they do not interfere with the electronic states involved in the optical properties. For pristine $MAPbBr_3$, the partial charge densities computed at the gap edges show states delocalized on all octahedra (Fig. 9D(a)). When a defect is created at the $MAPbBr_3$ surface, in the form of a bromide vacancy, a striking evolution occurs on the distribution of the conduction band minimum (CBM, Fig. 9D(b)). Similar defect passivation behaviors are observed in the case of O_2 and the superoxide O_2^- (Fig. 9D(c and d)): O_2 shows only partial passivation of the Pb* dangling bond (Fig. 9D(c)), whereas O_2^- exhibits complete passivation with both pDOS and charge densities pointing to a fully recovered CBM.

A similar case can be found in the triple-cation perovskite ($FA_{0.79}MA_{0.15}Cs_{0.06}Pb(I_{0.85}Br_{0.15})_3$) system. In the study by Szemjonov *et al.*, the issue of how iodide vacancies and O_2 molecules influence the local geometry and electronic structure as well as the stability properties was examined (Fig. 10).[48] Many calculations on the energetics at various lattice and vacancy sites in the $MAPbI_3$ structure have found that the iodide vacancy is the most favorable for O_2 and superoxide species. The insertion of O_2 into a vacancy is shown in Fig. 10A. In the lowest energy configuration, the O_2 species is inclined with respect to the Pb–I–Pb axis, in which both of the oxygen atoms bond to an adjacent Pb atom (Fig. 10B). Their calculations show that the introduction of O_2 passivates iodide vacancy induced gap states (Fig. 10D) in $FA_{0.79}MA_{0.15}Cs_{0.06}Pb(I_{0.85}Br_{0.15})_3$, resulting in enhanced luminescence efficiency (Fig. 10C).

As for the influence of oxygen passivation on the carrier recombination and stability of perovskite, Long *et al.* systematically studied the effect of oxygen, superoxide and peroxide passivation on the carrier dynamics and stability of $CsPbBr_3$ and $MAPbI_3$ based on time-domain *ab initio* analysis.[49] Previous experiments have shown that excess lead atoms accelerate charge recombination while oxygen passivation can heal the

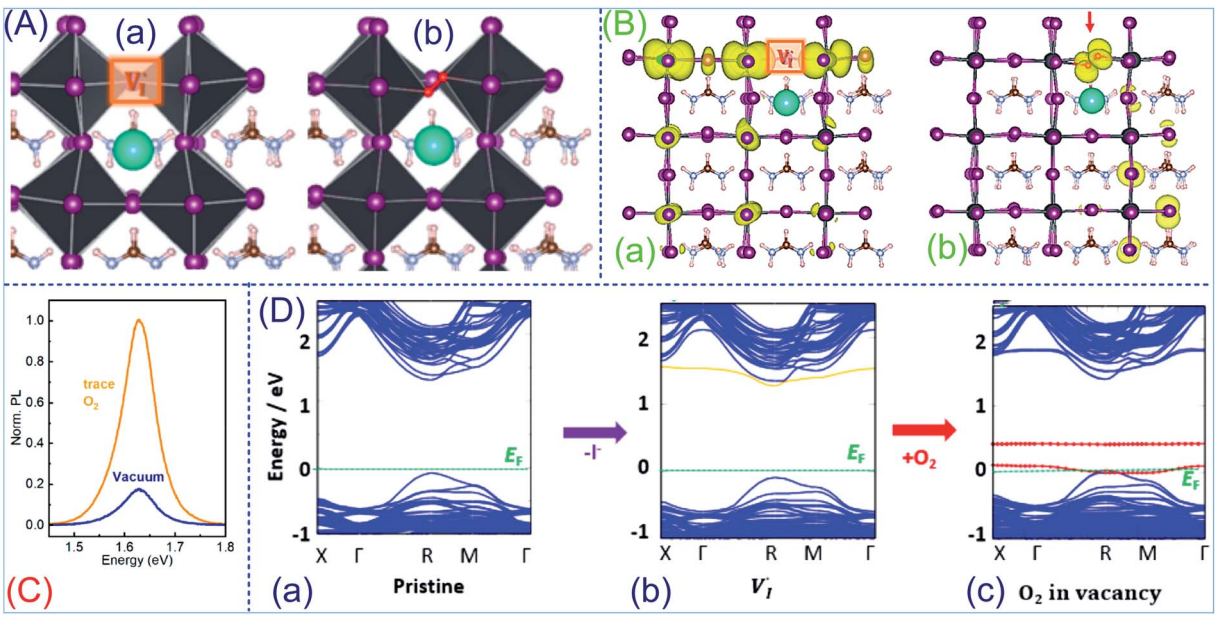

Fig. 10 (A) Local structure of $FA_{0.85}MA_{0.11}Cs_{0.04}PbI_3$ (a) around the iodide vacancy (V_I) site. (b) V_I occupied by an O_2 molecule. (B) Band-decomposed charge density of $FA_{0.85}MA_{0.11}Cs_{0.04}PbI_3$: (a) iodide vacancy (orange box); (b) O_2 molecule occupying the iodide vacancy (indicated with a red arrow). (C) PL measurements taken under trace oxygen conditions and under high vacuum (10^{-6} mbar). (D) Band structures: (a) pristine $FA_{0.85}MA_{0.11}Cs_{0.04}PbI_3$, (b) with an iodide vacancy, and (c) with an O_2 species occupying the iodide vacancy. Reprinted with permission from ref. 48. Copyright 2019 American Chemical Society.

defects and enhance the solar cell efficiency. It is found here that the surface Pb-dimer passivated by molecule oxygen can notably suppress charge recombination in $CsPbBr_3$ perovskite. They also demonstrated that an excess lead atom forms a Pb-dimer with a single surface lead atom of $CsPbBr_3$ (001) surface and creates a deep hole trap.[50] The electron–hole recombination is accelerated to over 10 ps *via* fast hole trapping or bypassing the hole trap compared to pristine $CsPbBr_3$, occurring in tens of picoseconds. The Pb-dimer passivated with oxygen molecules forms Pb–O bonds, breaks the Pb-dimer, and removes the trap state (Fig. S5A and B†), leading to a decrease in the recombination and extending excited-state lifetime to over 100 ps. This work advances our understanding of the excited-state dynamics of all-inorganic perovskites in the presence of excess lead and oxygen atmosphere.

In another study, they found that while superoxide/peroxide chemistry extends the charge carriers' lifetime, it undermines the chemical stability of $MAPbI_3$ when exposed to oxygen, simultaneously.[49] Combined nonadiabatic molecular dynamics simulations and time-domain *ab initio* DFT calculations have shown that superoxide and peroxide are the common forms of oxygen interacting with $MAPbI_3$ and that oxygen most readily interacts with iodine vacancies on the perovskite surface. They establish that the iodine vacancy decreases charge carrier lifetimes, because it localizes both electrons and holes, increasing their overlap. By passivating the vacancy, the oxygen species separate electrons and holes and increase the lifetimes by more than an order of magnitude. The pDOS is shown in Fig. S5C.† It is important that neither the I_V system nor the doped structures exhibit midgap states. From Fig. S5D,† the positively charged I_V contains no midgap states as well. Midgap states appear only when the vacancy is strongly reduced, corresponding to the removal of the I^+ cation. Similarly, to I_V, strongly reduced versions of the O_2-doped and O-doped I_V systems also contain midgap states.

4.2.3 Oxygen–halogen interstitial interaction and reversible oxygen passivation of MHPs. In view of the drastic PLQY enhancements upon exposure of perovskites to oxygen molecules and the reversible trap passivation by oxygen molecules reported, Angelis *et al.* proposed a mechanism based on DFT modeling whereby oxygen effectively inactivates deep hole traps associated with iodide interstitials by forming moderately stable oxidized products (Fig. 11A).[51] The small energy gain associated with trap passivation is in agreement with the reversibility of the process. The interaction of O_2 with negative interstitial iodine leads to the formation of coordinated IO^-, IO_2^-, and IO_3^- in the perovskite lattice with their thermodynamic ionization levels and calculated structures. Iodide oxidation on the surface is calculated to be exothermic by ~0.6–0.9 eV, compared to the ~0.1 eV endothermic reaction calculated for the bulk. He *et al.* unraveled the effects of the oxidation state of interstitial iodine and oxygen passivation on charge trapping and recombination in $MAPb_3$ perovskite by a time-domain *ab initio* study (Fig. 11B).[52] They show that electron–hole recombination in perovskites strongly depends on the oxidation state of interstitial iodine and oxygen passivation. The negative interstitial iodine delays charge recombination by a factor of 1.3. The deceleration is attributed to the fact that the interstitial iodine anion forms a chemical bond with its nearest lead atoms, eliminates the trap state, and decreases the

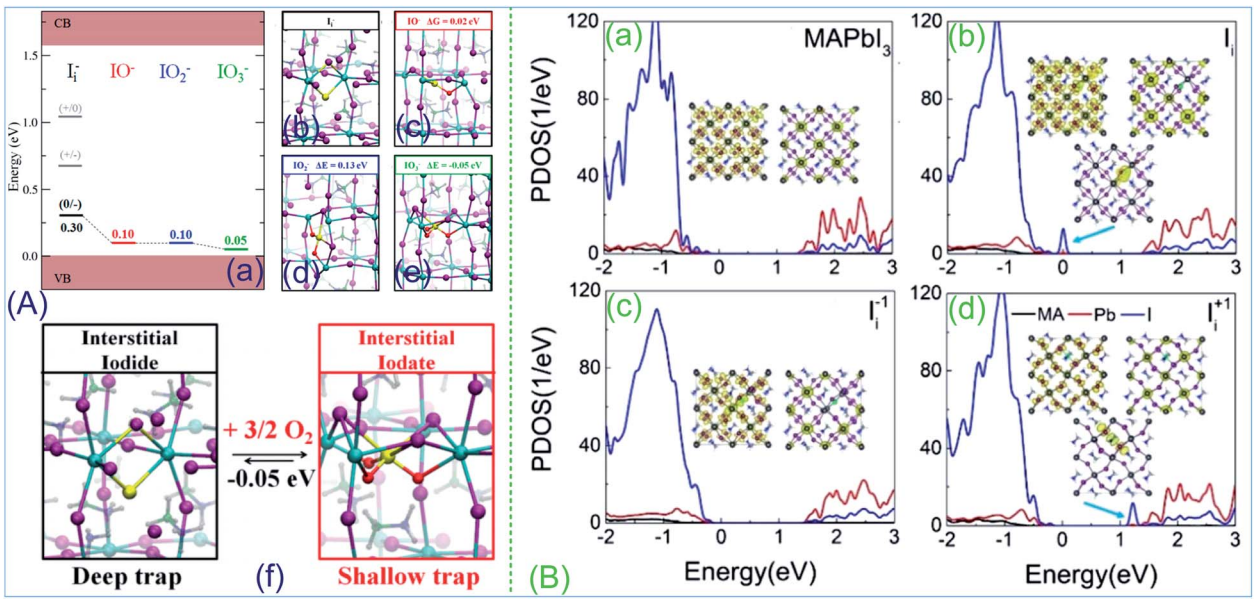

Fig. 11 (A) Thermodynamic ionization levels at the HSE06-SOC level for I_i^- (a); (b–e) structure of I_i^- and of its interaction products with 1/2 O_2, O_2, and 3/2 O_2 along with the calculated energetics (ΔE, eV). Atom color code: yellow, I_i; purple, I; red, O; light blue, Pb. The oxidation of interstitial iodine inactivates a source of deep traps with levels located in the $MAPbI_3$ band gap (f). Reprinted with permission from ref. 51. Copyright 2017 American Chemical Society. (B) PDOSs of (a) pristine $MAPbI_3$, (b) I_i, (c) I_i^- and (d) I_i^+ systems. The insets show the charge densities of the key electronic states involved in the charge trapping and recombination. Reprinted with permission from ref. 52. Copyright 2019 Royal Society of Chemistry.

nonadiabatic electron–phonon coupling. The positive interstitial iodine attracts its neighboring lattice iodine anions, resulting in the formation of an I-trimer and producing an electron trap. Electron trapping proceeds on a very fast timescale, tens of picoseconds, and captures the majority of free electrons available to directly recombine with free holes while inhibiting the recombination of free electrons and holes, delaying the recombination by a factor of 1.5. However, the positive interstitial iodine easily converts to a neutral iodine defect by capturing an electron, giving rise to a singly occupied state above the valence band maximum and acting as a hole trap.

In addition to these established achievements and consensus, there are also some disputes. Recently, Sienkiewicz *et al.* reported the differential response of the photoluminescence and photocurrent of polycrystalline $MAPbI_3$ and $MAPbBr_3$-based gas-sensing elements to exposure to oxygen and nitrogen (Fig. 12A).[53] Specifically, they found that under exposure to O_2 the PL responses of $MAPbI_3$ and $MAPbBr_3$ were markedly opposite (Fig. 12B and C); *i.e.*, the PL decreased for $MAPbI_3$, whereas it increased for $MAPbBr_3$. In contrast, under the exposure to N_2, the PL of $MAPbI_3$ increased, while it decreased for $MAPbBr_3$. A considerably differential behavior was also found for the PC responses. In particular, under recurrent exposures to both gaseous media, the PL and PC responses of $MAPbBr_3$ correlated, whereas for $MAPbI_3$ they anticorrelated. In conclusion, the distinctly opposite PL and PC responses of polycrystalline deposits of $MAPbI_3$ and $MAPbBr_3$ to O_2 and N_2 reported herein point to markedly contrasting properties of the surface carrier traps and defects for these two MHPs. The proposed schematic interpretation of the mechanisms underlying the diversified PL responses of the polycrystalline deposits of $MAPbI_3$ and $MAPbBr_3$ under exposure to light and O_2, as observed in this study, is shown in Fig. 12D. This work suggests that MHPs with different halogens can function as a differential gas detector due to their differential responses to exposure to O_2 or N_2.

All-inorganic cesium lead halide perovskites have been emerging as promising semiconductor materials for next-generation optoelectronics. Brovelli *et al.* revealed the role of nonradiative defects and environmental oxygen in exciton recombination processes in $CsPbBr_3$ perovskite nanocrystals (NCs) (Fig. 13).[54] They conducted spectro-electrochemical (SEC) experiments together with oxygen sensing measurements on $CsPbBr_3$ NCs for the first time (Fig. 13A(a)). They showed that the application of EC potentials controls the emission intensity by altering the occupancy of defect states without degrading the NCs (Fig. 13A(b and c)). Reductive potentials lead to strong (60%) emission quenching by trapping of photogenerated holes, whereas the concomitant suppression of electron trapping is nearly inconsequential to the emission efficiency. Consistently, oxidizing conditions result in minor (5%) brightening due to suppressed hole trapping, confirming that electron traps play a minor role in nonradiative decay. This behavior is rationalized through a model that links the occupancy of trap sites with the position of the NC Fermi level controlled by the EC potential (Fig. 13B(e)). Photoluminescence measurements in a controlled atmosphere reveal strong quenching by collisional

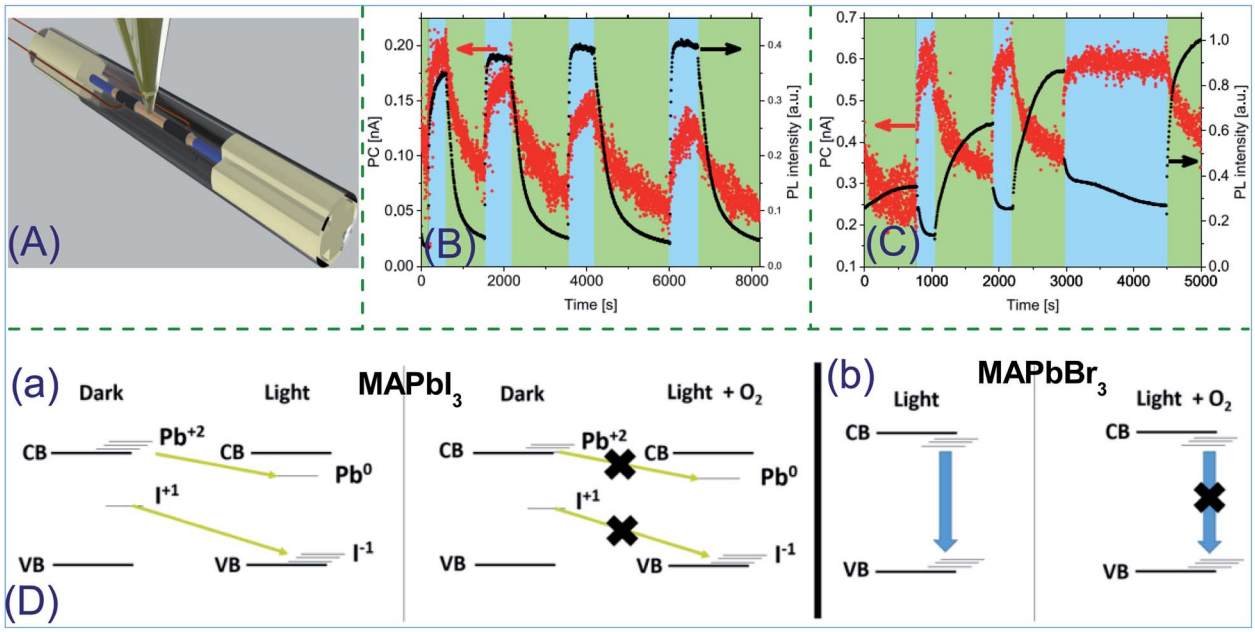

Fig. 12 (A) Schematic setup for the simultaneous monitoring of the PL and PC responses of the polycrystalline perovskite of 80 μm in diameter. (B) Evolutions of PC and PL for polycrystalline $MAPbI_3$ under recurrent exposures to either N_2 or O_2. (C) Evolutions of PC (red scattered points) and PL (black scattered points) for a polycrystalline deposit of $MAPbBr_3$ under recurrent exposures to either N_2 or O_2. (D) Schematic representation of the energy levels of shallow and deep quenching centers governing the processes of radiative and nonradiative recombination in $MAPbI_3$ (a) and $MAPbBr_3$ (b) under the combined exposure to above the band gap energy photons and O_2. Reprinted with permission from ref. 53. Copyright 2019 American Chemical Society.

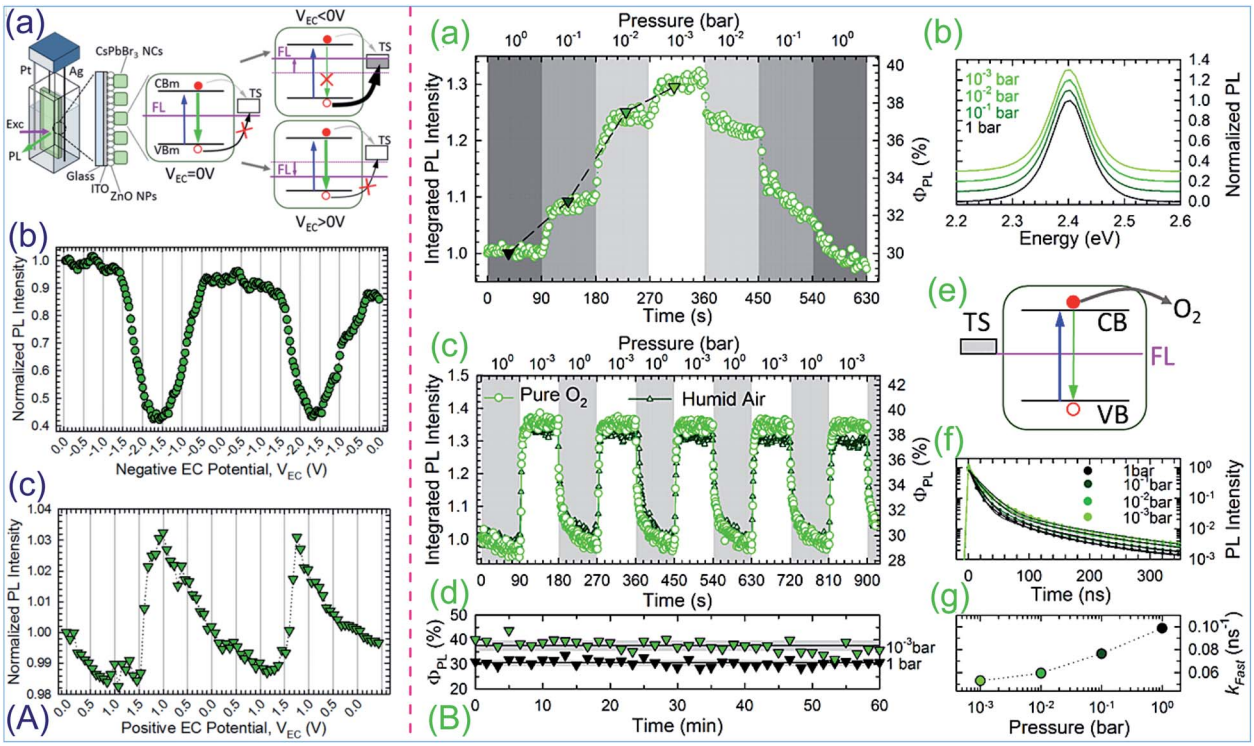

Fig. 13 (A) (a) Schematics of the SEC setup consisting of an EC cell with tetrabutylammonium perchlorate in propylene carbonate (0.1 M) as an electrolyte and a working electrode comprising an ITO-coated glass covered with a layer of ZnO nanoparticles and $CsPbBr_3$ perovskite NCs. (b) Spectrally integrated PL intensity as a function of V_{EC}. (c) Spectrally integrated PL intensity during a stepwise scan of the EC potential to positive values. (B) (a) Normalized spectrally integrated PL intensity and corresponding PL quantum yield, Φ_{PL}, of a $CsPbBr_3$ perovskite NC film during a stepwise pressure scan starting from $P = 1$ bar and lowering the pressure by 1 order of magnitude per step, down to $P = 10^{-3}$ bar. (b) Normalized PL intensity at each pressure level of panel (a) as indicated by the symbols. (c) Normalized spectrally integrated PL intensity and corresponding PL quantum yield of $CsPbBr_3$ NCs during O_2/vacuum cycles between $P = 1$ bar (highlighted with gray shades) and $P = 10^{-3}$ bar. (d) Φ_{PL} during continuous excitation at 3.1 eV in 10^{-3} bar vacuum (green triangles) and in 1 bar of pure O_2. (e) Schematic depiction of the interaction between O_2 and the NCs, showing direct extraction of photoexcited electrons from the conduction band (gray arrow) leading to the quenching of the PL (green arrow), while surface defects placed close to the Fermi level in the absence of external potentials are essentially unaffected by oxygen. The excitation light is indicated with a blue arrow. (f) Normalized PL decay curves (dotted lines) corresponding to the pressure levels indicated by symbols in panel (a) and respective double-exponential fitting curves (black lines). (g) Decay rate of the fast component of the double-exponential dynamics of the NCs as a function of the O_2 pressure. Reprinted with permission from ref. 54. Copyright 2017 American Chemical Society.

interactions with O_2, which is in contrast to the photobrightening effect observed in films and single crystals. This indicates that O_2 acts as a scavenger of photoexcited electrons without mediation by structural defects and, together with the asymmetrical SEC response, suggests that electron-rich defects are likely less abundant in nanostructured perovskites than in the bulk, leading to an emission response dominated by direct interaction with the environment.

After that, they reported O_2 as a molecular probe for non-radiative surface defects in $CsPbBr_3$ perovskite nanostructures and single crystals (Fig. 14).[55] Using O_2 as a molecular probe for the effects of surface states on the exciton recombination processes of nanocubes (NCs), nanowires (NWs), nanosheets (NSs) and bulk single crystals (SCs) of $CsPbBr_3$ perovskite, an in-depth systematic study of the surface trap-mediated processes in perovskite materials of different dimensionality has been conducted (Fig. 14A and B). Continuous wave and time-resolved PL experiments in a controlled O_2 atmosphere reveal the opposite optical response of NCs with respect to higher dimensional perovskites due to the different nature of the material surfaces. Specifically, O_2 passivates surface hole-traps in NWs, NSs and SCs, leading to PL brightening with unaltered recombination dynamics. Conversely, NCs appear to be free from such surface hole-traps and exposure to O_2 leads to direct extraction of photogenerated electrons that competes with radiative exciton recombination, leading to dimmed PL efficiency under atmospheric conditions (Fig. 14C). Further O_2/vacuum and vacuum/O_2 cycle measurements (Fig. 14D) reveal that the PL brightening of the NCs in a vacuum follows a single exponential function with a characteristic time $\tau_{NC} = 5.8$ s, slightly slower than the drop of the O_2 pressure over time. This opposite oxygen PL response demystifies the critical role of surface passivation in perovskite NCs in stark contrast to higher dimensional nanostructures and single crystals.

Lu *et al.* discovered the giant light-emission efficiency enhancement in $CsPbBr_3$ nanowires by surface oxygen passivation (Fig. 15).[56] The enhancement is close to 3 orders of magnitude as the perovskite dimensions decrease to the

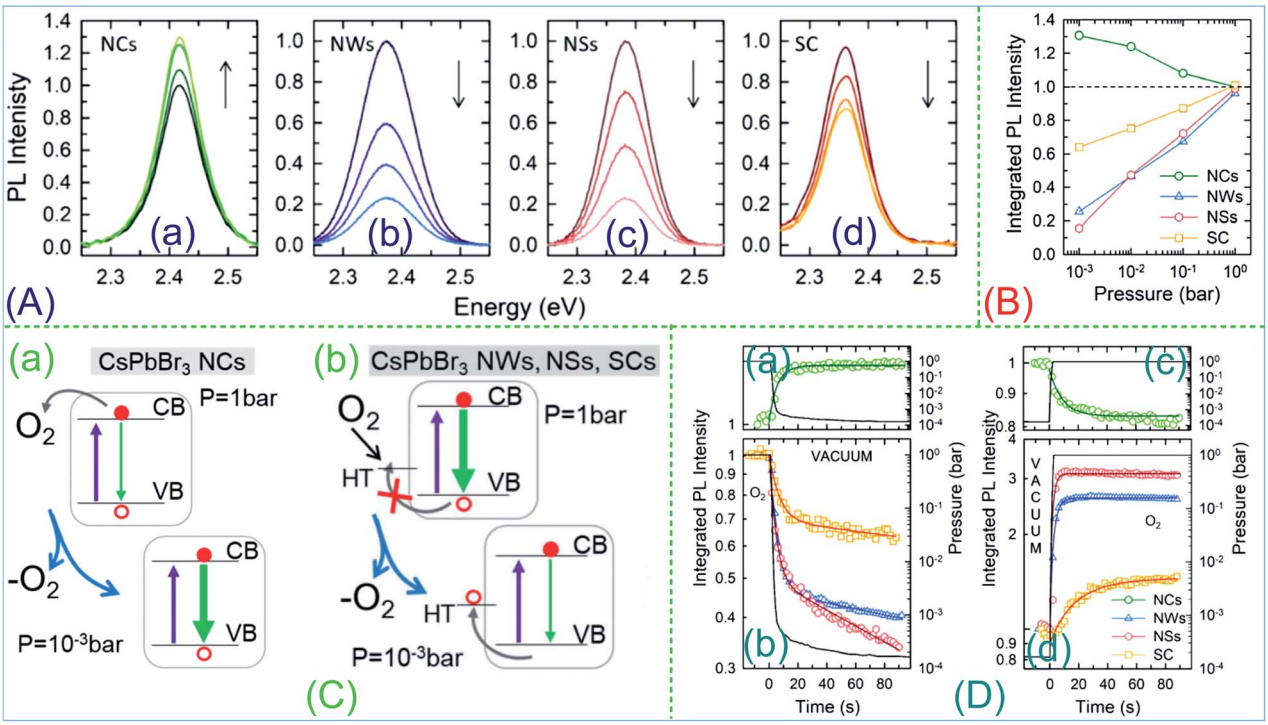

Fig. 14 (A) PL spectra of $CsPbBr_3$ NC (green), NW (blue), NS (pink) films and SCs (orange) at pressure $P = 1$ bar, $P = 10^{-1}$ bar, $P = 10^{-2}$ bar and $P = 10^{-3}$ bar (from dark to light colors). (B) Integrated PL intensity of the same systems collected at the end of each pressure step in (a) as a function of increasing O_2 pressure (logarithmic scale). (C) Schematics of the interaction mechanism between O_2 and $CsPbBr_3$ NCs (a) and NWs, NSs and SCs (b). (D) (a and b) Time dynamics of the PL pressure response of $CsPbBr_3$ NCs, NWs, NSs and SCs during the evacuation stage of an O_2/vacuum cycle. (c and d) Time evolution of the PL response during the refilling stage of the vacuum/O_2 cycle. Reprinted with permission from ref. 55. Copyright 2019 Royal Society of Chemistry.

nanoscale, improving external quantum efficiencies from <0.02% to over 12%. Along with about a 4-fold increase in spontaneous carrier recombination lifetimes, they show that oxygen exposure enhances light emission by reducing the nonradiative recombination channel. The light-emission efficiency enhancement factor was found to be proportional to the surface-to-volume ratio, 1/H (Fig. 15C). Supported by X-ray surface characterization and theoretical modeling, they propose that excess lead atoms on the perovskite surface create deep-level trap states that can be passivated by oxygen adsorption (Fig. 15D). By clarifying the general mechanism in solid-state halide perovskites, this study provides a guideline for achieving high-efficiency integrated optoelectronic devices, such as perovskite-based lasers.

Wang *et al.* reported dynamic switching between radiative exciton recombination and non-radiative carrier trapping in $CsPbBr_3$ by controlling the atmospheric conditions (Fig. 16).[57a] They showed that the PL intensity from the $CsPbBr_3$ crystals can be boosted by ~60 times by changing the surrounding from vacuum to air. Based on comprehensive characterization and DFT calculations (Fig. 16A), they unraveled that the physisorption of oxygen molecules, which repairs the trap states by passivating the PL-quenching bromine vacancies, is accountable for the enhanced PL in air. The band structures of $CsPbBr_3$ under different conditions were calculated. The defect-free $CsPbBr_3$ has a direct band gap with the valence band maximum and conduction band minimum (CBM) both located at the Γ point. For the $CsPbBr_3$ surface with bromine vacancies, the calculated results manifest the formation of new shallow energy levels at the bottom of the CBM. When O_2 is adsorbed at the location of the bromine vacancy, the shallow trap states at the bottom of the CBM are effectively removed. The schematic depiction of the O_2-physisorption induced PL switching phenomenon is illustrated in Fig. 16A(d). Specifically, the bromine vacancies, which are responsible for the PL-quenching in $CsPbBr_3$ crystals, tend to attract oxygen molecules and the adsorption of O_2 will repair the trap states introduced by V_{Br}, hence leading to a greatly enhanced PL signal (Fig. 16B). The presence of water vapor also has a positive effect on the PL enhancement. However, compared to the impact of O_2 molecules, the role played by H_2O in the PL switching phenomenon is minor. These results are helpful for better understanding the optical properties of all-inorganic perovskites.

4.3 Real-space observation of the structural defects and electronic properties of the surface and of surface defects

Surfaces plays a fundamental role in charge transport and trapping in polycrystalline thin films of MHPs as defect formation is facilitated at surfaces. It's reported that surface defects dominate ion migration and affect the stability of MHPs. Although surface/interface defect passivation has been widely reported, which has significantly improved the device

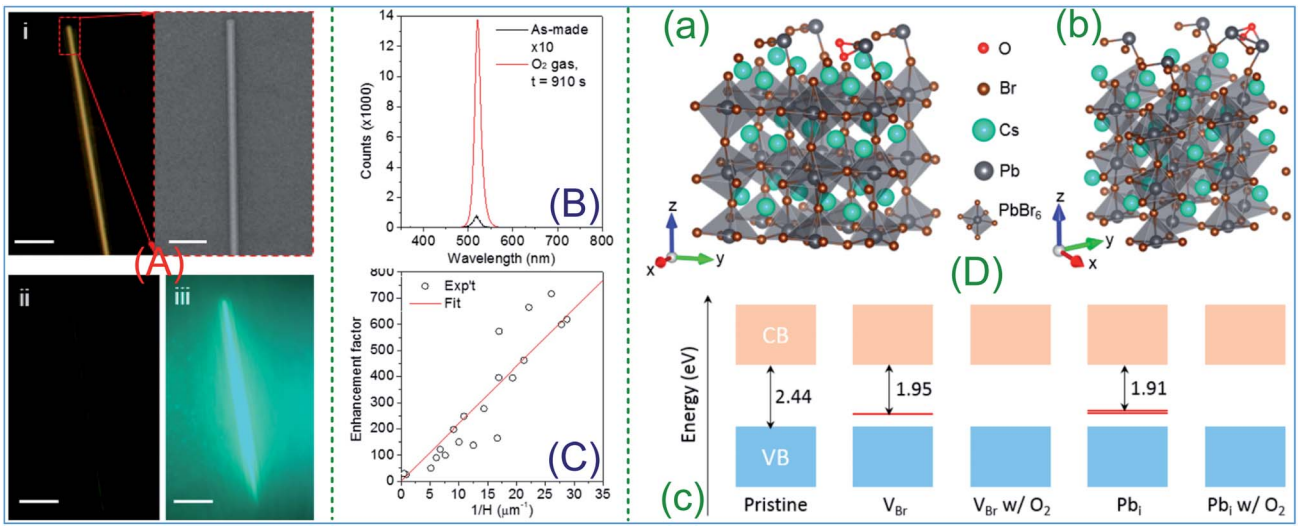

Fig. 15 (A) Optical dark-field image of a $CsPbBr_3$ NW ((i), scale bar, 10 μm) with a zoom-in SEM image (scale bar, 1 μm). Corresponding PL images for the NW before and after O_2 exposure are shown in (ii) and (iii), respectively (scale bar, 10 μm). (B) PL spectra for the as-made $CsPbBr_3$ NW (black line) and that after O_2 exposure for 910 s (red line). (C) PL enhancement factor plotted against 1/H for individual NWs with sizes varying from ~30 nm to a few microns (open circles). (D) Theoretical modeling and energy level calculation. (a and b) Theoretical models of the perovskite surface as a 2D slab with crystal structures for the V_{Br} (a) and Pb_i (b) defects adsorbed by an O_2 molecule. V_{Br}, a bromine atom removed from the surface; Pb_i, an extra lead atom added to the surface. (c) Theoretical calculated energy levels around the band gap for various defect structures. Bandgaps are shown as the energy difference between the top of the valence band and the bottom of the conduction band. The V_{Br} and Pb_i defects introduce occupied deep levels inside the band gap (red lines). In the case of Pb_i the defect levels are doubly degenerate. When O_2 is adsorbed onto the defect, the defect levels are removed. Reprinted with permission from ref. 56. Copyright 2018 American Chemical Society.

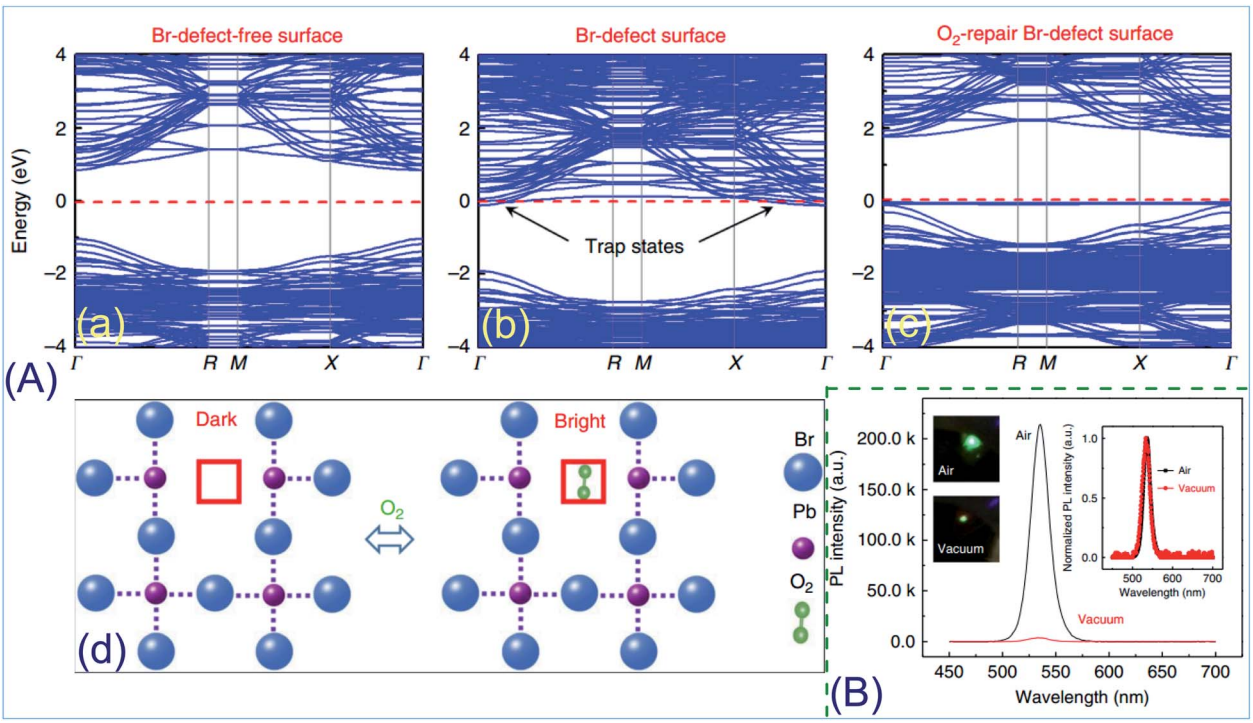

Fig. 16 (A) Band structure of Br-defect-free $CsPbBr_3$ (a). Band structure of $CsPbBr_3$ with Br vacancies (b) and band structure of $CsPbBr_3$ with Br vacancies and adsorption of oxygen molecules (c). Schematic illustration of PL switching behavior in $CsPbBr_3$ (d). (B) PL spectra of $CsPbBr_3$ in a vacuum and air. Reprinted with permission from ref. 57*a*. Copyright 2018 Nature Publishing Group.

performance of PSCs, our understanding of the surface structure and surface defect structure, electronic properties of the surface and of surface defects is far from clear. Comprehension of the phenomena occurring at the surface is thus crucial to increase solar cell efficiency and temporal stability. Very recently, several major advancements in the structural and electronic properties of the surface and of surface defects have been made.[57b]

4.3.1 Real-space observation of the structural defects, structural properties of the surface and of surface defects. Surface defects are expected to be intrinsic to perovskite crystals and may play an important role in the structural decomposition of perovskite materials. Understanding the nature of such

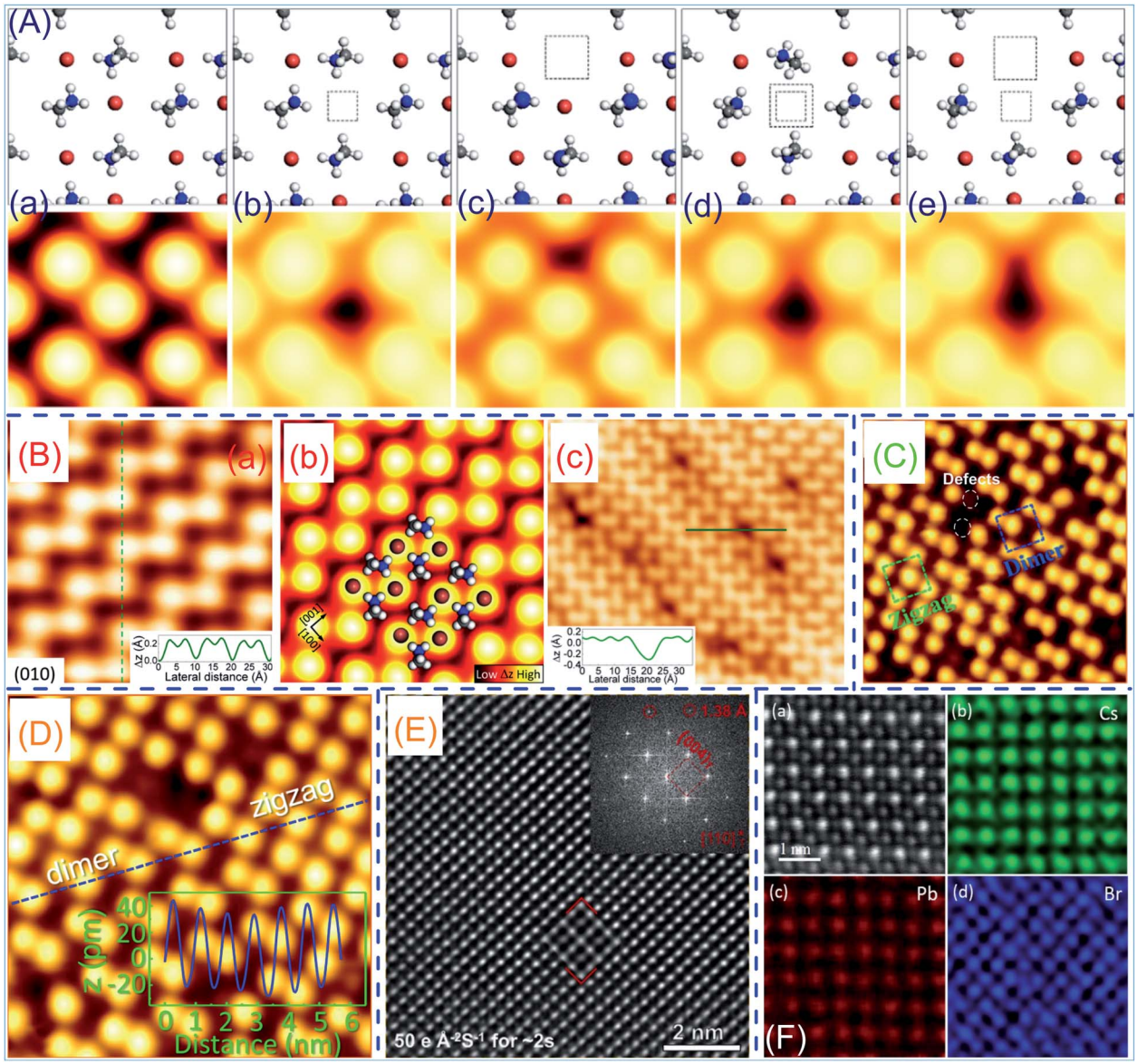

Fig. 17 (A) The top layer atoms and simulated STM images of (a) the pristine $MAPbBr_3$ (010) surface and a surface with (b) a Br vacancy V_{Br}, (c) a MA vacancy V_{MA}, (d) a Br–Pb double vacancy V_{Br-Pb}, and (e) a Br–MA double vacancy V_{Br-MA}. The squares show the position of the missing Br and Pb atoms or MA cations. Color code: N (blue), C (gray), H (white), and Br (brown). Reprinted with permission from ref. 57*c*. Copyright 2017 American Chemical Society. (B) Atomic resolution of $MAPbBr_3$. (a) Atomically resolved STM topography image of the perovskite surface. Inset: height profile along dashed line in the image. Image size: 31 × 31 $Å^2$. (b) Simulated STM image of the (010) plane of the orthorhombic crystal with surface reconstruction. Br and MA ions are overlaid. (c) STM image of defects on the surface. Reprinted with permission from ref. 57*d*. Copyright 2015 American Chemical Society. (C) High-resolution STM image of the $MAPbI_3$ film. Image size: 19 × 19 nm^2. Reprinted with permission from ref. 57*e*. Copyright 2017 Elsevier Inc. (D) STM image of the two phases coexisting on the (001) surfaces of the $MAPbI_3$ film (5.6 × 5.6 nm^2). Reprinted with permission from ref. 57*f*. Copyright 2015 American Chemical Society. (E) HRTEM image of $MAPbI_3$ shows a perfect $[110]_T$ lattice structure of $MAPbI_3$ with the corresponding Fast Fourier Transformation (FFT) shown in the inset. Reprinted with permission from ref. 57*g*. Copyright 2020 Elsevier Inc. (F) Atomic-resolution EDS elemental mapping of an orthorhombic $CsPbBr_3$ nanoplate. (a) HAADF-STEM image. (b) Cs-column mapping. (c) Pb-column mapping and (d) Br-column mapping. Reprinted with permission from ref. 57*h*. Copyright 2020 Wiley-VCH.

defects can provide some useful information toward understanding the instability of perovskite materials. Recent advances in various scanning probe microscopy techniques have demonstrated their extraordinary capability in real-space imaging and spectroscopic measurements of the structural and electronic properties of MHPs with atomic precision. For example, STM measurements not only enable a direct visualization of individual impurities and vacancies at the atomic scale, but also facilitate the unveiling of the electronic properties of these defects and their impact on the optoelectronic properties and chemical stability of MHPs. Lee *et al.* investigated the chemical identity of the intrinsic surface defects in $MAPbX_3$ perovskite crystals systematically with first-principles DFT calculations and STM simulations (Fig. 17A).[57c] The calculated STM images of all vacancy structures are shown in Fig. 17A. It should be mentioned that the dark STM feature observed in the V_{Br}, V_{Br-Pb}, and V_{Br-MA} vacancies is consistent with the previous experimental observations, in which one bright peak at the surface site of Br is replaced by a depression (Fig. 17B(c)), while the calculated STM image of the MA vacancy does not agree with the experimental measurements because the number of bright features remains unchanged. Qi *et al.* reported the real-space imaging of the atomic structure of a $MAPbBr_3$ single crystal with low-temperature STM (Fig. 17B).[57d] The surface reconstruction and the most stable surface structures of $MAPbBr_3$ have been successfully characterized, and local probing of defects has been demonstrated. Fig. 17B(a) shows an STM topography image with atomic resolution of the $MAPbBr_3$ single crystal surface. The obtained STM image of the reconstructed surface is shown in Fig. 17B(b), which agrees very well with the experimental results. In Fig. 17B(c) an area with a particularly high concentration of defects (about 10 defects per 100 nm^2) is presented. All defects shown in the image appear as depressions, the most predominant type observed on the surface, which are assigned to be Br vacancies.

As for the surface defects of prototypical perovskite $MAPbI_3$, Zhong *et al.* reported on the growth and interfacial structure of $MAPbI_3$ films on an Au (111) surface. Fig. 17C[57e] shows the high-resolution STM imaging of the OHP surface with atomic defects. The characteristic depressions are presumably attributed to Br vacancies and double Br–MA vacancies. A good agreement between the simulated STM image and experimental one further supports this structural assignment (Fig. 17A and B). It has been theoretically predicted that these types of vacancies are the most abundant defects on the MHP surface with relatively low formation energies. In their another study, a reconstructed surface phase with iodine dimers, coexisting with the pristine zigzag phase, was found at the MA-iodine-terminated (001) surfaces of the orthorhombic perovskite films deposited on Au (111) surfaces (Fig. 17D).[57f]

Cryo-TEM is another effective technique that can perform direct atomic scale characterization of the surface structure and defects in MHPs. With specific imaging conditions, Gu *et al.* were able to avoid the electron beam-induced structural damage of MHPs.[57g] Fig. 17E presents a typical high magnification cryo-TEM image of the $MAPbI_3$ particle under the protection of liquid N_2. The crystal structure of $MAPbI_3$ is well preserved and perfect squared lattices along the $[110]_T$ zone axis can be clearly seen.[57h] They also observed some structural defects, such as atomic surface steps and MAI-stacking faults, in single crystalline $MAPbI_3$, which shows the great potential of cryo-TEM in the observation of perovskite structure defects. Fig. 17F shows the atomic-resolution EDS elemental mapping of an orthorhombic $CsPbBr_3$ nanoplate by Han *et al.*[57h] The results show the distribution of Cs, Pb, and Br atomic columns constituting a perfect perovskite structure, demonstrating that this material was stable under the EDS mapping conditions and no beam-induced structural damage occurred.

4.3.2 Electronic structure and properties of the surface and of surface defects. MHPs have shown ultrasensitivity to atmospheres especially to O_2, which is due to the passivation effect of the surface defects. The identification of the chemical nature of the surface defects is thus of crucial importance for the fundamental understanding of these materials. To reveal the mechanisms of oxygen passivation on surface defects in $MAPbI_3$, Tian *et al.* systematically studied the adsorption of O_2 on all possible crystal defects on the (001) surface with three different possible terminations and it is finally identify that the vacancy defects of I and the interstitial defects of Pb are the two main surface defects responsible for the charge-carrier trapping (Fig. 18A).[57i] According to Fig. 18B(a–c), we can see that certain electrons can be transferred from a nearby Pb atom with low coordination to an oxygen molecule when O_2 is adsorbed at the vacant-V_I. Such electron transfer indicates strong bonding interaction between the oxygen and the Pb atom. The charge density differences, shown in Fig. 18B(d–f), confirm the electron transfer between the two Pb atoms and the oxygen molecule. With these results, we can conclude that the adsorption of O_2 causing the passivation of V_I and Pb_i may be ascribed to the existence of unsaturated coordinated Pb atoms and the interaction between O_2 and these Pb atoms. The presence of numerous iodine vacancies at the surface of the film formed by their evaporation during the thermal annealing process has been broadly shown to induce deep-level defects, cause nonradiative charge recombination, and induce photocurrent hysteresis, all of which limit the efficiency and stability of PSCs. In the work by Huang *et al.*, modifying the defective surface of perovskite films with cadmium iodide (CdI_2) effectively reduces the formation of halogen vacancies by filling the iodide vacancies and stabilizes iodine ions *via* the formation of strong Cd–I ionic bonds. The reduced surface halogen deficiency effectively decreased the density of surface defects and substantially suppressed nonradiative recombination, thus reducing the interfacial recombination loss to achieve a high V_{oc} of 1.20 V with a record small V_{oc} deficit of only about 0.31 V.[57j]

Angelis *et al.* investigated charge localization and trapping at the surface of the prototypical $MAPbI_3$ perovskite through advanced electronic-structure calculations by considering different surface terminations (Fig. 18C and D).[57k] It is found that both MAI- and PbI_2-terminated surfaces exhibit a clear spatial separation of hole and electron polarons, while a MAI-vacant surface induces charge localization at under-coordinated lead atoms. Notably, the PbI_2-terminated surface

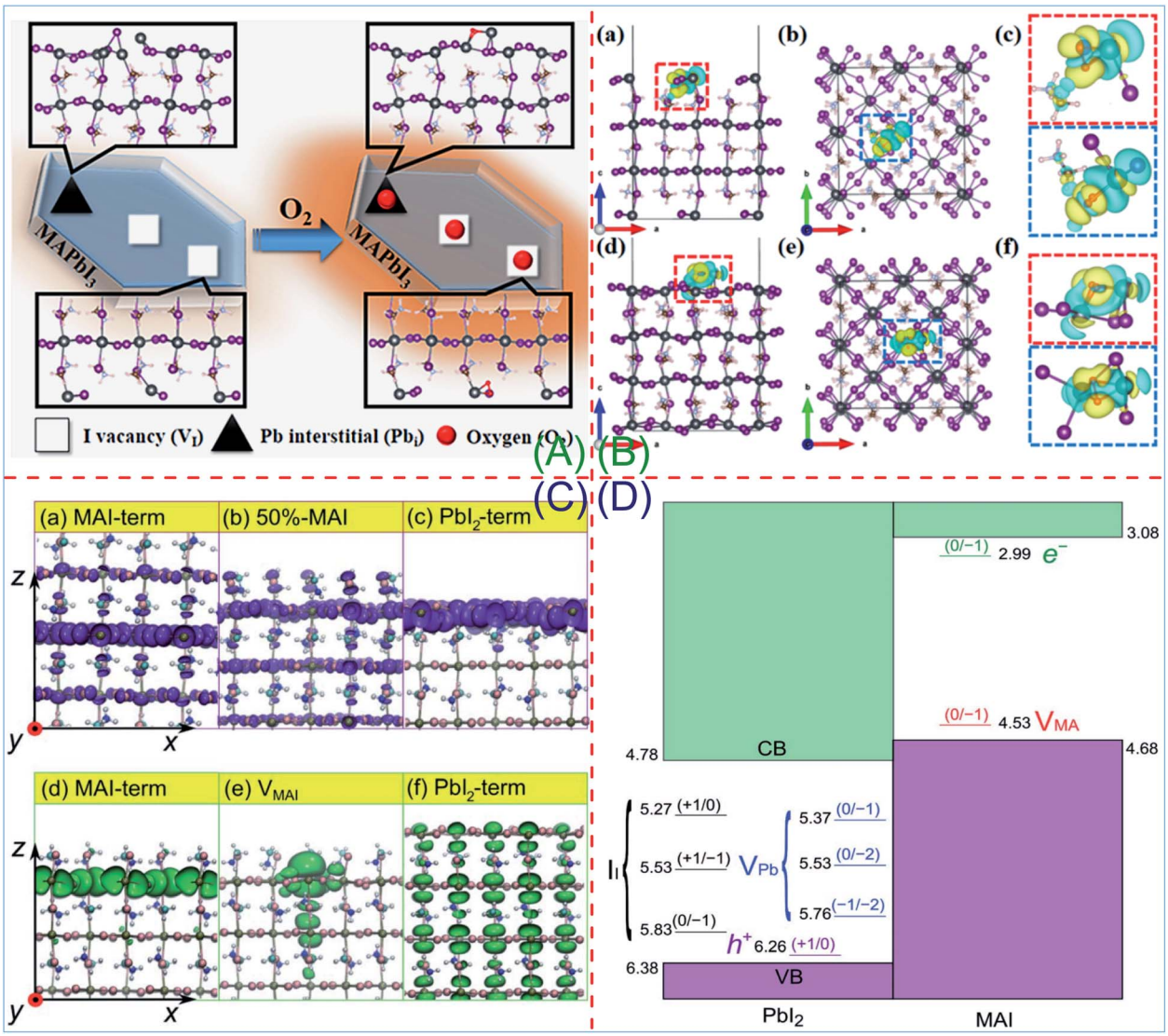

Fig. 18 (A) Mechanisms of oxygen passivation on surface defects in $MAPbI_3$. (B) (a) Side, (b) top, and (c) corresponding partial enlarged views of charge density differences for the optimized system where O_2 is adsorbed at the vacant-V_I. (d) Side, (e) top, and (f) corresponding partial enlarged views of charge density differences for the system where O_2 is adsorbed at the flat-Pb_i. The yellow and cyan regions represent charge accumulation and depletion, respectively. The atom O is shown in red. Reprinted with permission from ref. 57*i*. Copyright 2015 American Chemical Society. (C) Isodensity representations of an extra hole (purple, upper panels) for the (a) MAI surface, (b) 50% MAI-covered surface, and (c) PbI_2 surface. Isodensity representations of an extra electron (green, lower panels) for the (d) MAI surface, (e) MAI-vacant surface (V_{MAI}), and (f) PbI_2 surface. (D) Schematic representation of the energy levels of surface defects which are relevant for the MAI and PbI_2 terminations of the (001) surface of tetragonal MAPbI3. All energy levels are referenced to the vacuum level. Reprinted with permission from ref. 57*k*. Copyright 2020 Royal Society of Chemistry.

is sensitive to surface defects, which may either act as recombination centres or inhibit charge transfer at the surface, while the MAI-terminated surface is comparably more defect tolerant. It is thus suggested that perovskite growth under MAI-rich conditions should be beneficial to limit surface recombination, while the synthesis of $MAPbI_3$ in a PbI_2-rich environment should be accompanied by surface passivation strategies to counteract the negative impact of surface defects. In another study, they showed that the band edge energies of $MAPbI_3$ perovskite can in principle be varied by as much as 1 eV *via* postsynthetic MAI treatment. In particular, MAI-rich (PbI_2-rich) surfaces induce an energy upshift (downshift) of the perovskite band energies, and this can either inhibit or favor hole transfer at the perovskite/HTL interface (Fig. S6†).[57*l*]

5 Representative applications of the OIDH effect

5.1 Perovskite solar cells

By combining atmospheric and photoinduced post-treatments of solution-processed polycrystalline $MAPbI_3$ perovskites (Fig. 19A), Stranks *et al.* demonstrated perovskite polycrystalline

films that exhibit properties of single crystals with an improved diffusion length (77 μm), carrier lifetime (32 μs), and suppressed surface recombination velocity (0.4 cm s^{-1}).[58,59] The single crystal level of film quality ensures 19.2% (Fig. 19B) efficient nip PH-PSCs with a near-instant rise to a stabilized power output, due to the suppression of ion migration. Considering the observed micro-photoluminescence enhancements (Fig. 19C and D) and the theoretical evidence that oxygen diffusion into $MAPbI_3$ films is accompanied by photo-induced formation of superoxide species (O_2^-) at iodide vacancies (passivating effect of oxygen), a mechanism in which light creates superoxide species from oxygen that remove shallow surface states is proposed to explain such a result (Fig. 19E). This work reveals an industrially scalable post-treatment capable of producing state-of-the-art semiconducting films for advanced optoelectronic applications.

To address the remaining puzzle of the perovskite "photo-brightening" phenomenon of the increase in photo-luminescence during exposure to light in an ambient atmosphere, Snaith and Wenger *et al.* proposed a comprehensive mechanism for the reactivity of the archetypal perovskite, $MAPbI_3$, under ambient conditions and established the formation of lead-oxygen bonds by hydrogen peroxide (H_2O_2) as the key factor leading to perovskite photo-brightening (Fig. 20A).[19] It is demonstrated that H_2O_2 can be applied directly as an effective "post-treatment" to emulate the process

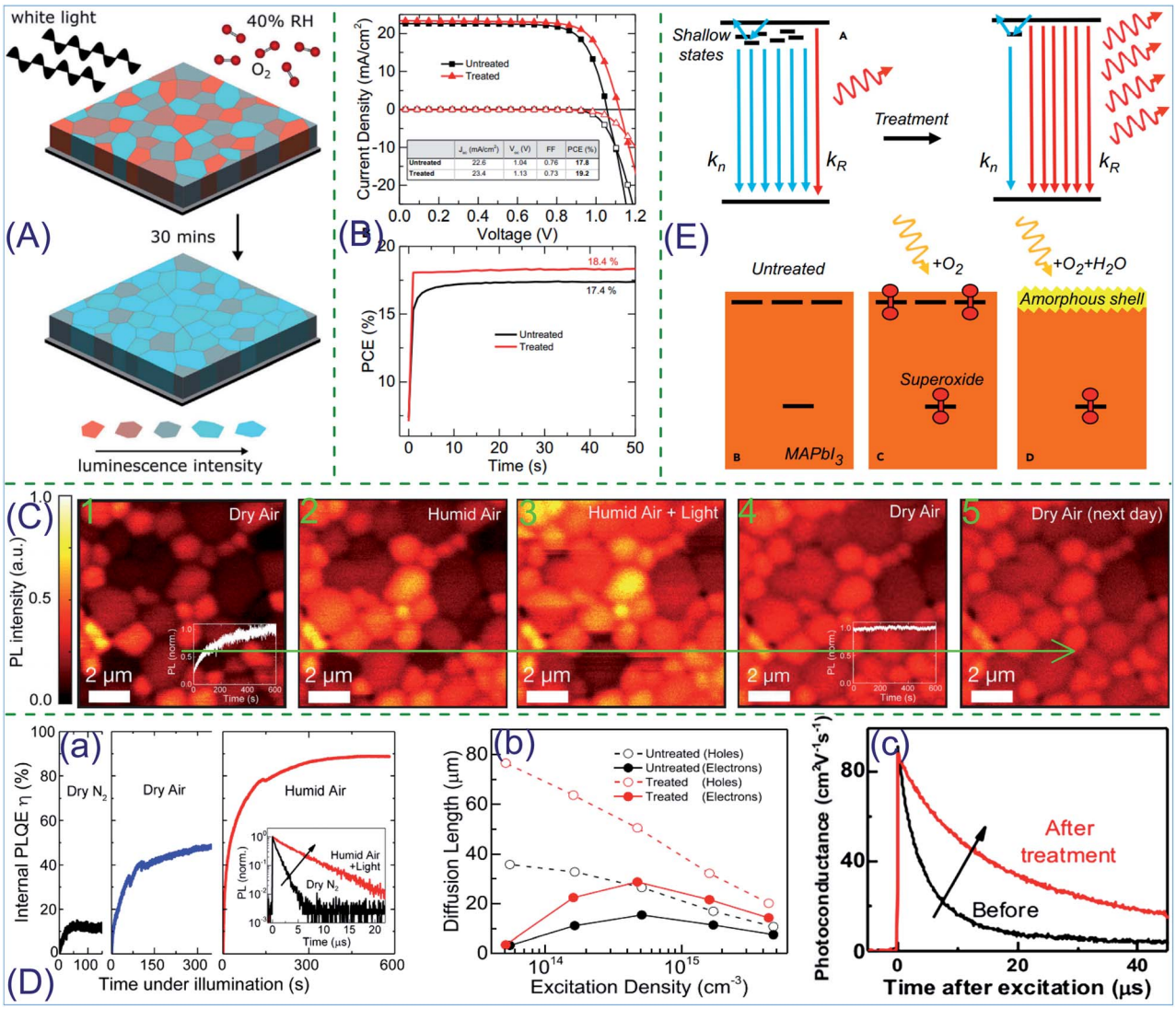

Fig. 19 PL enhancements of films under solar illumination (A). Light and dark *J*–*V* curves of champion devices which contain untreated (stored in dry air) and treated (light soaked in humid air) films measured under AM1.5 100 mW cm^{-2} simulated sunlight. Reprinted with permission from ref. 59. Copyright 2017 Elsevier Inc. (B). Stabilized power output of the devices presented in (a) measured by holding the devices at their maximum power point (as determined from *J*–*V* curves) for 50 s (C). *In situ* confocal PL maps with 405 nm excitation measured in (1) dry air, (2) humidified air, (3) after light soaking for 10 m under excitation with a 532 nm laser equivalent to 10 sun under humid air, and (4) after returning to dry air, and (5) measured the next day with storage in dry air (D). Mechanism of photo-brightening (E). Reprinted with permission from ref. 58. Copyright 2017 Elsevier Inc.

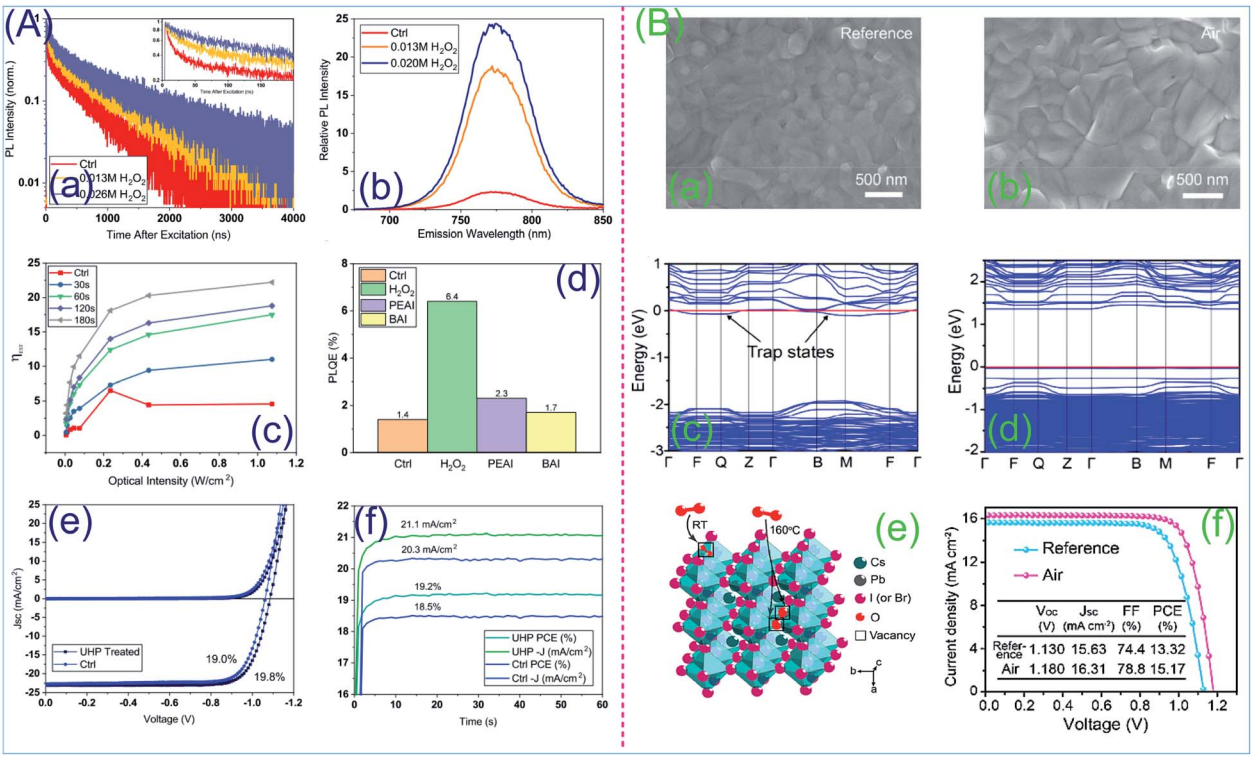

Fig. 20 (A) Oxidative passivation of a PSC: time-resolved (a) and steady-state (b) PL measurements of control and H_2O_2 treated $FA_{0.83}Cs_{0.17}Pb(I_{0.83}Br_{0.17})_3$ films. Intensity dependence of external PLQE values of the treated films (c) and PLQE of films after three different treatments (d). *J*–*V* curves (e) and steady-state power output (f) of devices treated with H_2O_2. Reprinted with permission from ref. 19. Copyright 2019 Elsevier Inc. (B) Oxidative passivation of an all-inorganic PSC: SEM images of the reference (a) and the air processed (b) $CsPbI_2Br$ film. Band structure of $CsPbI_2Br$ with halogen vacancy (c) and halogen vacancy and dissociated O atom passivation (d). Schematic of adsorbed oxygen molecule passivation and oxygen atom passivation (e). *J*–*V* curves and performance parameters of the corresponding devices (f). Reprinted with permission from ref. 20. Copyright 2012 American Chemical Society.

and substantially improve photoluminescence quantum efficiencies. For films treated with 13 and 26 mM solutions of H_2O_2 in isopropanol, we obtain lifetimes of 140 and 281 ns respectively, which represents a significant increase compared to a mean control value of 40 ns. The time-integrated PL intensities show a more than 10^3 increase with the H_2O_2 treatment (Fig. 20A(a and b)). The H_2O_2 treatment is more effective than some of the current best performing passivation agents in reducing the concentration of defects leading to non-radiative recombination (Fig. 20A(c and d)). Both of these findings suggest a large reduction in non-radiative pathways, consistent with the passivation of defects at the surface. Finally, they show that the treatment can be incorporated into photovoltaic devices to give a 50 mV increase in open-circuit voltage, delivering 19.2% steady-state power conversion efficiencies for inverted perovskite solar cells of the mixed halide, mixed cation perovskite $FA_{0.83}Cs_{0.17}Pb(I_{0.9}Br_{0.1})_3$ (Fig. 20A(e and f)).

Defect passivation using oxygen has been identified as an efficient and convenient approach to suppress nonradiative recombination and improve the photovoltaic performance of MHPs. However, oxygen can seriously undermine the chemical stability of MHPs due to the reaction of superoxide with protonated organic cations such as $CH_3NH_3^+$ and $[(NH_2)_2CH]^+$, thus hindering the deep understanding of how oxygen affects their defect properties. Liu *et al.* substituted free-proton inorganic Cs^+ for an organic moiety to avoid the negative effect of oxygen and then systematically investigated the oxygen passivation mechanism in an all-inorganic MHP $CsPbI_2Br$ from theory to experiment (Fig. 20B).[20] They found that, in contrast to conventional oxygen molecule passivation just through physisorption on the surface of perovskites, the oxygen atom can provide a better passivation effect due to its stronger interaction with all-inorganic perovskites. The key point to achieve O-passivated perovskites rather than O_2 is dry-air processing conditions, which can dissociate the O_2 into O during the annealing process. It is found that the grain size of the air-$CsPbI_2Br$ film was larger than that of the reference film. XPS measurement confirmed the Pb–O bond and indicated that oxygen was successfully introduced into $CsPbI_2Br$ films in the form of oxygen atoms under dry-air condition processing. ToF-SIMS and EDS measurements indicated that oxygen exists throughout the whole air-$CsPbI_2Br$ layer. DFT calculations suggests a stronger coupling of the O atom to the valence band of the perovskite compared with the O_2 molecule (Fig. 20B(c and d)) and the O atom has better capability to passivate halogen vacancies in perovskites than O_2. Similar to hybrid MHPs where surface halogen vacancies were favorable sites for oxygen molecule adsorption, oxygen molecules may be preferentially

adsorbed on surface iodide or bromine vacancies in $CsPbI_2Br$ at room temperature. In contrast, through the dry air fabrication process, oxygen atoms rather than molecules can be incorporated into the whole perovskite films instead of only the surface (Fig. 20B(e)). O-passivated MHP solar cells exhibit enhanced PCE and better air stability than O_2-passivated cells (Fig. 20B(f)), which is similar to the results reported by Che *et al.* These results not only provide deep insights into the passivation effect of oxygen on perovskites but also demonstrate the great potential of all-inorganic MHPs for high photovoltaic performance with simplified ambient processing.

The toxicity of lead soon leads to the invention of lead-free PSCs, among which Sn(II) halide perovskites have shown the highest PCE. However, the facile oxidation of Sn^{2+} to Sn^{4+} results in the rapid degradation of its optoelectronic properties. Chen *et al.* reported highly stable and efficient all-inorganic lead-free $Cs(Sn_{0.5}Ge_{0.5})I_3$ PSCs with native-oxide passivation, delivering a promising PCE of up to 7.11%.[60] The $Cs(Sn_{0.5}Ge_{0.5})I_3$ perovskite powder was used to evaporate thin films (Fig. 21A(a and b)) on a 10×10 cm^2 glass substrate. The extremely high oxidation activity of Ge^{2+} enables the rapid (within 30 s) formation of a stable and ultrathin (<5 nm) uniform native-oxide surface passivating layer on the $Cs(Sn_{0.5}Ge_{0.5})I_3$ perovskite as the perovskite thin films are exposed to air, endowing it with superior stability (Fig. 21B). XPS spectra at different incidence angles present a sharp drop in the Ge^{2+} content at incidence angles from 30 to 45°, indicating a distinct native-oxide layer comprising Ge^{4+} primarily (Fig. 19A(c)). The energy-level diagrams of the device with a native-oxide layer are shown in Fig. 21C(a). The *J–V* curves of the champion device with 7.03% PCE show negligible hysteresis (Fig. 21C(b)). This can be attributed to the suppression of recombination of photocarriers at the interface between the $Cs(Sn_{0.5}Ge_{0.5})I_3$ perovskite and the HTL, where the native oxide resides. More importantly, these PSCs show very high stability, with less than 10% decay in efficiency after 500 h of continuous operation in a N_2 atmosphere under one-sun illumination. The key to this striking performance of these PSCs is the formation of a full-coverage, stable native-oxide layer, which fully encapsulates and passivates the perovskite surfaces. The native-oxide passivation approach reported here represents an alternate avenue for boosting the efficiency and stability of lead-free PSCs.

5.2 Perovskite light emitting diodes

Mixed-halide perovskites, such as $MAPb(Br_xI_{1-x})_3$, are very promising candidates for wavelength-tunable LEDs due to their tunable band gaps, while uniform MHPs suffer from notorious phase separation into I-rich and Br-rich domains with different band gaps under light illumination or an electric field, which is detrimental to LEDs. As for LEDs, the emission wavelength will be pinned in the infrared range due to energy transfer from large-bandgap Br-rich domains to low-bandgap I-rich domains. Xiao *et al.* reported that such an issue can be addressed by

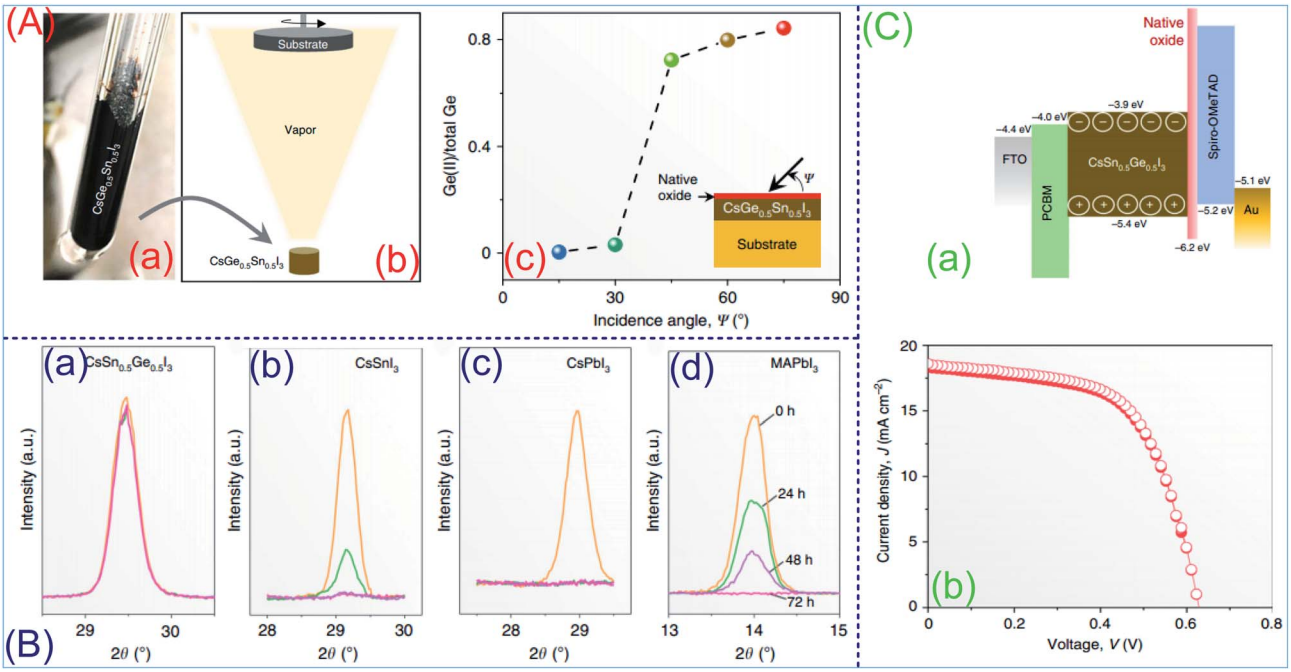

Fig. 21 All-inorganic lead-free PSC with native-oxide passivation: film synthesis and characterization (A): photograph of the as-synthesized $Cs(Sn_{0.5}Ge_{0.5})I_3$ perovskite solid using the melt-crystallization method (a). Schematic illustration of the single-source evaporation method for the deposition of an ultra-smooth $Cs(Sn_{0.5}Ge_{0.5})I_3$ film (b). Plot of the fraction of Ge(II) *vs.* the incidence angle during the XPS characterization (c). Thin-film stability (B): XRD patterns of perovskite films before and after exposure for 24, 48, and 72 h to light-soaking (1 sun) at approximately 45 °C and 80% RH: $Cs(Sn_{0.5}Ge_{0.5})I_3$ (a), $CsSnI_3$ (b), $CsPbI_3$ (c), and $MAPbI_3$ (d). Device performance (C): schematic illustration showing the energy-level diagram of the device (a) and *J–V* curves of the champion device (b). Reprinted with permission from ref. 60. Copyright 2019 Nature Publishing Group.

oxygen passivation under light illumination as oxygen atoms can effectively occupy halogen vacancies, thus suppressing halogen redistribution and phase separation (Fig. 22).[46] As shown in Fig. 22, the PL peaks gradually blue-shifted toward the absorption edges at 70 °C in an O_2 environment. This result suggests that heating can also accelerate the diffusion of oxygen into the perovskite film and enhance the passivation effect. It should be noted that it takes around 40 min for the phase-separated film to recover to the uniform state under 1 sun illumination, while it takes around 8 h for heating at 70 °C, which might be the reason for the systematic shift of PL during heating and the differences in the PL shift between heating and 1 sun illumination. The effect of O_2 passivation on the final LED device performance was tested. Fig. 22B shows the current density, external quantum efficiency, and electroluminescence (EL) spectra of the LEDs. The LED shows a strong EL peak at 660 nm after O_2 passivation initially, compared with 730 nm for control devices without passivation. This result further demonstrates the role of O_2 passivation in suppressing light (or electric field)-induced phase separation in MHPs. XPS measurement indicates a higher oxidation state of Pb and formation of a Pb–O bond, confirming the interfacial bonding between the MHP and oxygen. DFT calculations further confirm the oxidation passivation. The switchable emission color in N_2 and O_2 reported here may have potential application in light-emitting field-effect transistors, where the perovskite films are exposed to an external environment.

5.3 Oxygen/ozone sensors

In addition to the applications in the field of optoelectronics, oxygen/ozone sensing and detection based on the air-induced optical and electrical modulation of MHPs has also been reported. Stoeckel *et al.* reported a reversible, fast, and wide-range oxygen sensor based on nanostructured $MAPbI_3$ perovskite (Fig. 23).[61] This is the first experimental demonstration of the use of perovskite-based devices as an O_2 sensor. The electrical response of MHPs to oxygen is studied. A 3000-fold increase in the resistance of perovskite based lateral devices is found when measured in a full oxygen atmosphere (Fig. 23A(b and c)), which is ascribed to a trap healing mechanism originating from O_2-mediated iodine vacancy filling (Fig. 23A(f)). The effect is fast

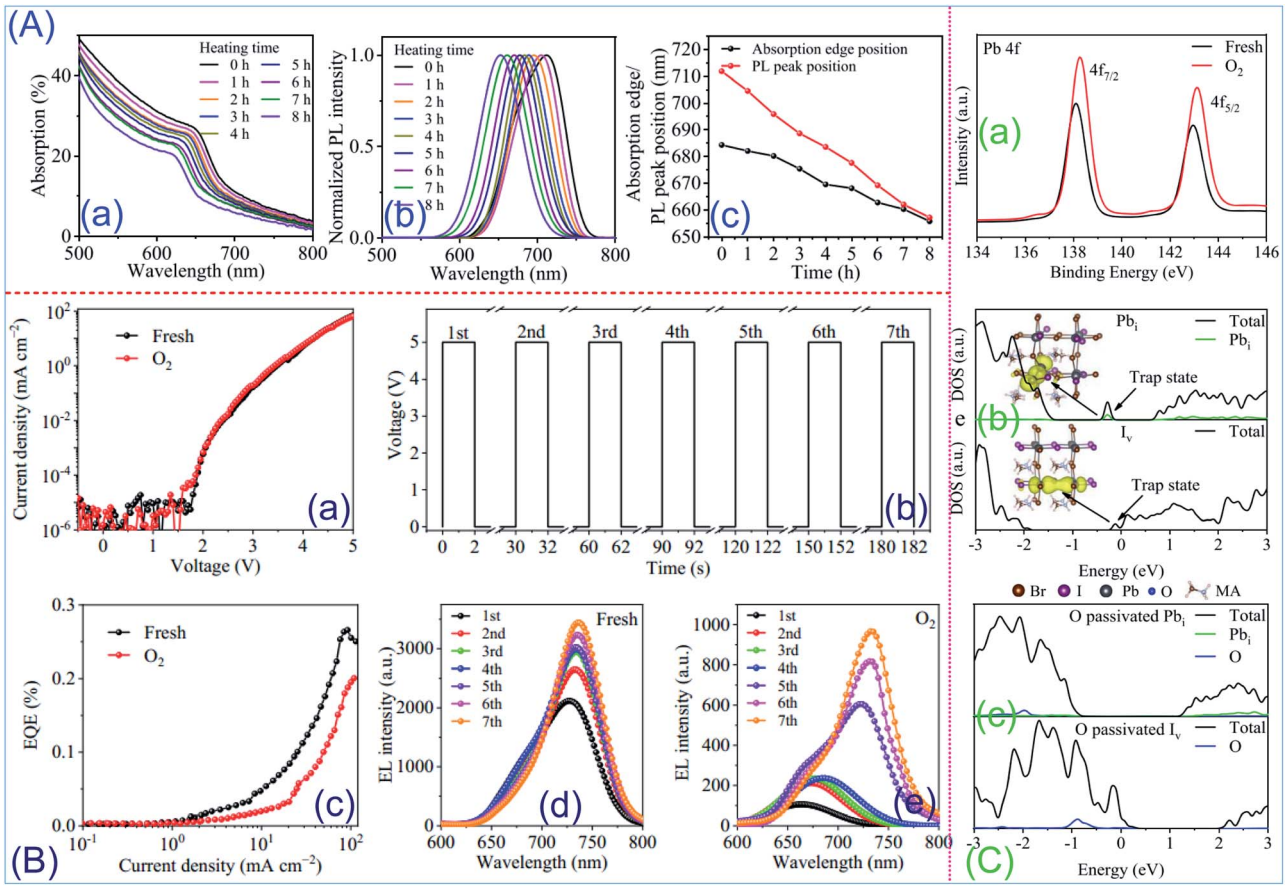

Fig. 22 (A) Perovskite characterization: absorption (a) and PL spectrum (b) of the $MAPb(Br_{0.4}I_{0.6})_3$ film with different heating times in an oxygen environment. The PL measurement was done in a pure oxygen environment with continuous excitation. Plot of absorption edges and PL peak positions *versus* heating time (c). (B) PLED characterization: current density (a) and EQE (b) of the perovskite LEDs based on $MAPb(Br_{0.4}I_{0.6})_3$. Voltage pulses applied on the devices for EL measurement (c). Normalized EL spectrum of perovskite LEDs using fresh films (d) and O_2 passivated films (e). (C) Interaction between the perovskite and oxygen: XPS core level spectra for Pb 4f (a) of the $MAPb(Br_{0.4}I_{0.6})_3$ film and the PDOS of Pb_i and I_V before (b) and after (c) O_2 passivation. Reprinted with permission from ref. 46. Copyright 2019 American Chemical Society.

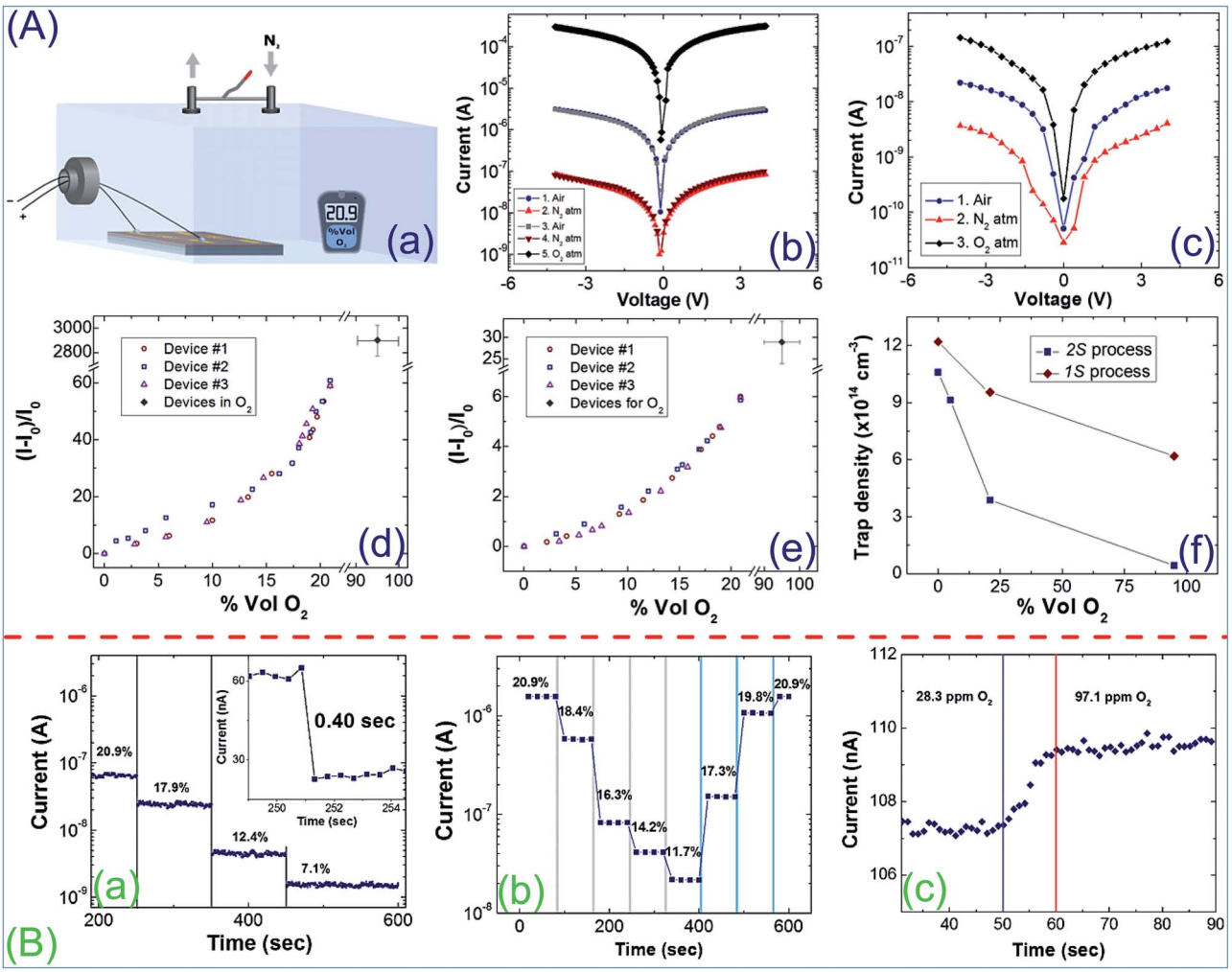

Fig. 23 (A) Experimental setup and device performance: experimental setup scheme used for device characterization (a). *I–V* curves at different O_2 concentrations for the 2S perovskite (b). *I–V* curves at different O_2 concentrations for the 1S perovskite (c). Sensor sensitivity *versus* O_2 concentration for (d) 2S and (e) 1S perovskites, measured upon applying 4 V between the electrodes. (f) Number of charge traps in the perovskite films at different oxygen concentration, obtained by fitting the *I–V* traces to the SCLC model. (B) Device response characteristics: real time change in the current measured in a 2S film in response to changes in the atmospheric composition (a). Inset: speed of the sensor response. Reversibility of the sensor (b). The O_2 concentration is firstly decreased from 20.9% to 11.7% and then increased back to 20.9%. In this case, measurements are performed every 20 s. Real-time current change corresponding to a 70 ppm O_2 variation in the sample atmosphere (c). The blue line indicates the instant at which oxygen gas is introduced into the chamber. After this moment, the oxygen content in the proximity of the sample increases slowly until it reaches an equilibrium state (marked by the red line). Reprinted with permission from ref. 61. Copyright 2017 Wiley-VCH.

(<400 ms) and fully reversible, making MHPs ideal active materials for oxygen sensing (Fig. 23B(a)). A variation as small as 70 ppm in the oxygen concentration can be detected (Fig. 23B(c)). They also showed that the device sensitivity is strongly affected by the nanoscale morphology of the perovskite films, which was controlled by the deposition method adopted. It is suggested that the effect of oxygen on the electrical characteristics of MHPs must be taken into deep consideration for the design and optimization of any other perovskite-based optoelectronic device working under ambient conditions.

In addition to the electrical response of perovskites to oxygen as the basis of oxygen sensing, oxygen induced photoluminescence-quenching is another mechanism that can be adopted. For the design of photoluminescence-quenching probes for molecular O_2, luminescent semiconductor NCs have been proposed as emerging candidates, but the inherent O_2 sensing of phosphorescent semiconductor NCs has not been reported so far. Lin *et al.* demonstrated the O_2 sensing capability of Mn^{2+}-doped $CsPbCl_3$ NCs (Mn:$CsPbCl_3$ NCs) and reveal the role of O_2 in the optical de-excitation process of such perovskite NCs.[62] It is found that by adjusting the amount and distribution of luminescent Mn^{2+} dopants, as well as the host-dopant energy transfer process in NCs, they highlight that O_2 can reversibly quench the Mn^{2+} emission due to the temporary disturbance to the ligand field of near-surface Mn^{2+} dopants in NCs. In phosphorescence mode, the PL intensity of the Mn:$CsPbCl_3$ NCs is quenched by 53% on increasing the O_2 concentration from 0 to 100%. The Stern–Volmer plot shows

a good linearity in the 0–12% O_2 concentration range. In addition, the sensing reversibility was demonstrated in 10 repeated cycles without obvious loss in performance (Fig. 24). As shown in Fig. 24, they evaluated the response and recovery time. In the presence of O_2, a phosphorescence quenching degree of 97% is achieved within 5 s. The test of the photostability in air suggests that although the phosphorescence intensity drops by 6% after 1 h, the constant peak position of Mn^{2+} emission rules out the possibility of permanent surface oxidation for the dopants. If they temporarily blow the film with pure N_2 again to accelerate the removal of absorbed O_2, the phosphorescence in air recovers to the initial intensity, which excludes the irreversible loss of Mn^{2+} dopants during limited photo-bleaching.

The photoluminescence of MHPs is very sensitive to their surface conditions, especially surface defect states, making the PL of small MHP crystals an effective way to probe the surface reactions and report their surface states. Vicente *et al.* reported single oxygen molecule sensitivity of MHP PL by quantitatively evaluating the interaction between a single surface defect and a single O_2 molecule (Fig. 25A and B).[63] In particular, they showed that the exposure of an MHP nanorod to single O_2 molecules under illumination could lead to the enhancement of its PL by facilitating the relaxation of an active trap, and effectively passivating it to prevent its further activation, which provide a potential strategy to design suitable interfacial chemistry for photovoltaic and optoelectronic devices and gas sensors.

Gas sensing technologies are of great importance in environmental monitoring, public security, air conditioning appliances/systems, and commercial and domestic safety. Apart from oxygen sensing of MHPs, their sensing properties in an ozone (O_3) environment have also been demonstrated.[64] Ozone is one of the six principal pollutants considered harmful to the public health and the environment. It has been established that

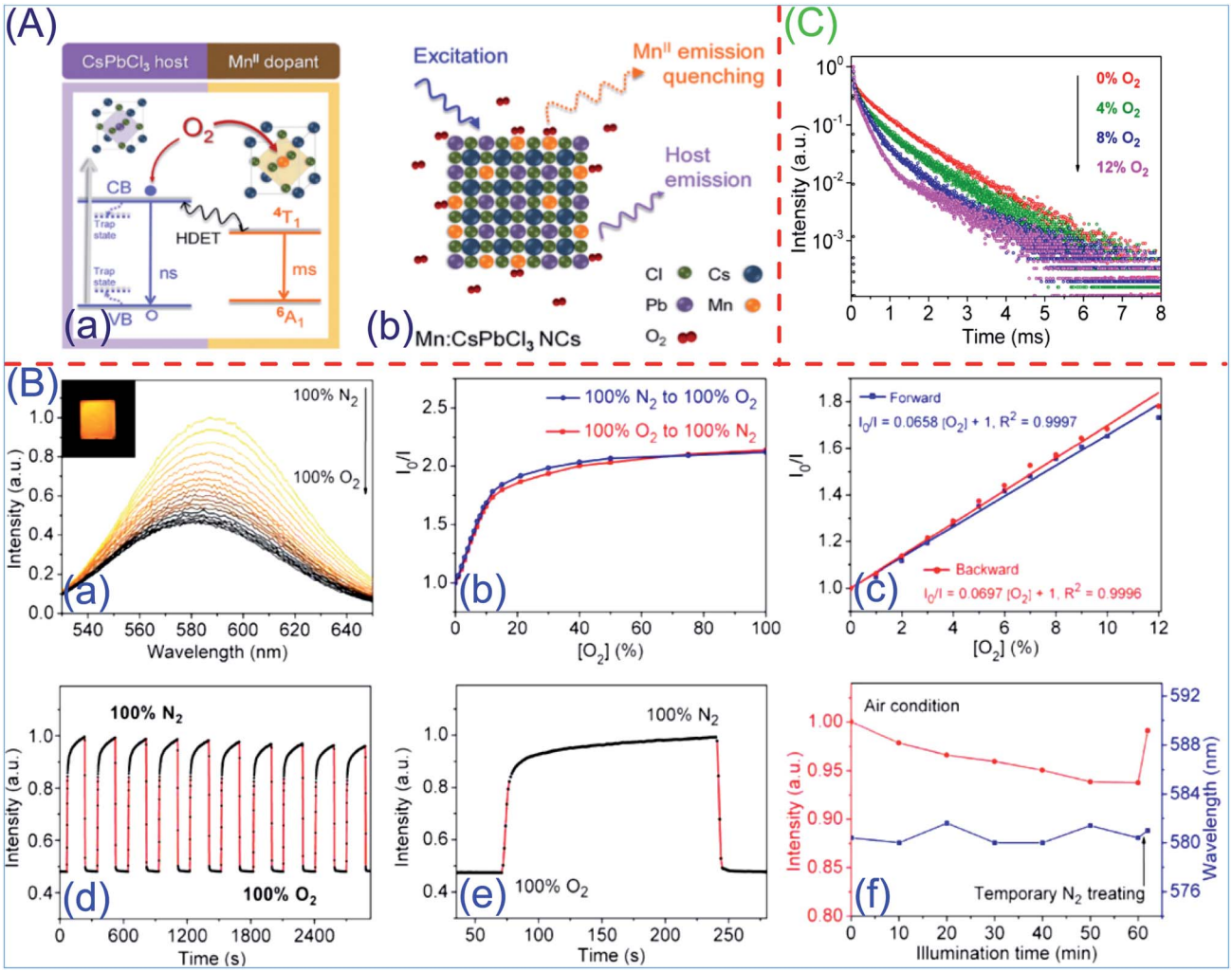

Fig. 24 (A) Schematic representation of the interaction mechanism between O_2 and Mn doped $CsPbCl_3$ NCs. (B) Sensing responses of the $Mn_{0.175}$:$CsPb_{0.825}Cl_3$ film to O_2: phosphorescence spectra under different O_2 fractions (a). The first-order reaction kinetics curves of the maximum phosphorescence intensities under different O_2 fractions (b). Stern–Volmer plot under the O_2 fractions between 0 and 12% (c). Reversibility test under alternating exposure to 100% O_2 or 100% N_2 (d). The response time curve within one cycle test (e). Photostability test under air conditions (f). (C) The Mn-related time-resolved PL decay of testing films under different O_2 fractions (0–12%). Reprinted with permission from ref. 62. Copyright 2018 American Chemical Society.

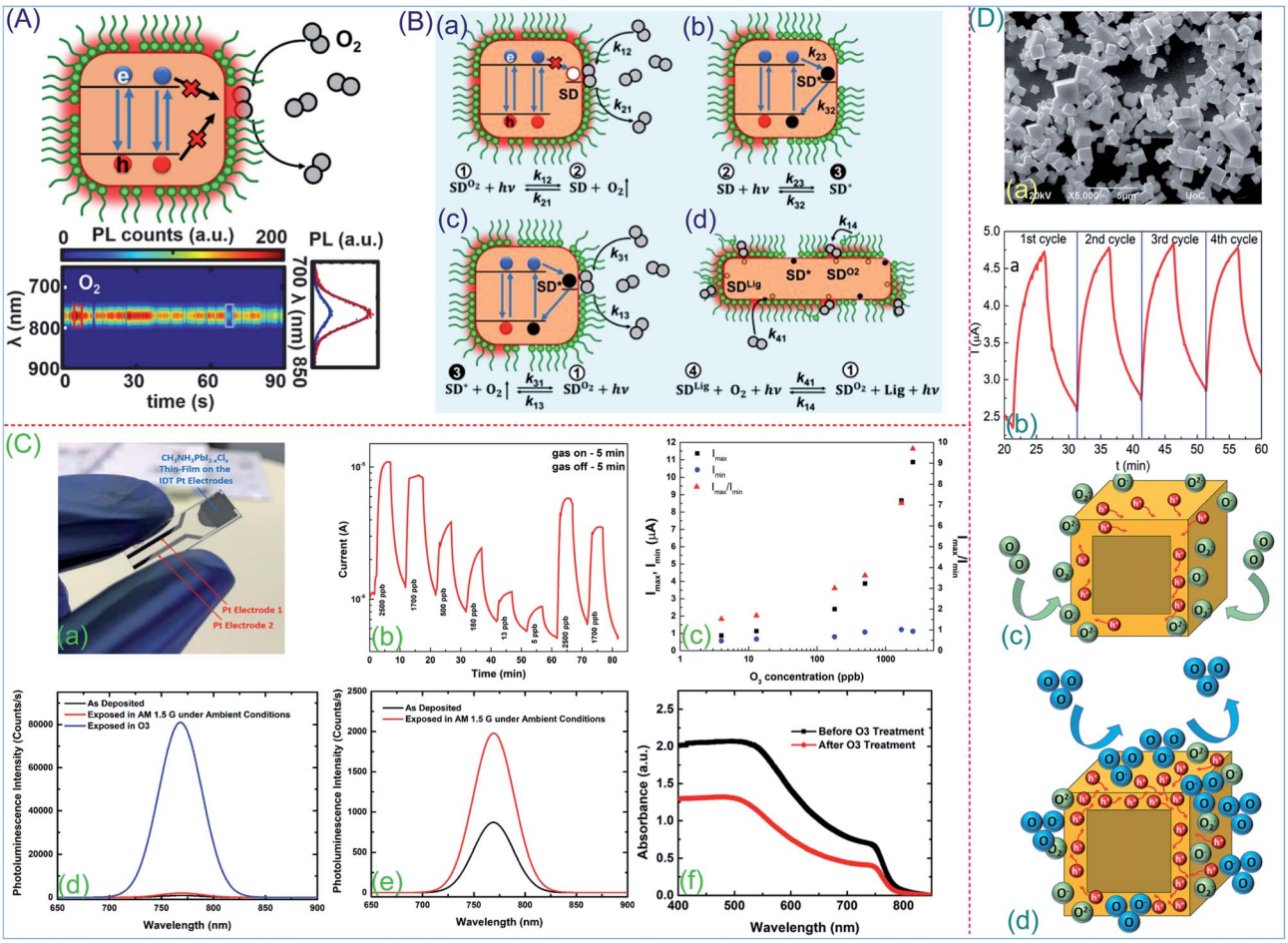

Fig. 25 Single-particle MHP PL as a probe: (A) conceptual schematic of single oxygen molecule sensitivity of MHP PL. (B) Proposed surface reaction mechanism (a–d). Reprinted with permission from ref. 63. Copyright 2019 American Chemical Society. (C) $MAPbI_{3-x}Cl_x$ based self-powered O_3 sensing element: image (a) and the electrical response of the device under various O_3 concentrations (b). Sensitivity as a function of the O_3 concentration (c). PL spectra of the pristine (black line) (d) and A.M.1.5G exposed (red line) and O_3 (e) exposed $MAPbI_{3-x}Cl_x$ films. Absorption spectra of the $MAPbI_{3-x}Cl_x$ films before and after exposure to O_3 (f). Reprinted with permission from ref. 65. Copyright 2017 American Chemical Society. (D) Time dependence of the ozone response upon four successive sensing scans (a) and SEM image of the all-inorganic perovskite nanocubes at the end of the sensing process (b). Schematic diagram of the gas sensing mechanism under ambient conditions (c) and after ozone exposure (d). Reprinted with permission from ref. 64 Copyright 2017 American Chemical Society.

high concentrations of this powerful oxidizing gas in the ambient atmosphere are hazardous to human health. Kakavelakis *et al.* reported a portable, flexible, solution processed $MAPbI_{3-x}Cl_x$ perovskite based self-powered and ultra-sensitive ozone sensing element that can be operated at room temperature (Fig. 25C).[65] The electrical resistance of the $MAPbI_{3-x}Cl_x$ sensing element was immediately decreased when exposed to an O_3 environment and it managed to recover its pristine electrical conductivity values within a few seconds after the complete removal of O_3 gas. Sensing measurements showed different response times at different gas concentrations with good repeatability, ultrahigh sensitivity and fast recovery time. Fig. 25C(d) shows the PL spectra of the $MAPbI_{3-x}Cl_x$ film before and after its exposure to simulated one sun irradiation, a typical procedure performed in such films for the improvement of its electronic quality, while Fig. 25C(e) depicts the substantially enhancement of the PL intensity after the exposure of the same film to an ozone environment. This enhancement is mainly attributed to the O_3 exposure that passivates the surface traps in the perovskite films and thus increases the intensity of the radiative recombination. However, the stability test suggests that the exposure of the sensors to ozone for prolonged periods has some detrimental effects that need further investigation. Brintakis *et al.* investigated ligand-free all-inorganic metal halide nanocubes for fast, ultra-sensitive and self-powered ozone sensors (Fig. 25D).[64] They demonstrated higher sensitivity (54% in 187 ppb) and faster response and recovery times compared to hybrid lead mixed halide perovskite ($MAPbI_{3-x}Cl_x$) layers with a new sensing mechanism proposed as shown in (Fig. 25D(c and d)). These studies demonstrate the great potential of MHPs as reliable sensing elements, serving the objectives of environmental control.

Zhang *et al.* reported the reversible air-induced optical and electrical modulation of $MAPbBr_3$ SCs (Fig. 26A and S7A(a and

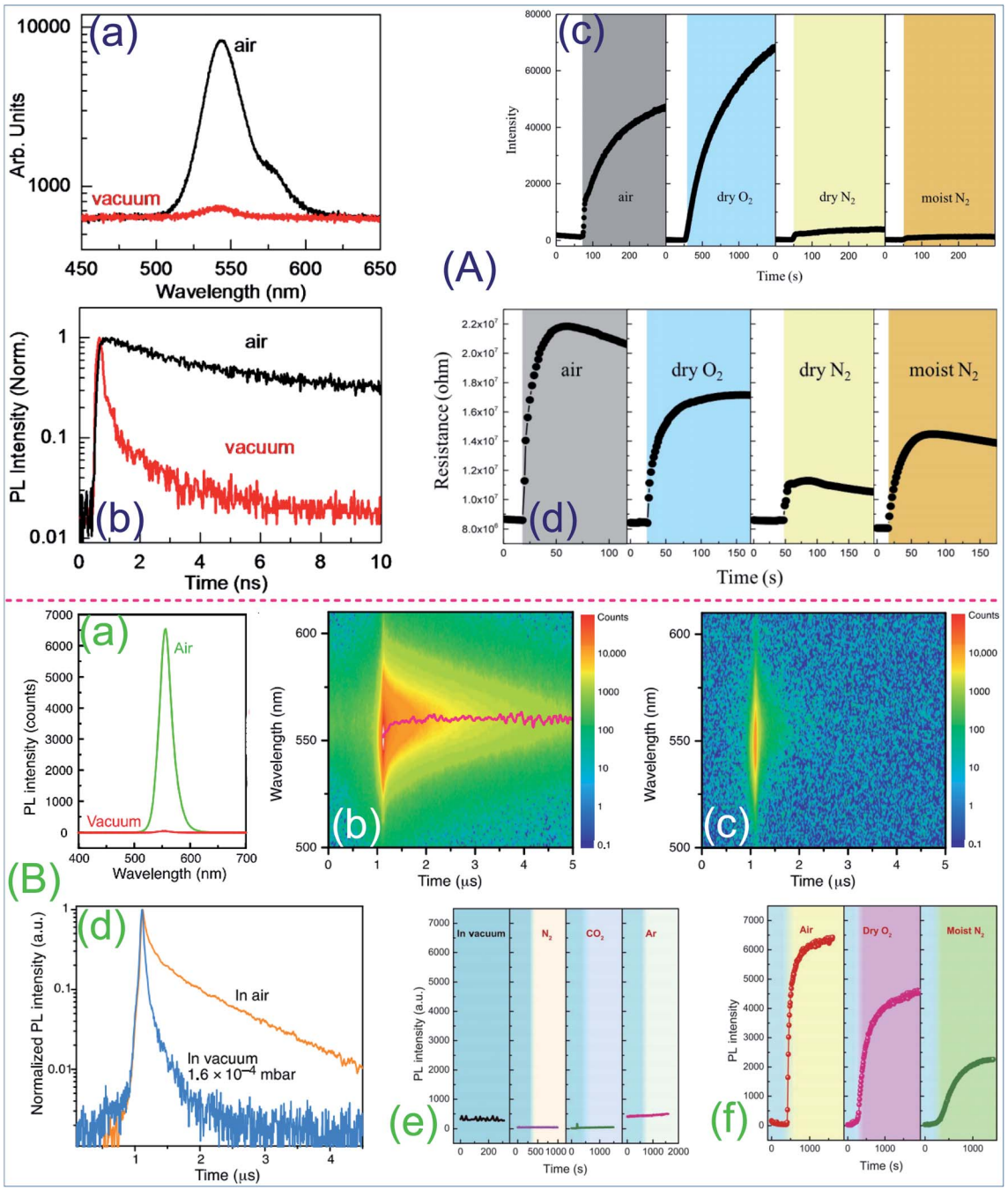

Fig. 26 (A) Reversible air-induced optical and electrical modulation of $MAPbBr_3$ SCs: steady PL (a) and PL decay (b) of $MAPbBr_3$ SCs in air and vacuum, respectively. The PL (c) and resistance (d) of $MAPbBr_3$ SCs as a function of time upon exposure to air, dry O_2, dry N_2 and moist N_2. Reprinted with permission from ref. 66. Copyright 2017 The Author(s). (B) PL spectra of $MAPbBr_3$ SCs in a vacuum and air (a). Two-dimensional (2D) pseudocolor plots of TRPL spectra taken in air (b) and vacuum (c). Decay of the PL at a wavelength of 560 nm in air and vacuum (d). Effect of exposure to different gaseous environments on the PL intensity of $MAPbBr_3$ SCs (c and d). Reprinted with permission from ref. 67. Copyright 2016 The Authors.

b)†).[66] It is observed that the PL intensity and lifetime of perovskite SCs decrease (Fig. 26A(a and b)), while the conductivity increases, with the change in the surrounding atmosphere from air to vacuum. Also, there is a positive correlation between the resistance of $MAPbBr_3$ SCs and the air pressure. DFT studies suggest that the shallow trap states associated with O_2 and H_2O molecules are considered as the key elements in PL and conductivity changes. Further electrical property measurements in different atmospheres (Fig. 26A(c and d) and S7A(b)†) clearly show that the $MAPbBr_3$ SCs are mainly influenced by oxygen and water molecules when exposed to air. These results highlight the important implications for the characterization and application of halide perovskites in a vacuum. The absence of trap states found in a vacuum here strongly suggests the

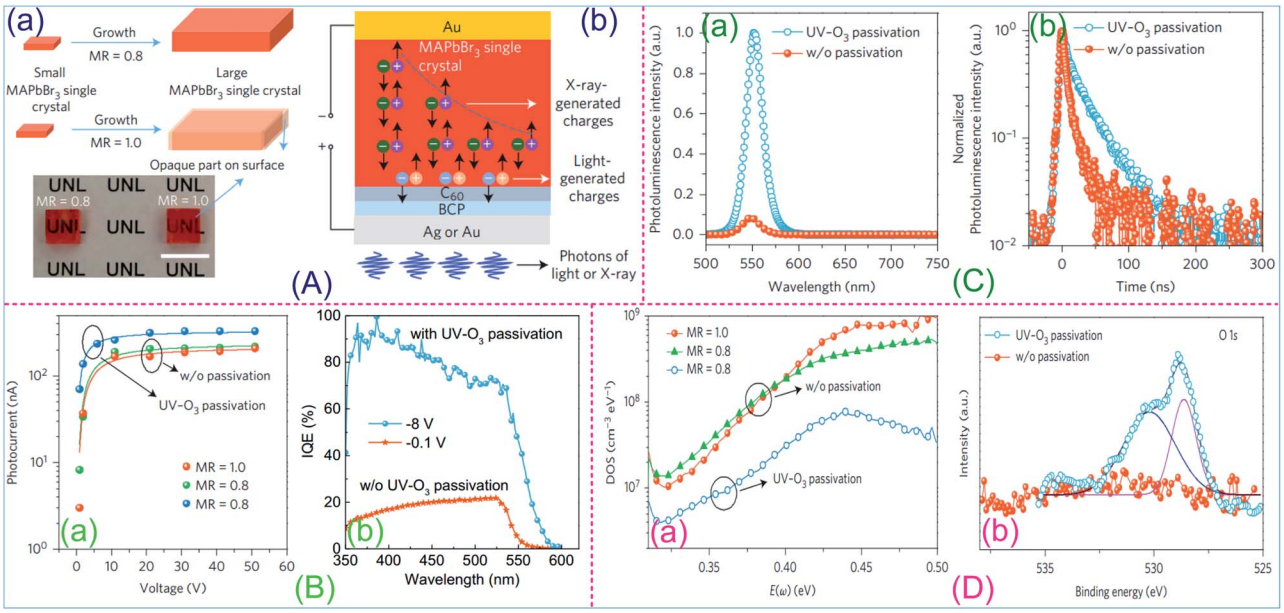

Fig. 27 (A) Scheme and photograph of $MAPbBr_3$ SCs with different molar ratios (a) and the X-radiation detector structure (b). (B) Photoconductivity of the devices with different molar ratios (MR) and surface treatments (a) and charge collection efficiency of the $MAPbBr_3$-MR0.8 SC device (b). (C) Steady (a) and transient (b) PL of a $MAPbBr_3$ SC in a vacuum before and after UV-O_3 treatment. (D) XPS spectra (a) and trap density states (b) of the $MAPbBr_3$ SC with different molar ratios, before and after UV-O_3 treatment. Reprinted with permission from ref. 68 Copyright 2016 Macmillan Publishers Limited.

possible application of halide perovskite materials without O_2 and H_2O, especially for space use. Fang *et al.* reported the ultrahigh sensitivity of a $MAPbBr_3$ SC device to environmental gases (Fig. 26B and S7B(a and b)†).[67] They demonstrated that the surface recombination rate (or surface trap state density) in $MAPbBr_3$ SCs can be fully and reversibly controlled by the physisorption of oxygen and water molecules, leading to a modulation of the PL intensity by over two orders of magnitude (Fig. 26B(a) and S7B(e)†). To understand how the presence of air affects the PL, the dynamics of photoexcitation in the $MAPbBr_3$ SCs in different environments (Fig. 26B(b and c)) were investigated. It was found that the decay time of the crystal measured in air shows an initial fast component with a lifetime of ≈59 ns (77.2%) and a slower component with a lifetime of ≈818 ns (22.8%) (Fig. 26B(d)). From Fig. 26B(e, f) and S7B(f),† the exposure of the crystal to dry N_2, CO_2, or Ar has no obvious influence on the PL intensity, while the PL intensity increases rapidly in the presence of air, dry O_2, and moist N_2. Note that the most rapid and intense PL enhancement is observed in the air-exposed SC, whereas the PL intensity recovers much more slowly in dry O_2 and moist N_2. These data clearly indicate that the PL enhancement is due to the molecular properties of O_2 and H_2O. These findings highlight the importance of environmental conditions in the investigation and fabrication of high-quality, perovskite-based devices and offer a new potential application of these materials to detect oxygen and water vapor.

5.4 X-ray detectors

Apart from the common application of solar cells and LEDs, the OIDH effect has also found its application in X-ray detectors. Wei *et al.* reported the first sensitive X-ray detectors made of $MAPbBr_3$ SCs, whose sensitivity is four times higher than that of α-Se X-ray detectors (Fig. 27A).[68] A record-high $\mu\tau$ product of 1.2×10^{-2} cm^2 V^{-1} and an extremely small surface charge recombination velocity of 64 cm s^{-1} are realized by reducing the bulk defects *via* a non-stoichiometry precursor (Fig. 27A(a)) and passivating surface traps with UV-O_3 oxidization. The enhancement of these material properties has contributed to improved photo-current and IQE of the final X-ray detectors (Fig. 27B). From comprehensive optoelectronic characterization, it is found that the oxidized $MAPbBr_3$-MR0.8 SCs have 12 times stronger PL intensity and three times longer radiative recombination lifetime than pristine $MAPbBr_3$ SCs under vacuum conditions (Fig. 27C). The trap density of the UV-O_3 passivated $MAPbBr_3$ SC (3×10^6 and 7×10^7 cm^{-3} eV^{-1}) was reduced by approximately tenfold, which is the lowest measured trap density of all known SCs. XPS further confirms this passivation effect as the XPS measurements could not remove the chemically attached oxygen species, which verifies the permanent passivation effect of UV-O_3 passivation (Fig. 27D).

6 Conclusions and outlook

During the last several years, the great commercial potential of halide perovskite optoelectronic devices, such as perovskite based solar cells and light-emitting diodes, has been demonstrated with rapid development. As a process that limits the maximum achievable efficiency of such devices, a common challenge is the urgent need to suppress the nonradiative recombination due to all kinds of trap states within the perovskite.

In this review, recent advances in the oxygen-induced defect-healing (OIDH) effect and photo-brightening of halide perovskite semiconductors have been summarized, highlighting their related phenomenon, science and applications. In spite of the exciting achievements fulfilled in the past few years, these effects still need to be promoted for their practical application in other optoelectronic devices. Here, some major outlooks are presented to address these issues:

(1) OIDH and photo-brightening effects are well adopted to fabricate efficient perovskite solar cells and oxygen sensors, while their usage in other optoelectronic devices (such as humidity sensors[69,70] and any other gas or organic solvent sensors,[71–73] photo-detectors,[74,75] filed effect transistors, memristors,[76,77] LEDs,[75] lasers[75] and even energy storage devices[78]) has seldom been reported. As an efficient way of defect passivation, the OIDH and photo-brightening effects may have great potential in any other halide perovskite (mixed cation perovskites, 3D, 2D, 0D or mixed dimensional perovskites, *etc.*) and perovskite-like semiconductor based optoelectronic applications, which awaits the community's intense exploration. For example, it would be interesting to passivate the defect of low dimensional perovskites (such as perovskite quantum dots) with a high surface area with oxygen.

(2) In spite of the consensus mentioned in the main text, there are still some controversial observations and views. For example, Sienkiewicz *et al.* reported the differential response of the photoluminescence and photo-current of polycrystalline $MAPbI_3$ and $MAPbBr_3$-based gas-sensing elements to the same atmosphere. This suggests that the defect passivation effect of oxygen is halogen ion dependent. Therefore, further in-depth work is needed to identify the specific defects being passivated and elucidate universal mechanisms.

(3) The presently reported studies on oxygen induced defect passivation are mainly focused on the halogen vacancy and interstitial defects, while the passivation of many other defects within the perovskite has seldom been mentioned in the published studies.

(4) Apart from the photo-brightening effect as reported, there have also been some reports on the photo-darkening effect,[79] which can be a competitive process. For example, in the work by Míguez *et al.*,[40] photo-brightening was observed followed by photo-darkening, implying the excess oxygen as a fluorescence quenching center with an extended oxygen exposure. This suggests that further work is needed to identify the specific defects being passivated and elucidate universal mechanisms.

(5) As also reported in some published work, accompanied by the photo-brightening effect, is the notorious photo-degradation effect of halide perovskites,[79] which may cause the stability issue of the perovskite and perovskite-based devices. How to make full use of the oxygen induced photo-brightening effect to achieve high efficiency while inhibiting the photo-oxygen degradation to ensure high stability of the device can be a major challenge that needs to be careful addressed.

(6) Despite the encouraging results achieved, there are also concerns about the stability and durability of the OIDH effect. This is a natural doubt because it is possible for oxygen to desorb and leave the perovskite lattice. This depends on the form (oxygen–halogen interstitial interaction, oxygen–lead interaction, *etc.*) and intensity of the interaction between oxygen and the perovskite lattice, external conditions (such as temperature, light, *etc.*), *etc.* Considering the working conditions of PSCs, the oxygen ions bound to the perovskite lattice may be activated by the combined effects of an electric field, high temperature and illumination, thus degassing from the perovskite lattice. For solar cells and light-emitting diodes, this reversibility of the oxygen passivation can be unfavorable, while, such reversibility of oxygen adsorption/passivation and desorption/degassing can be necessary for oxygen/ozone detectors. Anyway, controlled oxygen adsorption/passivation and desorption will be necessary and highly expected, which requires further in-depth research by the entire research community.

We believe that the present understanding and successful application of the OIDH effect in the as-mentioned devices will find wide application in other optoelectronic devices such as filed-effect transistors, photodetectors, *etc.*

CRediT authorship contribution statement

Like Huang: conceptualization, investigation, methodology, writing the original draft, writing the review & editing, validation, visualization, project administration, and funding acquisition. Ziyi Ge: project administration, supervision, and funding acquisition. Xiaoli Zhang: review & editing. Yuejin Zhu: project administration and supervision.

Conflicts of interest

The authors declare no competing financial interest.

Acknowledgements

This work was supported by the National Natural Science Foundation of China (61904182, 51773212, and 21805296), National Science Fund for Distinguished Young Scholars (21925506), and National Postdoctoral Program for Innovative Talents (BX20180322) of China sponsored by the China Postdoctoral Science Foundation and China National Postdoctoral Council. The authors also gratefully acknowledge the support from the National Key R&D Program of China (2017YFE0106000), Zhejiang Provincial Natural Science Foundation of China (LY20B040002), Ningbo S&T Innovation 2025 Major Special Programme (2018B10055), Ningbo Municipal Science and Technology Innovative Research Team (2015B11002 and 2016B10005), and CAS Key Project of Frontier Science Research (QYZDB-SSW-SYS030) and the K. C. Wong Magna Fund at Ningbo University.

References

1 A. Kojima, K. Teshima, Y. Shirai and T. Miyasaka, Organometal halide perovskites as visible-light sensitizers

for photovoltaic cells, *J. Am. Chem. Soc.*, 2009, **131**(17), 6050–6051.
2 National Renewable Energy Laboratory, Best Research-Cell Efficencies Chart, https://www.nrel.gov/pv/cell-efficiency.html.
3 P. Lopez-Varo, J. A. Jimenez-Tejada, M. Garcia-Rosell, S. Ravishankar, G. Garcia-Belmonte, J. Bisquert and O. Almora, Device physics of hybrid perovskite solar cells: theory and experiment, *Adv. Energy Mater.*, 2018, **8**(14), 1702772.
4 (*a*) Y. Chen, M. He, J. Peng, Y. Sun and Z. Liang, Structure and growth control of organic-inorganic halide perovskites for optoelectronics: from polycrystalline films to single crystals, *Adv. Sci.*, 2016, **3**, 1500392; (*b*) H. Zhu, Z. Zhao, H. Cao, H. Yu, J. Li, X. Chen, S. Dong, L. Yang and S. Yin, Determination of bandgaps of photoactive materials in perovskite solar cells at high temperatures by in situ temperature-dependent resistance measurement, *Optoelectron. Lett.*, 2016, **12**, 337–339.
5 S. Akin, N. Arora, S. M. Zakeeruddin, M. Grätzel, R. H. Friend and M. I. Dar, New strategies for defect passivation in high-efficiency perovskite solar cells, *Adv. Energy Mater.*, 2019, **10**, 1903090.
6 E. Aydin, M. Bastiani and S. Wolf, Defect and contact passivation for perovskite solar cells, *Adv. Mater.*, 2019, **31**, 1900428.
7 Q. Jiang, Y. Zhao, X. Zhang, X. Yang, Y. Chen, Z. Chu, Q. Ye, X. Li, Z. Yin and J. You, Surface passivation of perovskite film for efficient solar cells, *Nat. Photonics*, 2019, **13**, 460–466.
8 B. Chen, P. N. Rudd, S. Yang, Y. Yuan and J. Huang, Imperfections and their passivation in halide perovskite solar cells, *Chem. Soc. Rev.*, 2019, **48**, 3842–3867.
9 J. M. Ball and A. Petrozza, Defects in perovskite-halides and their effects in solar cells, *Nat. Energy*, 2016, **1**, 16149.
10 N. K. Noel, A. Abate, S. D. Stranks, E. S. Parrott, V. M. Burlakov, A. Goriely and H. J. Snaith, Enhanced photoluminescence and solar cell performance via Lewis base passivation of organic-inorganic lead halide perovskites, *ACS Nano*, 2014, **8**(10), 9815–9821.
11 D. W. Dequilettes, S. Koch, S. Burke, R. Paranji, A. J. Shropshire, M. E. Ziffer and D. S. Ginger, Photoluminescence lifetimes exceeding 8 μs and quantum yields exceeding 30% in hybrid perovskite thin films by ligand passivation, *ACS Energy Lett.*, 2016, **1**(2), 438–444.
12 S. Yang, J. Dai, Z. Yu, Y. Shao and X. Zhou, Tailoring passivation molecular structures for extremely small open-circuit voltage loss in perovskite solar cells, *J. Am. Chem. Soc.*, 2019, **141**(14), 5781–5787.
13 Y. Ding, M. Sugaya, Q. Liu, S. Zhou and T. Nozaki, Oxygen passivation of silicon nanocrystals: influences on trap states, electron mobility, and hybrid solar cell performance, *Nano Energy*, 2014, **10**, 322–328.
14 Y. Zhang, D. Zherebetskyy, N. D. Bronstein, S. Barja, L. Lichtenstein, A. P. Alivisatos, L. W. Wang and M. Salmeron, Molecular oxygen induced in-gap states in PbS quantum dots, *ACS Nano*, 2015, **9**(10), 10445–10452.
15 X. Liu, C. Chen, L. Wang, J. Zhong, M. Luo, J. Chen, D. J. Xue, D. Li, Y. Zhou and J. Tang, Improving the performance of Sb_2Se_3 thin film solar cells over 4% by controlled addition of oxygen during film deposition progress in photovoltaics, *Prog. Photovolt: Res. Appl.*, 2015, **23**(12), 1828–1836.
16 C. Schwermann, T. Stiehm, P. Tonndorf, R. Schneider and N. L. Doltsinis, Incorporation of oxygen atoms as a mechanism for photoluminescence enhancement of chemically treated MoS_2, *Phys. Chem. Chem. Phys.*, 2018, **20**(25), 16918–16923.
17 H. Nan, Z. Wang, W. Wang, Z. Liang, Y. Lu, Q. Chen, D. He, P. Tan, F. Miao and X. Wang, Strong photoluminescence enhancement of MoS_2 through defect engineering and oxygen bonding, *ACS Nano*, 2014, **8**(6), 5738–5745.
18 R. Brenes, D. Guo, A. Osherov, N. K. Noel, C. Eames, E. M. Hutter, S. K. Pathak, F. Niroui, R. H. Friend, M. S. Islam, H. J. Snaith, V. Bulović, T. J. Savenije and S. D. Stranks, Metal halide perovskite polycrystalline films exhibiting properties of single crystals, *Joule*, 2017, **1**(1), 155–167.
19 J. S. W. Godding, A. J. Ramadan, Y.-H. Lin, K. Schutt, H. J. Snaith and B. Wenger, Oxidative passivation of metal halide perovskites, *Joule*, 2019, **3**(11), 2716–2731.
20 S. Liu, Z. Li, Y. Yang, X. Wang, Y. Chen, D. Xue and J. Hu, Investigation of oxygen passivation for high-performance all-inorganic perovskite solar cells, *J. Am. Chem. Soc.*, 2019, **141**, 18075–18082.
21 P. Delugas, A. Filippetti and A. J. Mattoni, Methylammonium fragmentation in amines as source of localized trap levels and the healing role of Cl in hybrid lead-iodide perovskites, *Phys. Rev. B: Condens. Matter Mater. Phys.*, 2015, **92**(4), 045301.
22 G. Nan, X. Zhang, M. Abdi-Jalebi, Z. Andaji-Garmaroudi, S. D. Stranks, G. Lu and D. J. Beljonne, How methylammonium cations and chlorine dopants heal defects in lead iodide perovskites, *Adv. Energy Mater.*, 2018, **8**(13), 1702754.
23 D. R. Ceratti, Y. Rakita, L. Cremonesi, R. Tenne and V. Kalchenko, Self-healing inside $APbBr_3$ halide perovskite crystals, *Adv. Mater.*, 2018, **30**(10), 1706273.
24 F. Lang, N. H. Nickel, J. Bundesmann, S. Seidel, A. Denker, S. Albrecht, V. V. Brus, J. Rappich, B. Rech and G. Landi, Radiation hardness and self-healing of perovskite solar cells, *Adv. Mater.*, 2016, **28**, 8726–8731.
25 W. Nie, J. C. Blancon, A. J. Neukirch, K. Appavoo, H. Tsai, M. Chhowalla, M. A. Alam, M. Y. Sfeir, C. Katan and J. Even, Light-activated photocurrent degradation and self-healing in perovskite solar cells, *Nat. Commun.*, 2016, **7**(1), 11574.
26 J. Fan, Y. Ma, C. Zhang, L. Chong and Y. Mai, Thermodynamically self-Hhealing 1D-3D hybrid perovskite solar cells, *Adv. Energy Mater.*, 2018, **8**(16), 1703421.
27 W.-J. Yin, H. Chen, T. Shi, S.-H. Wei and Y. Yan, Origin of high electronic quality in structurally disordered $CH_3NH_3PbI_3$ and the passivation effect of Cl and O at grain boundaries, *Adv. Electron. Mater.*, 2015, **1**(6), 1500044.

28 Z. Ren, A. Ng, Q. Shen, H. Gokkaya, J. Wang, L. Yang, W. Yiu, G. Bai, A. Djurisic and W. Leung, Thermal assisted oxygen annealing for high efficiency planar CH3NH3PbI3 perovskite solar cells, *Sci. Rep.*, 2014, **4**(1), 6752.

29 S. Pathak, A. Sepe, A. Sadhanala, F. Deschler, A. Haghighirad, N. Sakai, K. C. Goedel, S. D. Stranks, N. Noel, M. Price, S. Hüttner, N. A. Hawkins, R. H. Friend, U. Steiner and H. J. Snaith, Atmospheric influence upon crystallization and electronic disorder and itsimpact on the photophysical properties of organic-inorganic perovskite solar cells, *ACS Nano*, 2015, **9**(3), 2311–2320.

30 B. J. Bruijnaers, E. Schiepers, C. H. L. Weijtens, S. C. J. Meskers, M. M. Wienk and R. Janssen, The effect of oxygen on the efficiency of planar p-i-n metal halide perovskite solar cells with a PEDOT:PSS hole transport layer, *J. Mater. Chem. A*, 2018, **6**(16), 6882–6890.

31 G. Grancini, V. D'Innocenzo, E. R. Dohner, N. Martino, A. R. Srimath Kandada, E. Mosconi, F. De Angelis, H. I. Karunadasa, E. T. Hoke and A. Petrozz, $CH_3NH_3PbI_3$ perovskite single crystals: surface photophysics and its interaction with the environment, *Chem. Sci.*, 2015, **6**(12), 7305–7310.

32 W. Hao, X. Chen and S. Li, Synergistic effects of water and oxygen molecule co-adsorption on (001) surfaces of tetragonal $CH_3NH_3PbI_3$: a first-principles study, *J. Phys. Chem. C*, 2016, **120**(50), 28448–28455.

33 W. Kong, A. Rahimi-Iman, G. Bi, X. Dai and H. Wu, Oxygen intercalation induced by photocatalysis on the surface of hybrid lead-halide perovskites, *J. Phys. Chem. C*, 2016, **120**(14), 7606–7611.

34 L. Zhang and P. Sit, Ab initio study of the role of oxygen and excess electrons in the degradation of $CH_3NH_3PbI_3$, *J. Mater. Chem. A*, 2017, **5**(19), 9042–9049.

35 N. Aristidou, C. Eames, I. Sanchezmolina, X. Bu, J. Kosco, M. Saiful Islam and S. Haque, Fast oxygen diffusion and iodide defects mediate oxygen-induced degradation of perovskite solar cells, *Nat. Commun.*, 2017, **8**(1), 15218.

36 B. Philippe, B. W. Park, R. Lindblad, J. Oscarsson, S. Ahmadi, E. M. J. Johansson and H. Rensmo, Chemical and electronic structure characterization of lead halide perovskites and stability behavior under different exposures-A photoelectron spectroscopy investigation, *Chem. Mater.*, 2015, **27**(5), 1720–1731.

37 M. Ralaiarisoa, I. Salzmann, F. Zu and N. Koch, Materials effect of water, oxygen, and air exposure on $CH_3NH_3PbI_{3-x}Cl_x$ perovskite surface electronic properties, *Adv. Electron. Mater.*, 2018, **4**, 1800307.

38 A. Zohar, N. Kedem, I. Levine, D. Zohar and D. Cahen, Impedance spectroscopic indication for solid state electrochemical reaction in $CH_3NH_3PbI_3$ films, *J. Phys. Chem. Lett.*, 2015, **7**(1), 191–197.

39 J. F. Galisteo-López, M. Anaya and M. E. Calvo, Environmental effects on the photophysics of organic-inorganic halide perovskites, *J. Phys. Chem. Lett.*, 2015, **6**(12), 2200–2205.

40 M. Anaya, J. F. Galisteo-López, M. E. Calvo, J. P. Espinos and H. Míguez, Origin of light induced photophysical effects in organic metal halide perovskites in the presence of oxygen, *J. Phys. Chem. Lett.*, 2018, **9**(14), 3891–3896.

41 Y. Tian, P. Maximilian, U. Eva, A. Mohamed, K. Zheng, T. Pullerits, A. Yartsev, V. Sundström and I. G. Scheblykin, Mechanistic insights into perovskite photoluminescence enhancement: light curing with oxygen can boost yield thousand fold, *Phys. Chem. Chem. Phys.*, 2015, **17**(38), 24978–24987.

42 Y. Tian, A. Merdasa, E. Unger, M. Abdellah, K. Zheng, S. R. McKibbin, A. Mikkelsen, T. Pullerits and A. Sundstrom, Enhanced organo-metal halide perovskite photoluminescence from nanosized defect-free crystallites and emitting sites, *J. Phys. Chem. Lett.*, 2015, **6**(20), 4171–4177.

43 S. G. Motti, M. Gandini, A. J. Barker, J. M. Ball, A. R. Srimath Kandada and A. Petrozza, Photoinduced emissive trap states in lead halide perovskite semiconductors, *ACS Energy Lett.*, 2016, **1**(4), 726–730.

44 W. Li, Y.-Y. Sun, L. Linqiu, Z. Zhou and J. Tang, Control of charge recombination in perovskites by oxidation state of halide vacancy, *J. Am. Chem. Soc.*, 2018, **140**(46), 15753–15763.

45 R. Brenes, C. Eames, V. Bulović, M. S. Islam and S. Stranks, The impact of atmosphere on the local luminescence properties of metal halide perovskite grains, *Adv. Mater.*, 2018, **30**(15), 1706208.

46 W. Fan, Y. Shi, T. Shi, S. Chu, W. Chen, K. Ighodalo, J. Zhao, X. Li and Z. Xiao, Suppression and reversion of light-induced phase separation in mixed-halide perovskites by oxygen passivation, *ACS Energy Lett.*, 2019, **4**(9), 2052–2058.

47 X. Che, B. Traore, C. Katan and H. H. Fang, Charge trap formation and passivation in methylammonium lead tribromide, *J. Phys. Chem. C*, 2019, **123**(22), 13812–13817.

48 A. Szemjonov, K. Galkowski, M. Anaya, Z. Andaji-Garmaroudi, T. K. Baikie, S. Mackowski, I. D. Baikie, S. D. Stranks and M. Saiful Islam, Impact of oxygen on the electronic structure of triple-cation halide perovskites, *ACS Mater. Lett.*, 2019, **1**(5), 506–510.

49 J. He, W. H. Fang, R. Long and O. V. Prezhdo, Superoxide/peroxide chemistry extends charge carriers' lifetime but undermines chemical stability of $CH_3NH_3PbI_3$ exposed to oxygen: time-domain *ab initio* analysis, *J. Am. Chem. Soc.*, 2019, **141**(14), 5798–5807.

50 L. Qiao and R. Long, Surface Pb-dimer passivated by molecule oxygen notably suppresses charge recombination in $CsPbBr_3$ perovskites: time-domain *ab initio* analysis, *J. Phys. Chem. Lett.*, 2019, **10**(18), 5499–5506.

51 D. Meggiolaro, E. Mosconi and F. De Angelis, Mechanism of reversible trap passivation by molecular oxygen in lead-halide perovskites, *ACS Energy Lett.*, 2017, **2**(12), 2794–2798.

52 J. He, W. H. Fang and R. Long, Unravelling the effects of oxidation state of interstitial iodine and oxygen passivation on charge trapping and recombination in $CH_3NH_3PbI_3$ perovskite: a time-domain *ab initio* study, *Chem. Sci.*, 2019, **10**(43), 10079–10088.

53 K. Mantulnikovs, A. Glushkova, M. Kollár, L. Forró, E. Horváth and A. Sienkiewicz, Differential response of the

photoluminescence and photocurrent of polycrystalline $CH_3NH_3PbI_3$ and $CH_3NH_3PbBr_3$ to the exposure to oxygen and nitrogen, *ACS Appl. Electron. Mater.*, 2019, **1**(10), 2007–2017.

54 M. Lorenzon, L. Sortino, Q. A. Akkerman, S. Accornero and S. Brovelli, Role of nonradiative defects and environmental oxygen on exciton recombination processes in $CsPbBr_3$ perovskite nanocrystals, *Nano Lett.*, 2017, **17**(6), 3844–3853.

55 C. Rodà, A. L. Abdelhady, J. Shamsi, M. Lorenzon, V. Pinchetti, M. Gandini, F. Meinardi, L. Manna and S. Brovelli, O_2 as a molecular probe for nonradiative surface defects in $CsPbBr_3$ perovskite nanostructures and single crystals, *Nanoscale*, 2019, **11**, 7613–7623.

56 D. Lu, Y. Zhang, M. Lai, A. Lee, C. Xie, J. Lin, T. Lei, Z. Lin, C. S. Kley and J. Huang, Giant light-emission enhancement in lead halide perovskites by surface oxygen passivation, *Nano Lett.*, 2018, **18**(11), 6967–6973.

57 (*a*) Y. Wang, Y. Ren, S. Zhang, J. Wu, J. Song, X. Li, J. Xu, C. H. Sow, H. Zeng and H. Sun, Switching excitonic recombination and carrier trapping in cesium lead halide perovskites by air, *Commun. Phys.*, 2018, **1**(1), 1–8; (*b*) L. K. Ono and Y. Qi, Surface and interface aspects of organometal halide perovskite materials and solar cells, *J. Phys. Chem. Lett.*, 2016, **7**, 4764–4794; (*c*) Y. Liu, K. Palotas, X. Yuan, T. Hou and S. T. Lee, The atomistic origins of surface defects in CH3NH3PbBr3 perovskite and their electronic structures, *ACS Nano*, 2017, **11**, 2060–2065; (*d*) R. Ohmann, L. K. Ono, H. S. Kim, H. Lin, M. V. Lee, Y. Li, N. G. Park and Y. Qi, Real-space imaging of the atomic structure of organic-inorganic perovskite, *J. Am. Chem. Soc.*, 2015, **137**, 16049–16054; (*e*) L. She, M. Liu, X. Li, Z. Cai and D. Zhong, Growth and interfacial structure of methylammonium lead iodide thin films on Au (111), *Surf. Sci.*, 2017, **656**, 17–23; (*f*) L. She, M. Liu and D. J. Zhong, Atomic structures of CH3NH3PbI3(001) surfaces, *ACS Nano*, 2016, **10**, 1126–1131; (*g*) Y. Zhu, Z. Gui, Q. Wang, F. Meng, S. Feng, B. Han, P. Wang, L. Huang, H. L. Wang and M. Gu, Direct atomic scale characterization of the surface structure and planar defects in the organic-inorganic hybrid $CH_3NH_3PbI_3$ by Cryo-TEM, *Nano Energy*, 2020, **73**, 104820; (*h*) K. Song, L. Liu, D. Zhang, M. P. Hautzinger, S. Jin and Y. Han, Atomi-resolution imaging of halide perovskites using electron microscopy, *Adv. Energy Mater.*, 2020, 1904006; (*i*) Y. Zhou, X. Hu, D. Xie and Y. Tian, Mechanisms of oxygen passivation on surface defects in MAPbI3 revealed by first-principles study, *J. Phys. Chem. C*, 2020, **124**, 3731–3737; (*j*) W. Wu, P. N. Rudd, Z. Ni, C. Henry Van Brackle, H. Wei, Q. Wang, B. R. Ecker, Y. Gao and J. Huang, Reducing surface halide deficiency for efficient and stable iodide-based perovskite solar cells, *J. Am. Chem. Soc.*, 2020, **142**, 3989–3996; (*k*) F. Ambrosio, D. Meggiolaro, E. Mosconi and F. Angelis, Charge localization and trapping at surfaces in lead-iodide perovskites: the role of polarons and defects, *J. Mater. Chem. A*, 2020, **8**, 6882; (*l*) D. Meggiolaro, E. Mosconi, A. H. Proppe, R. Quintero-Bermudez and F. De Angelis, Energy level tuning at the MAPbI3 perovskite/contact interface using chemical treatment, *ACS Energy Lett.*, 2019, **4**, 2181–2184.

58 R. Brenes, D. Guo, A. Osherov, N. Noel, C. Eames, E. Hutter, S. Pathak, H. Snaith, V. Bulović and S. Stranks, Metal Halide Perovskite Polycrystalline Films Exhibiting Properties of Single Crystals, *Joule*, 2017, **1**(1), 155–167.

59 S. Brandon, Tailoring perovskite thin films to rival single crystals, *Joule*, 2017, **1**(1), 23–25.

60 M. Chen, M. Ju, H. F. Garces, A. D. Carl, L. K. Ono, Z. Hawash, Y. Zhang, T. Shen, Y. Qi, R. L. Grimm, D. Pacifici, X. Zeng, Y. Zhou and N. P. Padture, Highly stable and efficient all-inorganic lead-free perovskite solar cells with native-oxide passivation, *Nat. Commun.*, 2019, **10**(1), 16.

61 M. Stoeckel, M. Gobbi, S. Bonacchi, F. Liscio, L. Ferlauto, E. Orgiu and P. Samori, Reversible, fast, and wide-range oxygen sensor based on nanostructured organometal halide perovskite, *Adv. Mater.*, 2017, **29**, 1702469.

62 F. Lin, F. Li, Z. Lai, Z. Cai, Y. Wang, O. S. Wolfbeis and C. Xi, Interfaces Mn^{II}-doped cesium lead chloride perovskite nanocrystals: demonstration of oxygen sensing capability based on luminescent dopants and host-dopant energy transfer, *ACS Appl. Mater. Interfaces*, 2018, **10**(27), 23335–23343.

63 J. R. Vicente, A. Miandashti, K. Piecco, J. Pyle, M. Kordesch and J. Chen, Interfaces single-particle organolead halide perovskite photoluminescence as a probe for surface reaction kinetics, *ACS Appl. Mater. Interfaces*, 2019, **11**(19), 18034–18043.

64 K. Brintakis, E. Gagaoudakis, A. Kostopoulou, V. Faka, A. Argyrou, V. Binas, G. Kiriakidis and E. Stratakis, Ligand-free all-inorganic metal halide nanocubes for fast, ultra-sensitive and self-powered ozone sensors, *Nanoscale Adv.*, 2019, **1**, 2699–2706.

65 G. Kakavelakis, E. Gagaoudakis, K. Petridis, V. Petromichelaki and E. Kymakis, Solution processed $CH_3NH_3PbI_{3-x}Cl_x$ perovskite based self-powered ozone sensing element operated at room temperature, *ACS Sens.*, 2017, **3**(1), 135–142.

66 H. Zhang, Y. Liu, H. Lu, W. Deng and K. Yang, Reversible air-induced optical and electrical modulation of methylammonium lead bromide ($MAPbBr_3$) single crystals, *Appl. Phys. Lett.*, 2017, **111**, 103904.

67 H. H. Fang, S. Adjokatse, H. Wei, J. Yang, G. R. Blake, J. Huang, J. Even and M. A. Loi, Ultrahigh sensitivity of methylammonium lead tribromide perovskite single crystals to environmental gases, *Sci. Adv.*, 2016, **2**(7), 1600534.

68 H. Wei, Y. Fang, P. Mulligan, W. Chuirazzi, H. H. Fang, C. Wang, B. R. Ecker, Y. Gao, M. A. Loi and L. Cao, Sensitive X-ray detectors made of methylammonium lead tribromide perovskite single crystals, *Nat. Photonics*, 2016, **10**(5), 333–339.

69 W. Xu, F. Li, Z. Cai, Y. Wang, F. Luo and X. Chen, An ultrasensitive and reversible fluorescence sensor of humidity using perovskite $CH_3NH_3PbBr_3$, *J. Mater. Chem. C*, 2016, **4**(41), 9651–9655.

70 M. Haque, A. Syed, F. Akhtar, R. Shevate, S. Singh, K. Peinemann, D. Baran and T. Wu, Giant humidity effect on hybrid halide perovskite microstripes: reversibility and sensing mechanism, *ACS Appl. Mater. Interfaces*, 2019, **11**(33), 29821–29829.

71 Z. Zhaohua, S. Qian, Z. Zhipeng, D. Jie, X. Guichuan, L. Shaozhou and H. Xiao, Metal halide perovskites: stability and sensing-ability, *J. Mater. Chem. C*, 2018, **6**, 10121.

72 H. Chen, M. Zhang, R. Bo, C. Barugkin, J. Zheng, Q. Ma, S. Huang, A. W. Y. Ho-Baillie, K. R. Catchpole and A. Tricoli, Superior self-powered room-temperature chemical sensing with light-activated inorganic halides perovskites, *Small*, 2018, **14**(7), 1702571.

73 Y. Zhuang, W. Yuan, L. Qian, S. Chen and G. Shi, High-performance gas sensors based on a thiocyanate ion-doped organometal halide perovskite, *Phys. Chem. Chem. Phys.*, 2017, **19**(20), 12876–12881.

74 H. Wang and H. Dong, Perovskite-based photodetectors: materials and devices, *Chem. Soc. Rev.*, 2017, **46**(17), 5204–5236.

75 F. Yan, S. T. Tan and X. Li, Light generation in lead halide perovskite nanocrystals: LEDs, color converters, lasers, and other applications, *Small*, 2019, **15**(47), 1902079.

76 X. Zhao, H. Xu, Z. Wang, Y. Lin and Y. Liu, Memristors with organic-inorganic halide perovskites, *InfoMat*, 2019, **1**, 183–210.

77 W. Tress, Metal halide perovskites as mixed electronic-ionic conductors: challenges and opportunities-from hysteresis to memristivity, *J. Phys. Chem. Lett.*, 2017, **8**(13), 3106–3114.

78 W. Lee, H. Li, A. B. Wong, D. Zhang and P. Yang, Ultralow thermal conductivity in all-inorganic halide perovskites, *Proc. Natl. Acad. Sci. U. S. A.*, 2017, **114**(33), 8693–8697.

79 J. F. Galisteo-López, M. Anaya, M. E. Calvo and H. Míguez, Environmental effects on the photophysics of organico-norganic halide perovskites, *J. Phys. Chem. Lett.*, 2015, **6**(12), 2200–2205.

